# Numerical modeling of the effect of preferential flow on hillslope hydrology and slope stability

Shao, Wei

**DOI**
10.4233/uuid:6d192fe2-de18-4556-873a-d3cd56ab96a6

**Publication date**
2017

**Document Version**
Final published version

**Citation (APA)**
Shao, W. (2017). *Numerical modeling of the effect of preferential flow on hillslope hydrology and slope stability*. [Dissertation (TU Delft), Delft University of Technology]. https://doi.org/10.4233/uuid:6d192fe2-de18-4556-873a-d3cd56ab96a6

# NUMERICAL MODELING OF THE EFFECT OF PREFERENTIAL FLOW ON HILLSLOPE HYDROLOGY AND SLOPE STABILITY

# NUMERICAL MODELING OF THE EFFECT OF PREFERENTIAL FLOW ON HILLSLOPE HYDROLOGY AND SLOPE STABILITY

## Proefschrift

ter verkrijging van de graad van doctor
aan de Technische Universiteit Delft,
op gezag van de Rector Magnificus prof. ir. K. C. A. M. Luyben,
voorzitter van het College voor Promoties,
in het openbaar te verdedigen op Woensdag 11 Januari 2017 om 15:00 uur

door

**Wei SHAO**

Master of Science in Hydrology and Water Resources,
Hohai University, Nanjin, China.
geboren te Xinjiang, China.

This dissertation has been approved by the
promotor: Prof. dr. ir. M. Bakker
copromotor: Dr. T. A. Bogaard

Composition of the doctoral committee:

| | |
|---|---|
| Rector Magnificus, | chairman |
| Prof. dr. ir. M. Bakker | Delft University of Technology |
| Dr. T. A. Bogaard | Delft University of Technology |

Independent members:

| | |
|---|---|
| Prof. dr. ir. T. J. Heimovaara | Delft University of Technology |
| Prof. dr. C. Jommi | Delft University of Technology |
| Prof. dr. J. A. Huisman | Forschungszentrum Jülich |
| Dr. M. Berti | Università di Bologna |
| Dr. C. J. van Westen | Universiteit Twente |
| Prof. dr. ir. H. H. G. Savenije | Delft University of Technology, reserve member |

*Keywords:* Preferential flow, Dual-permeability model, Slope stability, Landslide, Hillslope hydrology,

*Printed by:* Ipskamp Drukkers

*Front & Back:* Designed by W. Shao; cover photo by Blue Hermiony (bluelagoon, website http://openwalls.com/bluelagoon)



ISBN 978-94-028-0482-9

An electronic version of this dissertation is available at
http://repository.tudelft.nl/.

*To my parents*

# CONTENTS

# SUMMARY

The topic of this thesis is the quantification of the influence of preferential flow on landslide-triggering in potentially unstable slopes. Preferential flow paths (e.g., cracks, macropores, fissures, pipes, etc.) commonly exists in slopes. Flow velocities in preferential flow paths can be significantly larger than in the matrix. Under large rainfall or snowmelt events, preferential flow can bypass the adjacent soil matrix and directly reach the groundwater table. The fast pressure build-up caused by preferential flow can reduce the effective stress and shear strength, which is an important triggering factor for landslides. Single-permeability models can not appropriately simulate preferential flow. Hence, hydro-mechanical models of landslide need the inclusion of preferential flow.

Preferential flow also affects tracer transport in subsurface flow systems. The celerity in unsaturated flow represents the maximum water velocity in a soil, and it may be used to predict the first arrival time of a conservative tracer. The celerity function is derived from the soil hydraulic conductivity function for unsaturated flow, and is used to derive the breakthrough curve of a conservative tracer under advective transport. Analysis of the bimodal hydraulic function for a dual-permeability model shows that different parameter sets may result in similar soil hydraulic conductivity behavior, but distinctly different celerity behavior.

In Chapter 4, a 2D hydro-mechanical model is developed using COMSOL multiphysics modeling software to couple a dual-permeability model with a linear-elastic model. Numerical experiments are conducted for two different rainfall events on a synthetic slope. The influence of preferential flow on slope stability is quantified by comparing the simulated slope failure area for single-permeability model and dual-permeability models. The single-permeability model only simulate regular wetting fronts propagating downward without representing the preferential flow. In contrast, the dual-permeability model can simulate the influence of preferential flow including the enhanced drainage that facilities pressure dissipation under low-intensity rainfall, as well as the fast pressure build-up that may trigger landslides under high-intensity rainfall. The dual-permeability model resulted in a smaller failure area than the corresponding single-permeability model under low-intensity rainfall, while the dual-permeability model resulted in a larger failure area and earlier timing than the corresponding single-permeability model for high-intensity rainfall.

In Chapter 5, a parsimonious 1D hydro-mechanical model is developed for field application by coupling a 1D dual-permeability model with an infinite slope stability anal-

ysis approach. The numerical model is benchmarked against the HYDRUS-1D for the simulation of non-equilibrium flow. In Chapter 6, the model is applied to simulate the pressure response in a clay-shales slope located in northern Italy. In the study area, preferential flow paths such as tension cracks and macropores are widespread. Intense rain-pulses in the summer can cause nearly-instant pressure responses which may re-activate landslide movement. The water exchange coefficient of the dual-permeability model is calibrated for two single-pulse rainfall-events in the summer, while all other parameters are obtained from field investigations. Results from the dual-permeability model are compared to previously published outcomes using a linear-diffusion equation, where the diffusion coefficient was calibrated for each rainfall event separately. The dual-permeability model explicitly accounts for the influence of both matrix flow and preferential flow on water flow and pressure propagation in variably saturated soils, and is able to simulate the measured pressure response to multi-pulse rainfall-events quite well even in the winter time. Results indicate that the dual-permeability model may be more appropriate for the prediction of landslide-triggering when the pore water pressure response is influenced by preferential flow under high-intensity rainfall.

# 1

# INTRODUCTION

## 1.1. RESEARCH BACKGROUND

Landslide is a general term describing downslope movement of slope material that occurs on curved (rotational slide) or planar (translational slide) slip surfaces [Highland et al., 2008]. Landslide material is commonly categorized as rock, debris, and soil, and the types of displacement can be classified as fall, topple, slide, spread, and flow [Highland et al., 2008; Varnes, 1978]. Landslides are common geological processes in landform evolution and their occurrence may cause causalities and heavy economic loss [Dai et al., 2002]. A global dataset during a 7-year period from 2004 to 2010 showed that 2620 landslides caused a total of 32,322 recorded fatalities [Petley, 2012]. The landslide hazard has drawn more attention in recent years, and extensive studies have been conducted to improve process understanding and modeling as well as the assessment of landslide susceptibility which is important for land-use planning [Aleotti and Chowdhury, 1999; Dai et al., 2002; Westen et al., 2006].

In landslide-prone hillslopes, slope stability can be evaluated by the factor of safety, which is defined as the ratio of the maximum shear strength over the shear stress along the potential slip surface. The soil strength is affected by cohesion, friction forces, suction stress, and root strength [Ng and Pang, 2000; Lehmann and Or, 2012; Ghestem et al., 2011; Lu et al., 2010], and the shear stress is affected by gravitational driving forces and external loads. Various factors can induce landslides [Highland et al., 2008], including geological activities (e.g., earthquakes, volcanoes), weathering processes, vegetation dynamics (root growth and decomposition), human activities (e.g., excavation), and hydrological / meteorological events (excessive precipitation and snow-melt). In addition, slope stability can be gradually affected by long-term processes such as weathering and internal erosion of the hillslope [Hencher, 2010]. However, landslides are triggered by short-term processes or events, such as earthquakes, excavations, or precipitation [Bo-

gaard, 2001]. The challenge of landslide-prediction is how to represent the antecedent conditions and diagnose the common triggering mechanisms.

Rainfall-triggered landslides are strongly related to hydrological processes because soil mechanical properties are affected by soil moisture dynamics and pore water pressure changes in the subsurface flow system [Bogaard, 2001; Lu and Godt, 2013]. Precipitation is the most common landslide-triggering factor, as rainfall-infiltration can increase the weight and the pore water pressure of the soil , and decrease the strength of the slope material [Asch et al., 1999]. On the other hand, drainage, evaporation, and transpiration decrease the pore water pressure and enhance the soil strength. Consequently, the simulation of pore water pressure and water content is necessary to calculate the effective stress and soil strength for slope stability analysis .

To deterministically predict the timing and magnitude of rainfall-triggered landslides, a hydro-mechanical model can be developed by integrating theories from both subsurface hydrology and soil mechanics [Rahardjo et al., 2012; Griffiths and Lu, 2005]. At the catchment scale, conceptual hydrological models have been extensively used to represent the storage-discharge relationship [Kirchner, 2009], in which the storage is linked to landslide probability [Krzeminska et al., 2012]. At the hillslope scale, the Darcy-Richards equation or the Boussinesq equation are widely-used single-permeability models as part of hydro-mechanical models for combined seepage and slope stability analysis [e.g., Talebi et al.; Lu et al., 2012]. However, the influence of preferential flow on soil mechanics is not considered in most of the existing hydro-mechanical models, so that the prediction of the timing and magnitude of rainfall-triggered landslides might deviate from reality when preferential flow dominates the water transport and pressure propagation.

Preferential flow in heterogeneous soils affects hillslope hydrology and pressure propagation, which increases the complexity of transport phenomena and landslide-triggering mechanisms [Beven and Germann, 2013; Uchida et al., 2004; Hencher, 2010]. Preferential flow paths (e.g., cracks, macropores, fissures, pipes, etc.) in highly heterogeneous slopes can facilitate fast solute transport and pressure propagation when preferential flow bypasses the adjacent soil matrix and directly reaches the groundwater table [Beven and Germann, 2013; Nimmo, 2007]. In turn, tracer experiments provide convincing evidence of the existence of preferential flow in soil porous medium [Beven and Germann, 2013; Krzeminska et al., 2014]. Regarding the effect of preferential flow on slope stability, two different mechanisms have been recognized [Uchida et al., 2001; Hencher, 2010]. Highly permeable preferential flow paths can facilitate drainage and pressure dissipation, having a positive effect on slope stability [Krzeminska et al., 2012; Pierson, 1983]. On the contrary, during high-intensity rainfall, preferential flow can cause a more rapid and deeper water movement and pressure response, which has a negative effect on slope stability [Ghestem et al., 2011; Hencher, 2010; Hendrickx and Flury, 2001].

Quantification of the influence of preferential flow on landslide-triggering is still a challenge that needs to integrate state-of-the-art preferential flow models with slope stability analysis approaches [Uchida et al., 2004]. Many modeling approaches for representing preferential flow paths and simulating preferential flow have been proposed, such as the pore-network model, and the dual- or multi-continuum conceptualization of the soil porous medium. The dual-permeability model uses two coupled Darcy-Richard equations can simulates both matrix and preferential flow. This approach can represent non-equilibrium phenomena related to different water contents, specific discharges, and solute concentrations in the two domains, which has also been observed in the field [Köhne et al., 2009; Gerke and Köhne, 2004]. The dual-permeability model simulates two different pore water pressures, one in the preferential flow domain and one in the matrix domain, which brings up fundamental question which pore water pressure should be used to calculate the effective stress and soil strength at the slip surface. This might be the most important reason why very few studies have quantified the effects of preferential flow on soil mechanics even though the discussions of such effects are widespread. In conclusion, there is an urgent need to explore effective approaches to couple dual-permeability models with slope stability models.

## 1.2. RESEARCH QUESTIONS

The main objective of this thesis is to investigate the influence of preferential flow on hillslope hydrology and landslide-triggering by a numerical modeling approach that couples a dual-permeability model with a slope stability analysis.

The specific questions to be investigated are:

1. How can pore-scale water velocity distribution be derived from the soil hydraulic properties?

2. How can the pore water pressures of a dual-permeability model be coupled with a soil mechanical model to quantify the influence of preferential flow on subsurface hydrology, pore water pressure, and landslide-triggering?

3. Do single and dual permeability models predict different timing and magnitude of rainfall-triggered landslides? Can the difference be quantified? Which hydrometeorological and soil conditions require application of a dual-permeability model, and for which condition is a single-permeability model sufficient?

## 1.3. THESIS OUTLINE

This thesis is composed of 7 chapters. Chapter 1 is a general introduction, and Chapter 2 is a review of the theoretical background. First, the slope failure theory is introduced and the influence of pore water pressure on soil mechanics. Second, the influence of pref-

erential flow on hillslope hydrology, tracer transport, and slope stability is illustrated. Third, the modeling approach of preferential flow and slope stability analysis are summarized.

In Chapter 3, the theoretical relationships between the water retention curves, soil hydraulic function, pore water velocity distribution function, and breakthrough curves are presented. The pore water velocity distribution in soil porous medium is inferred from several soil hydraulic conductivity functions. The theoretical basis provided in this chapter can be used to quantify the first arrival time of contamination transport.

The influence of preferential flow on slope stability is quantified in Chapter 4 for a synthetic slope. A 2D numerical model is developed using COMSOL multi-physics modeling software, which couples a dual-permeability model with a linear-elastic model for combined hydrology and soil mechanics analysis. The slope stability condition is analysed by a local factor of safety approach, a stress-field based approach that uses the calculated effective stress to quantify the failure area and timing. The effect of preferential flow on slope stability is assessed through comparison of the failure area when subsurface flow is simulated with a dual-permeability model as compared to a single-permeability model.

In Chapter 5, a parsimonious 1D hydro-mechanical model is developed to investigate the influence of preferential flow on pore water pressure propagation. The model uses a modified dual-permeability model to calculate the vertical pressure propagation in a synthetic hillslope, and the slope stability is computed with an infinite-slope stability analysis approach. The proposed model was benchmarked with HYDRUS-1D by comparing the simulated results of two vertical infiltration problems in a dual-permeability soil. Finally, the model is applied to a synthetic case to simulate the pressure response and landslide-triggering under transient hydrological conditions.

In Chapter 6, the 1D hydro-mechanical model developed in Chapter 5 is applied to quantify the pressure propagation and landslide triggering in a clay-shales slope at the study site in northern Italy. Prior to this study, the linear-diffusion model was applied to simulate the observed pressure response in the study area; calibration of the linear diffusion model was difficult, because no effective approach was found to estimate or constrain the diffusion coefficient. In Chapter 6, the 1D hydro-mechanical model is applied to analyze the influence of preferential flow on pressure propagation in the study area. Simulated results are compared to field observations and the outcomes of the linear-diffusion model. The pros and cons of both approaches are discussed.

Finally, in Chapter 7 all scientific findings are summarized and recommendations are given for further research.

# 2

# REVIEW OF THEORIES AND MODELING APPROACHES FOR PREFERENTIAL FLOW AND SLOPE STABILITY

*In this chapter, a summary is given of existing theories and modeling approaches for preferential flow and slope stability. Slope stability can be affected by both long-term processes and short-term triggering factors. The pore water pressure increase under heavy rainfall or snow-melt is the most common trigger of landslides. Hydro-mechanical models can simulate the impact of hydrological processes on landslide-triggering. Most of the hydro-mechanical models conceptualize soil as single-continuum and neglect the impact of preferential flow. Preferential flow through macropores, fissures, or other local high-permeability zones has a significantly larger velocity than in matrix flow. Under heavy rainfall, the occurrence of preferential flow can affect pressure propagation and slope stability. Many preferential flow models have been developed based on a dual-continuum approach. The coupling between a dual-permeability model and a soil mechanical model can be a promising approach to quantify the impact of preferential flow on slope stability.*

## 2.1. THE ROLE OF WATER IN SLOPE STABILITY

In a hillslope, local failure can occur when the gravitational driving force (shear stress) is larger than the material strength. To assess the stability of a slope, the factor of safety is often used as the prime indicator, and is defined as the ratio between the shear strength and the gravity-induced shear stress along a potential failure surface [Bogaard, 2001; Lu and Godt, 2013; Baum et al., 2010]. In such an approach, the slope failure is expected to occur when the factor of safety is smaller than 1.0.

Under variably-saturated conditions, the dynamics of the pore water pressure is strongly coupled with soil mechanics and slope stability [Aleotti and Chowdhury, 1999; Ng and Shi, 1998]. Pore water pressure affects the soil stress according to Terzaghi's effective stress principle. The effective stress-field in a soil skeleton below the groundwater table is affected by positive pore water pressures. In the unsaturated zone, negative pore water pressures influence the tension forces and suction stresses.

The effective stress is a function of the pore water pressure and can be expressed as:

$$\sigma^{'} = \sigma - \chi p \tag{2.1}$$

where $\sigma^{'}$ is the effective stress, $\sigma$ is the total stress, $p$ is the pore water pressure, and $\chi$ is the matrix suction coefficient.

The soil strength can be described with the Mohr–Coulomb failure criterion linking soil strength with effective stress.

$$\tau = c^{'} + \sigma^{'} \tan\phi^{'} \tag{2.2}$$

where $\tau$ is the shear strength , $c^{'}$ is the cohesion, and $\phi^{'}$ is the angle of internal friction.

In a potentially unstable slope, the landslide material can be stabilized by shear strength determined by cohesion, frictional forces, and suction forces [Lu et al., 2010]. Consequently, the stability of a slope decreases by either decreased shear strength or increased gravitational driving force. These can work on different time-scales [Bogaard, 2001; Bogaard and Greco, 2016]. A list of factors influencing the slope stability at different time scales is shown in Table 2.1 (from Bogaard [2001]).

Examples of long-term processes causing instability are weathering and internal erosion [Hencher, 2010], while triggering factors such as earthquakes, excavations, or precipitation, can directly initiate slope failure [Krzeminska et al., 2012; Highland et al., 2008]. Slope stability can also be affected by vegetation through both root-reinforcement and transpiration-induced suction; root growth and decay can also affect soil hydraulic and mechanical properties [for review see Sidle and Bogaard, 2016]. Rainfall is one of the most common triggering factors of landslides. Precipitation-induced pore water pressure dynamics influences the frequency and timing of landslide occurrence [Guzzetti

Table 2.1: , Classification and examples of mechanisms of landslides-triggering (from Bogaard [2001])

| Classification of processes | | Short time scale | Long time scale |
|---|---|---|---|
| Shear strength decrease | Increase of pore water pressure | Instantaneous hydrological triggers<br>*Intense rainfall or snowmelt*<br>*Reservoir water level variations*<br>*Poor drainage* | Long-term hydrological factors<br>*Regional climate change*<br>*Land-use change* |
| | Decrease of material strength | Instantaneous strength variations<br>*Liquefaction of weak layer*<br>*Freezing and thawing*<br>*Shrink and swelling* | Long-term strength variations<br>*Weathering of slope material*<br>*Root growth and decay* |
| Shear stress increase | | Instantaneous gravitational factors<br>*Earthquake shaking*<br>*Anthropogenic disturbances of excavation, road building* | Long-term gravitational changes<br>*Erosion or accumulation* |

et al., 2007].

## 2.2. MODELING APPROACH FOR HYDRO-MECHANICAL MODELS

The timing and magnitude of landslides can be quantified by hydro-mechanical models that couple a slope stability analysis with subsurface hydrological modelling [Bogaard and Greco, 2016; Lu et al., 2012; Lehmann and Or, 2012]. Subsurface flow is usually regarded as laminar flow, the specific discharge and pressure head are simulated with the Darcy-Richards equation [Kampf and Burges, 2007] as:

$$\frac{\partial \theta(h)}{\partial t} = \nabla \left[ K(h) \left( \nabla h + \nabla z \right) \right] \tag{2.3}$$

where $\theta$ is the volumetric water content (-), $h$ is the pressure head (L), $t$ is time (T), $z$ is the vertical coordinate (positive upward), and $K$ is the isotropic hydraulic conductivity ($LT^{-1}$). Note that both $\theta$ and $K$ are function of $h$.

The subsurface hydrological processes may be integrated with slope stability analysis approaches to simulate the timing and magnitude of landslides. Two common approaches for slope stability analysis are the limit-equilibrium approach and the shear strength reduction approach [Griffiths and Lane, 1999; Lu et al., 2012]. The limit-equilibrium approach (Figure 2.1a) is based on stress-field methods, and the slope stability is evaluated by searching for the critical slip surface that has the lowest factor of safety [Lu and Godt, 2013]. The method of calculating the driving and resistance forces on a potential slip surface varies among the different limit-equilibrium approaches, such as the Morgenstern-Price, Bishop, Ordinary, Fellenius/Petterson, Janbu, etc. [Lu and Godt, 2013; Krahn, 2004]. The limit-equilibrium approach may be integrated with the 2D Darcy-Richards equation to predict water flow and the dynamic pore water pressure distribu-

tion [Mukhlisin et al., 2008; Wilkinson et al., 2002]. The gravitational driving force or stress field can be calculated by a force equilibrium approach (e.g., limit equilibrium approach), or a momentum balance equation combined with a stress-stain constitutive relationship [Lu et al., 2012; Griffiths and Lane, 1999].



The infinite slope stability approach (Figure 2.1b) is a 1D limit-equilibrium method that simplifies the failure plane of the landslide into a infinitely long, straight sliding surface [Baum et al., 2010; Simoni et al., 2008]. The approach gives reasonably accurate estimates of the factor of safety for a shallow landslides where the depth of failure surface is much smaller than its length [Lu and Godt, 2008; Iverson, 2000; Crosta and Frattini, 2003; Rosso et al., 2006; Griffiths et al., 2011]. A benchmark study showed that the factor of safety estimated with the infinite slope approach agrees well with those estimated by the shear-strength reduction approach (combined with the finite element method) for shallow landslides, in which the ratio of length (L) to height (H) (L/H) is larger than 16 [Griffiths and Lane, 1999]. Milledge et al. [2012] employed a Monte Carlo approach to conduct 5000 synthetic slope stability analyses covering a wide range of parameters, and the results showed that the difference between the estimated safety factors for these two approaches is less than 5% when L/H is larger than 25. The infinite slope stability approach may be coupled with hydrological models of various complexity and has been applied to predict the timing and location of rainfall-induced shallow landslides in mountainous areas [Baum et al., 2010; Krzeminska et al., 2013; Talebi et al.]. The infinite slope stability approach has been combined with a 1D infiltration model [e.g., Lehmann and Or, 2012], the linear diffusion equation [e.g., Iverson, 2000; D'Odorico et al., 2005], the Boussinesq equation [e.g., Talebi et al.], and the Darcy-Richards equation [e.g., Baum et al., 2010] for combined hillslope hydrology and slope stability analysis.

Deformation-field based methods (Figure 2.1c) simulate transient hydrological conditions using a finite element implementation of the Darcy-Richards equation coupled with a momentum balance equation using a predefined stress-stain constitutive relationship; the shear strength reduction method (FE-SRM) is commonly used to calculate the factor of safety. For a potentially unstable slope, the shear strength reduction approach proportionally reduces the effective cohesion and friction angle till the scenarios of large plastic deformation (i.e., obvious post-failure displacement) are captured. The factor of safety can be determined from the strength reduction factor. The main advantage of the shear-strength reduction method is that the factor of safety is estimated through the analysis of plastic deformation without introducing any prior assumptions of failure surface or an extra failure mechanism [Griffiths and Lane, 1999]. The location, shape, and magnitude of the plastic deformation area can be used to quantify the slip surface and factor of safety. Geotechnical engineering software and numerical models – such as FLAC [Itasca, 2002], PLAXIS [Brinkgreve et al., 2010] (based on the strength re-

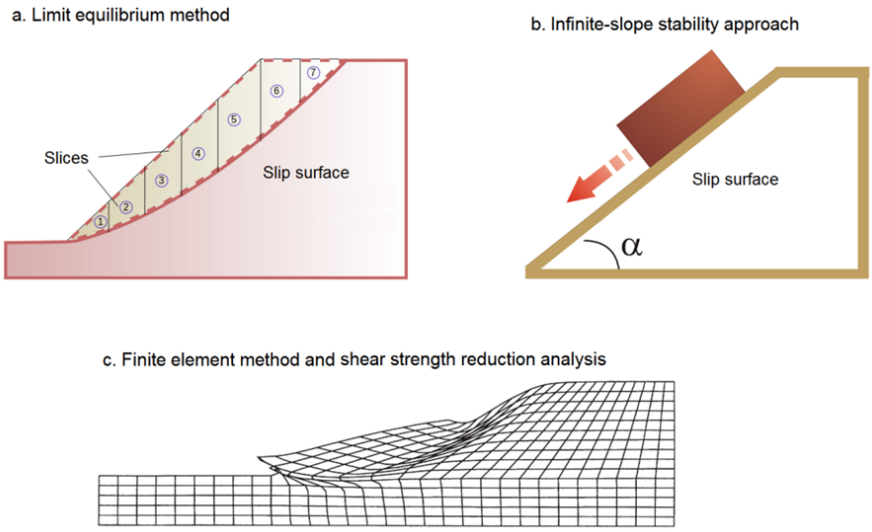


Figure 2.1: Different slope stability analysis approaches (Figure modified from Griffiths and Lane [1999])

duction method) – have been applied for slope stability analysis under the influence of transient hydrological conditions, such as rainstorms [Mukhlisin et al., 2008] or reservoir water level variations [Zhou et al., 2014].

## 2.3. PREFERENTIAL FLOW PATHS

Soil heterogeneity is ubiquitous at all scales in a subsurface hydrological system [McDonnell et al., 2007; Beven and Germann, 2013]. The microscopic-scale heterogeneity is caused by complex pore-size distributions, such as preferential flow networks, while macroscopic-scale heterogeneity is related to, e.g., soil layering, slope morphology, and ecological controls. Specifically, preferential flow paths usually have significantly larger pore-sizes and hydraulic conductivities than the surrounding soil matrix [Hencher, 2010; Jarvis, 2007], which can be generated by biological activity (e.g., root growth, earthworm digging), weathering (e.g., chemical weathering, root decomposition), and physical processes (e.g., internal erosion by pipe flow, shrinkage in expansive soil). Moreover, the preferential flow paths can be related to water repellency, air-entrapment, and heterogeneous distribution of soil hydraulic conductivity [van Schaik, 2010; DiCarlo, 2013; Steenhuis et al., 2013].

Preferential flow can be categorized into three types: macropore flow, fingered flow, and funneled flow, depending on their hydraulic characteristics (Figure 2.2) [Nimmo, 2007; Hendrickx and Flury, 2001]. Macropore flow usually occurs in high-permeable

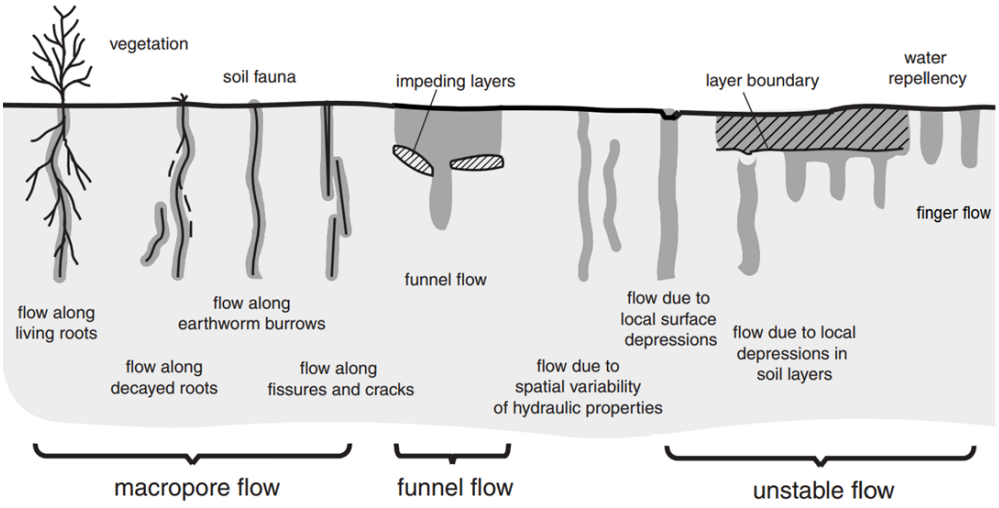


Figure 2.2: Different preferential flow mechanisms (Figure from Hendrickx and Flury [2001])

conduits like animal burrows, decayed and live roots, pipes, fissures, and fractures in soil and bedrock, in which film flow or turbulent flow might occur [Beven and Germann, 2013; Sidle et al., 2001; Greco, 2002]. Fingered flow may occur below an regular wetting front in a relative homogenous porous medium [van Schaik, 2010]. For example, the wetting front of gravity-driven infiltration in sandy soils is, to some extent, stable and laterally uniform, but may become and develop into finger-shape preferential flow paths [DiCarlo, 2013]. The occurrence of gravity-driven finger flow may be related to discontinues pore water pressure fields, and the irregular wetting front occurs when water stored in all pores cannot flow with the same velocity simultaneously [Steenhuis et al., 2013]. Finally, funneled flow is caused by large impeding structures such as clay lenses or large stones [van Schaik, 2010].

Even though individual macropores may not be continuous or connected directly to ponded water, they can affect lateral subsurface storm flow through self-organized preferential flow networks [Nieber and Sidle, 2010]. The self-organization of preferential flow paths can be caused by hydraulic connections between macropores, pipes, and other high-permeable soil zones [Sidle et al., 2001]. Interconnected macropore networks can consist of, e.g., earthworm burrows that are vertically continuous from the soil surface deep into the subsoil, existing decayed plant roots, and cracks and fissures between soil aggregation [Beven and Germann, 2013; Sidle et al., 2001]. The hydraulic connection between physically discontinues preferential flow paths can be achieved by either the water exchange between macropores and micropores [Nieber and Sidle, 2010], or pres-

sure propagation in saturated soils [McDonnell et al., 2007]. The hydraulic interaction is also related to antecedent wetness and topography [Blume and van Meerveld, 2015]. Preferential flow can dominate transport phenomena when the soil moisture or rainfall intensity is larger than a certain threshold [Nimmo, 2012; Uchida et al., 2001, 2004].



## 2.4. HYDROLOGICAL CONSEQUENCES OF PREFERENTIAL FLOW PATHS FOR WATER/SOLUTE TRANSPORT AND SOIL MECHANICS

Preferential flow through macropore, fissures, and other local high-permeability zones occurs within a small volumetric fraction of soil, which has a distinct larger flow velocity than that in the matrix flow [Jarvis, 2007; Hendrickx and Flury, 2001]. Consequently, preferential flow will affect not only the hillslope hydrology, but also the transport of solutes and the stability of the slope [Krzeminska et al., 2012; Uchida et al., 2001].

The most convincing evidence of preferential flow is obtained from a tracer experiment [Beven and Germann, 2013]. Preferential flow can affect tracer transport in terms of reducing travel time, increasing penetration depth, affecting solute concentrations in drainage flow, etc. [Jarvis, 2007]. Fast tracer transport accompanied by high-volume preferential flow can bypass the soil matrix and rapidly reach groundwater and river channels [Köhne et al., 2009; Christiansen et al., 2004]. Consequently, a solute breakthrough curve is often characterized by a bimodal behavior of an early-initial breakthrough and an extensive tailing [Brusseau and Rao, 1990].

At the hillslope and catchment scale, the analysis of the temporal behavior of environmental tracers such as stable water isotopes, silica or chloride in discharge time series has resulted in what has been called the “double paradox behavior” [Kirchner, 2003]. During a high-intensity rainstorm a large amount of “old” water residing in the subsurface is flushed into the stream, while meanwhile the labeled “new” water of the rainfall appears to appear in the stream immediately after infiltration through a fast flow path [Kirchner, 2003; Phillips, 2010]. Travel time distributions of tracer transport are related to the pore water velocity distribution in the numerous flow paths in subsurface hydrological systems. The study of the influence of preferential flow is essential to unravel the complex tracer transport behavior [McDonnell et al., 2007].

Preferential flow in self-organized macropores or pipes networks affects water transport in terms of vertical infiltration, lateral subsurface flow, and stream-flow generation in hillslope and headwater catchments [Sidle et al., 2001]. Hydraulic connections of preferential flow path can be formed during high-intensity or long-duration rainfall, resulting in subsurface stormflow that significantly contributes to peak flow [Beven and Germann, 2013; Nieber and Sidle, 2010; Sidle et al., 2001]. Under high-intensity storms, the

contribution of preferential flow to the peak flow can be upward of 90 % [Uchida et al., 2001].

For landslide-prone areas, landslide-triggering can be related to preferential flow, which increases fast pressure response in the subsurface following rainfall [Bogaard, 2001; Hencher, 2010; Krzeminska et al., 2012]. The internal erosion in macropores such as soil pipes can further decrease the cohesion and soil strength. Additionally, when flow reaches a closed-end pipe or macropore, the pressure build-up in certain preferential flow paths my result in a non-equilibrium pressure phenomenon, which can further influence timing and frequency of the landslide [Hencher, 2010; Uchida et al., 2004; Ghestem et al., 2011].

## 2.5. MODELING APPROACHES FOR PREFERENTIAL FLOW

In a single-permeability model, the Darcy-Richards equation may be used to calculate the average pore water velocity [Köhne et al., 2009]. The single-permeability model is based on a continuum modeling approach that conceptualizes discrete soil pores and water particles as a continuum in a representative element volume (REV). The soil hydraulic properties and the state variables (e.g., volumetric water content and capillary pressure) are lumped at the scale of an REV. Models based on a single-continuum conceptualization are not able to simulate preferential flow [Beven and Germann, 2013]. Many studies found that single-permeability models are not able to adequately simulate and predict water flow and tracer transport when preferential flow dominates the transport process [Jarvis, 2007]. Therefore, mechanisms and influences of preferential flow have been extensively studied [Beven and Germann, 1982; Hendrickx and Flury, 2001; Gerke, 2006].

Preferential flow influences the non-equilibrium solute transport process [Köhne et al., 2009]. The conventional single-permeability model that couple the Darcy-Richards equation and advection-diffusion equation cannot adequately describe non-equilibrium preferential flow and transport [Beven and Germann, 2013]. Increasingly sophisticated models have been developed to overcome this [Gerke, 2006; Šimůnek et al., 2003]. There are several main approaches of modeling preferential flow based on either the multi-continuum approach or the discontinuous modeling approach (Figure 2.3) [Köhne et al., 2009; Hendrickx and Flury, 2001]. The dual/multi-continuum approach conceptualizes the soil porous medium as two or more pore domains [Greco, 2002; Dusek et al., 2008; Wu et al., 2004]. The flow in each pore domain is described by individual continuum equations (e.g., Darcy-Richards equation, kinematic wave equation). In contrast, the discontinuous approaches explicitly simulates the flow in the preferential flow network [Nieber and Sidle, 2010; Chang et al., 2014; Moonen et al., 2008].

The mobile-immobile model (Figure 2.3 a) is a dual-continuum approach consisting

of two pore domains [Šimůnek et al., 2003]. The mobile domain represents the macropore system, in which the flow is described with the Darcy-Richards equation. The immobile domain represents the micropores with stagnant water. Water and solute is exchanged between two domains.

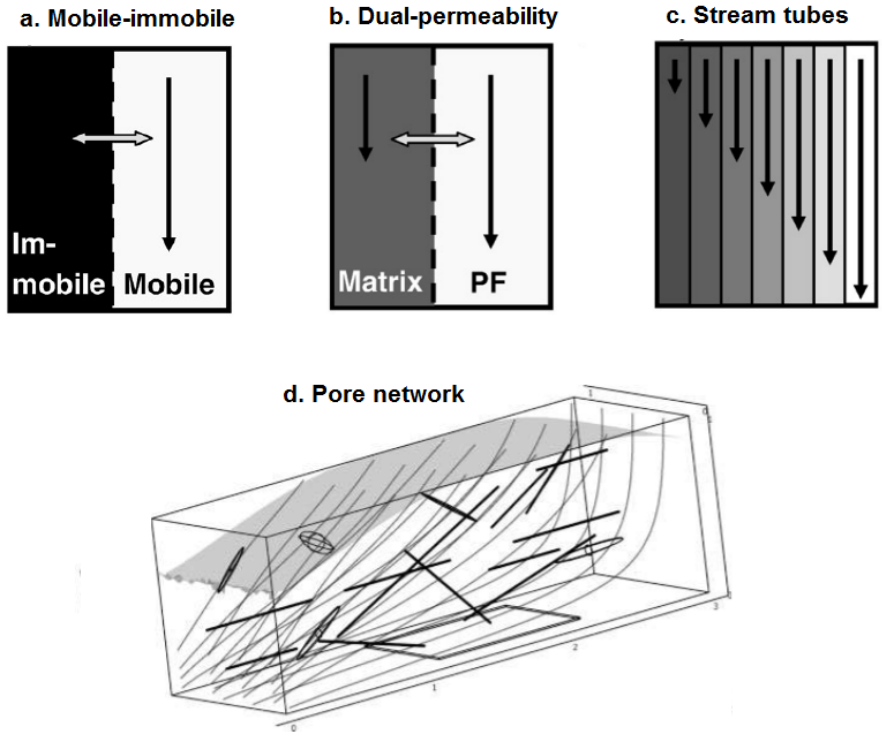


Figure 2.3: Typical preferential flow models (Figure modified from Köhne et al. [2009] and Nieber and Sidle [2010])

The dual-permeability model (Figure 2.3 b) is probably the most widely-used for the simulation of preferential flow. The dual-permeability model approximates a soil as two overlapping pore domains, the preferential flow domain with high permeability represents the preferential flow paths, such as macropores, fractures, cracks or any other large pores between the soil aggregate, while the matrix domain with relatively low permeability represents the micropore or soil matrix. Water and solute exchange may occur between the two domains [Gerke, 2006; Gerke and van Genuchten, 1993a]. Three types of dual-permeability models can be distinguished based on different underlying assumptions and equations [Köhne et al., 2009].

The first type of dual-permeability models is the capillary preferential flow model using two Darcy-Richards equations to simulate both preferential flow and matrix flow.

This approach has been adopted in HYDRUS [Šimůnek et al., 2008] and HydroGeoSphere [Therrien and Sudicky, 2005] software to simulate coupled water, solute, and heat transport. Extra parameters are needed to describe the soil hydraulic characteristics of the preferential flow domain. The solution of the coupled system of equations may be computationally intensive.

A second type of dual-permeability models is the gravity-driven preferential flow model. The water and solute transport in the matrix domain are based on the Darcy-Richards equation and advection-diffusion equation, while the preferential flow in the vertical direction is simulated by a kinematic wave equation that neglects the influence of capillary forces. For example, the one-dimensional gravity-driven preferential flow model MACRO uses a kinematic wave equation [Jarvis et al., 1991; Larsbo and Jarvis, 2003], that has been coupled with the 3D groundwater hydrology model MIKE SHE to simulate contamination transport at the catchment scale [Christiansen et al., 2004]. An another example is the modified DSFDM model [Mulungu et al., 2005], which simulates macropore flow and interflow in soil pipes in the top soil layer with the kinematic wave equation, which requires fewer parameters than the Darcy-Richards equation. It is difficult to simulate the positive pore water pressure build-up in macropore domains by the kinematic wave equation because its bottom boundary usually adopts a gravitational drainage condition.

A third type of dual-permeability models uses relatively-simple infiltration functions to describe preferential flow. For example, a Poiseuille's law can be used to calculate the macropore flow as in the CRACK-NP model [Armstrong et al., 2000]. The relatively simple preferential flow equation may be more suitable for hydrological modelling at the catchment-scale. The modified DSHVM model [Beckers and Alila, 2004] uses a Green-Ampt equation for the simulation of matrix flow, together with an instantaneous routing approach to calculate the contribution of threshold-triggered preferential flow on peak flow generation.

Figure 2.3c includes another type of model that conceptualizes the soil porous medium as many pore groups, in which water moves with distinct velocities. A piecewise linear approximation of the hydraulic conductivity can be used to identify the velocity in each pore group [Steenhuis et al., 1990]. This approach has been used to numerically simulate breakthrough curves to quantify solute transport in fully saturated soils [Steenhuis et al., 1990]. Such models have been extended to simulate infiltration and evaporation in the unsaturated zone [Ogden et al., 2015].

The discontinuous (or discrete) model (e.g., Figure 2.3d) directly simulates preferential flow in an explicit described fissure, pipe, or fracture networks [Köhne et al., 2009]. Several field studies [Hencher, 2010] and numerical experiments [Chang et al., 2014; Tsutsumi and Fujita, 2008] have focused on the investigation and simulation of pipe

flow (in soil) and fracture flow (in rock). Numerical simulations of flow in macropore networks require large amounts of geometry information [Nieber and Sidle, 2010] and large amounts of computational time, so that it is limited to small-scale studies with a limited number of pipes [Tsutsumi and Fujita, 2008] or cracks [Moonen et al., 2008].



Most of the current hydro-mechanical models for hillslope hydrology and slope stability are based on the continuum modeling approach as explicitly simulating preferential flow is difficult. Incorporating of a dual-permeability model in a hydro-mechanical model to quantify slope stability or slope deformation can be an option to simultaneously simulate the influence of both matrix and preferential flow on water transport and pressure propagation. However, a preferential flow approach results in two different pore water pressures for the two flow domains. The difficulty in estimating the pore water pressure in heterogeneous soils may be the most important reason why very few studies have focused on the quantification of the effect of preferential flow on soil mechanics. It is important to extend the current single-domain hydro-mechanical models to a dual-permeability conceptualization for slope stability assessment.

# 3

# THE CELERITY FUNCTION IN UNSATURATED SOILS

*A theoretical analysis is presented based on the pore bundle model to show that the celerity in unsaturated flow is equivalent to the maximum velocity. The celerity function can be used to derive a breakthrough curve to quantify the advective tracer transport. Breakthrough curves are computed for 5 typical soil textures using the the Brooks-Corey model, and both the unmodified and modified Mualem-van Genuchten models. It is shown that under near-saturated condition, celerity can be 5-100 times larger than the saturated hydraulic conductivity, and that a small volumetric fraction (< 15 %) of pores contributes more than 50% of the specific discharge. The first arrival time and the extensive tailing of the breakthrough curves are controlled by the maximum velocity and velocity distribution, respectively. The kinematic ratio of the Brooks-Corey model is constant for a specific soil and can be used to quantify the ratio of maximum tracer velocity over average tracer velocity. Furthermore, it is shown that a dual-permeability function with a bimodal soil hydraulic function may results in similar soil hydraulic conductivity functions for different parameter sets, but their celerity is different. Finally, the celerity function may be used to predict the first arrival time of a conservative tracer.*

## 3.1. INTRODUCTION

The terminologies of velocity and celerity have commonly been used to describe fluid dynamics of water in various hydrological systems, such as river channels [Lighthill and Whitham, 1955; Wong, 1996; Singh, 1996], estuaries [Savenije and Veling, 2005], and soils [Singh, 1997; Germann and Beven, 1985]. The celerity in subsurface flow represents the perturbation-induced pressure wave that is caused by precipitation, evaporation, and fluid injection and extraction [Rasmussen et al., 2000; Davies and Beven, 2012]. In saturated soils, the difference between velocity and celerity can be illustrated by a virtual experiment [McDonnell and Beven, 2014]:

"....in a cylinder full of sand and saturated with water, changing the flow rate or head at the input boundary will immediately cause a change in flow at the output boundary. While the water flow velocity through the sand is slow, the celerity in this case is (theoretically) instant, hence the immediate response. At larger scales, this case is analogous to a confined aquifer with incompressible water and rock. Allowing for the compressibility will slow the celerity a little, but the velocities of flow will still be much less than the celerities."

The celerity in confined saturated flow is nearly instant, caused by the low compressibility of the water and porous medium. In unsaturated soils, the pressure propagation has different mechanisms as determined by the variation of capillary pressure. In the unsaturated zone, the celerity is defined as the derivative of the specific discharge with respect to the water content [Singh, 2002; Rasmussen et al., 2000; Charbeneau, 1984]. More specifically, a fast response of the pore water pressure in unsaturated soils can be caused by either preferential flow [Nimmo, 2007] or pressure waves through entrapped air [Wang et al., 1997]. Therefore, identification of the cause-effect mechanism of the pressure response remains a challenge [Rasmussen et al., 2000].

The velocity in numerous flow paths is a function of the pore connectivity, tortuosity, and pore-size distribution [Nielsen et al., 1986; Bear, 1988]. For gravity-driven flow, integration of the velocities in all flow paths results in the soil hydraulic conductivity function [Peters et al., 2011]. Based on a pore bundle model, the hydraulic properties of each flow path are equivalent to that of a cylindrical tube [Mualem, 1976; Burdine et al., 1953; Childs and Collis-George, 1950]. Each tube conducts viscous flow. The relationship between the equivalent tube radius and the capillarity pressure and hydraulic conductivity can be described by a capillary rise equation (the Young-Laplace equation) and a pipe/cylinder liquid flow equation (the Hagen-Poiseuille equation), respectively. Many studies exist that use the pore bundle model to derive hydraulic conductivity functions by up-scaling the pore water velocities to the REV (representative elementary volume) scale [Mualem, 1976; Burdine et al., 1953; Childs and Collis-George, 1950]. The hydraulic conductivity functions integrated from pore velocity distributions can indirectly reflect the pore-scale hydraulic properties [Celia et al., 1995].

Mathematical derivations for the celerity and kinematic ratio were presented by Rasmussen et al. [2000]. Their work did not discuss the relation between tracer transport and pressure propagation. Wang et al. [2002] and Mohammadi et al. [2009] derive the tracer breakthrough curve directly from the soil hydraulic conductivity functions, which yields satisfying results when compared to their experiments. The work of Wang et al. [2002] and Mohammadi et al. [2009] was based on the soil hydraulic functions of either Brooks and Corey or the van Genuchten model for a single-permeability model.



The objective of this chapter is to illustrate the concept of celerity in unsaturated flow, derive new equations for the velocity distribution, and quantify the advective breakthrough curves. In Section 3.2.1, the definitions of the velocity and celerity are given for flow in the unsaturated zone. Based on a pore bundle model, the equivalence between celerity in the unsaturated soil and the maximum velocity among all flow paths is presented in Section 3.2.2. The celerity function is used to derive equations for breakthrough curves in Section 3.2.4. Functions for the celerity in dual-permeability models are derived in Section 3.2.5. Velocity distributions and breakthrough curves are analyzed for different soil textures in section 3.3, followed by a discussion and conclusions.

## 3.2. THEORY

### 3.2.1. DEFINITIONS

In the subsurface, the vertical component $q$ ($\mathrm{LT}^{-1}$) of the specific discharge vector (i.e. the volume flux of water per unit cross-sectional area, positive downward), can be formulated using Darcy's law as:

$$q = -K\frac{\partial}{\partial z}(h - z) \tag{3.1}$$

where $K$ ($\mathrm{LT}^{-1}$) is the hydraulic conductivity, $h$ (L) is the pressure head, and $z$ (L) is the vertical coordinate (positive downward). The average vertical velocity $\bar{v}$ ($\mathrm{LT}^{-1}$) is defined as:

$$\bar{v} = \frac{q}{\theta - \theta_r} \tag{3.2}$$

where $\theta$ (-) is the volumetric water content, and $\theta_r$ (-) is the residual water content.

The continuity equation for one-dimensional vertical flow is:

$$\frac{\partial \theta}{\partial t} + \frac{\partial q}{\partial z} = 0 \tag{3.3}$$

The derivative of the specific discharge $q$ with respect to $z$ may be written as:

$$\frac{\partial q}{\partial z} = \frac{\partial q}{\partial \theta}\frac{\partial \theta}{\partial z} \tag{3.4}$$

Substitution of Equation 3.4 for $\partial q/\partial z$ in Equation 3.3 results in the advection equation:

$$\frac{\partial \theta}{\partial t} + c\frac{\partial \theta}{\partial z} = 0 \tag{3.5}$$

where $c$ ($LT^{-1}$) is the celerity [Rasmussen et al., 2000]:

$$c = \frac{\partial q}{\partial \theta} \tag{3.6}$$



The advection equation theoretically represents the advection of the moisture content $\theta$ with a speed $c$. When $c$ is constant, this means that an arbitrarily shaped pulse of $\theta$ moves with constant speed $c$ without changing shape. The celerity $c$ is not a constant, however, but a function of the moisture content. Hence, the celerity is approximately equal to the advection of a small change in the moisture content.

The ratio between the celerity and the average velocity is called the kinematic ratio $\alpha_K$ (-), as defined by Rasmussen et al. [2000]:

$$\alpha_K = \frac{c}{\bar{v}} \tag{3.7}$$

### 3.2.2. CELERITY AND MAXIMUM VELOCITY

The pore bundle model approximates the soil as a bundle of nonintersecting, parallel, cylindrical tubes with varying radii [e.g. Wang et al., 2002; Mohammadi et al., 2009]. Each tube group represents the same fraction $\Delta\theta$ of the pore space and is either entirely filled with water or entirely empty. Pores are filled with water from the smallest tube group ($i = 1$) to the largest pore group ($i = N$). Under unsaturated condition, $M$ of the $N$ tube groups are filled with water. The pore water velocity $v_i$ ($LT^{-1}$) in tube group $i$ is related to the head gradient as:

$$v_i = -k_i \frac{\partial}{\partial z}(h - z) \tag{3.8}$$

where $k_i$ ($LT^{-1}$) is a coefficient relating the head gradient and the average velocity in tube group $i$.

The specific discharge $q$ ($LT^{-1}$) through the soil can be obtained from a summation:

$$q = \sum_{i=1}^{M} v_i \Delta\theta \tag{3.9}$$

where $M$ is the largest tube group filled with water. Substitution of Equation 3.8 for $v_i$ in Equation 3.9 gives:

$$q = \sum_{i=1}^{M} -k_i \frac{\partial}{\partial z}(h - z)\,\Delta\theta = -K\frac{\partial}{\partial z}(h - z) \tag{3.10}$$

where the hydraulic conductivity $K$ is defined as

$$K = \sum_{i=1}^{M} k_i \Delta\theta \tag{3.11}$$

The integral equivalent of Equation 3.9 is

$$q = \int_{\theta_r}^{\theta} v d\theta \tag{3.12}$$

while the integral equivalent of Equation 3.11 is

$$K = \int_{\theta_r}^{\theta} k d\theta \tag{3.13}$$

The celerity may be obtained with Equation 3.6 and 3.12 as

$$c(\theta) = \frac{\partial q}{\partial \theta} = v|_{\theta_r}^{\theta} = v(\theta) \tag{3.14}$$

where $v(\theta)$ is the velocity of the tube group with the largest diameter that is filled with water. Hence, the celerity is equal to the maximum velocity corresponding to a certain water content $\theta$.

### 3.2.3. DIFFERENT SOIL HYDRAULIC MODELS

The remainder of this chapter deals with a uniform vertical flow through the soil. A uniform flow is equivalent to the case that the pressure head $h$ is uniform everywhere and the specific discharge is equal to the hydraulic conductivity: $q = K$. This situation is also called the unit hydraulic gradient condition, as $\partial(h - z)/\partial z = -1$, because $h$ is constant.

Equations for the celerity and the kinematic ratio for the Brooks-Corey model and the modified Mualem-van Genuchten model [Vogel et al., 2000b; Schaap and Van Genuchten, 2006] are presented in Table 3.1. A similar table was presented by Rasmussen et al. [2000], but they included only the unmodified Mualem-van Genuchten model, which is obtained by setting the air entry pressure $h_s$ to zero, so that the parameter $\varepsilon$ equals one. The kinematic ratio and celerity in the unmodified Mualem-van Genuchten model approach an infinite value in near-saturated soil. The modified Mualem-van Genuchten model takes into account a non-zero air entry pressure.

The kinematic ratio for the Brooks-Corey model is a constant value of $\frac{2}{n_{\mathrm{BC}}} + 3$, which is equal to the power of the effective saturation $\Theta$ in the hydraulic conductivity function. The kinematic ratio of subsurface flow is also a constant value for other power functions that describe the unsaturated hydraulic conductivity [e.g., Mualem and Dagan, 1978; Campbell], and its value usually falls in a range between 2.5 and 24.5 [Mualem

Table 3.1: Constitutive relationships under the unit hydraulic gradient condition for the Brooks-Corey model and the modified Mualem -van Genuchten model

| Property | Definition | Brooks-Corey | Modified Mualem-van Genuchten |
|---|---|---|---|
| Water retention | $\Theta = \frac{\theta-\theta_r}{\theta_s-\theta_r}$ | $\Theta = \begin{cases} \lvert\alpha_{BC}h\rvert^{-n_{BC}}, & \alpha_{BC}h < -1 \\ 1, & \alpha_{BC}h > -1 \end{cases}$ | $\varepsilon\Theta = \begin{cases} \left[1+\lvert\alpha_{VG}h\rvert^{n_{VG}}\right]^{-m_{VG}}, & h < h_s \\ 1, & h \geq h_s \end{cases}$ |
| Specific capacity | $\frac{d\theta}{dh}$ | $\alpha_{BC}n_{BC}(\theta_s-\theta_r)\Theta^{1+1/n_{BC}}$ | $m_{VG}n_{VG}\alpha_{VG}(\theta_s-\theta_r)\Theta^{1/m_{VG}}\left(1-\Theta^{1/m_{VG}}\right)^{m_{VG}}$ |
| Specific discharge | $q = K$ | $K_s\Theta^{\frac{2}{n_{BC}}+3}$ | $K_s\Theta^{l_{VG}}\left[\frac{1-\left(1-(\varepsilon\Theta)^{1/m_{VG}}\right)^{m_{VG}}}{1-(1-\varepsilon^{1/m_{VG}})^{m_{VG}}}\right]^2$ |
| Celerity | $c = \frac{dK}{d\theta}$ | $\frac{a_K K_s}{\theta_s-\theta_r}\Theta^{\frac{2}{n_{BC}}+2}$ | $\frac{a_K K_s}{\theta_s-\theta_r}\Theta^{l_{VG}-1}\left[\frac{1-\left(1-(\varepsilon\Theta)^{1/m_{VG}}\right)^{m_{VG}}}{1-\left(1-\varepsilon^{1/m_{VG}}\right)^{m_{VG}}}\right]^2$ |
| Kinematic ratio | $\alpha_K = c/\bar{v}$ | $\frac{2}{n_{BC}}+3$ | $l_{VG}+\frac{2\left[1-(\varepsilon\Theta)^{1/m_{VG}}\right]^{m_{VG}-1}(\varepsilon\Theta)^{1/m_{VG}}}{1-\left[1-(\varepsilon\Theta)^{1/m_{VG}}\right]^{m_{VG}}}$ |

Notation: $\Theta = \frac{\theta-\theta_r}{\theta_s-\theta_r}$ is effective saturation, $\theta_s$ is saturated water content, $\alpha$ ($LT^{-1}$), $n$ (-), and $m$(-) are the fitting parameters for the Brooks-Corey model (subscript of "BC") and Mualem-van Genuchten model (subscript "VG" ). $\varepsilon = \frac{\theta_s-\theta_r}{\theta_m-\theta_r}$ , which is used as a correction factor to modify the van-Genuchten model with $\theta_m = \theta_r + (\theta_s-\theta_r)\left[1+\lvert\alpha_{VG}h_s\rvert^{n_{VG}}\right]^{m_{VG}}$. $h_s$ is the air entry pressure, which is zero when $\theta_m = \theta_s$ . $l_{VG}$ is pore connectivity parameter, and is usually assumed to be 0.5.

and Dagan, 1978]. The kinematic ratio for surface flow is much smaller. It is equal to 1.67, as derived from Manning's equation in a kinematic wave equation [Wong, 1996].

### 3.2.4. BREAKTHROUGH CURVES

Transport of a conservative tracer in a porous medium is governed by advection, dispersion, and molecular diffusion, among which advection and dispersion are a function of the velocity distribution. In this chapter, the breakthrough of a conservative tracer is derived from the velocity distribution using the pore bundle model following the work of Wang et al. [2002] and Mohammadi et al. [2009]. Flow is one-dimensional and uniform (unit hydraulic gradient condition), and the water content is constant and equal to $\theta_w$. $M$ of the $N$ tube groups are filled with water, so that the water content $\theta_w$ may be written as

$$\theta_w = \frac{M}{N}\theta_s \tag{3.15}$$

where $\theta_s$ is the water content at saturation.

Consider a vertical soil column with length $L$. At time $t = 0$, the concentration of the water entering at the top of the column is raised by $\Delta C$ from $C_0$ to $C_0 + \Delta C$. Water that starts in tube group $i$ remains in tube group $i$ from the top of the column to the bottom of the column. The travel time $t_i$ through tube group $i$ with velocity $v_i$ is

$$t_i = \frac{L}{v_i} \tag{3.16}$$

Hence, at time $t_i$, water in all tube groups $j > i$ have traveled from the top of the column

to the bottom of the column. The velocity-averaged concentration of water that flows out of the bottom of the column at time $t_i$ may be computed through summation as

$$C(t_i) = C_0 + \frac{\sum_{j=i}^{M} v_j \Delta\theta}{\sum_{j=1}^{M} v_j \Delta\theta} \Delta C \tag{3.17}$$

The integral equivalent of Equation (3.17) is

$$C(t_c) = C_0 + \frac{\int_{\theta_c}^{\theta_w} v d\theta}{\int_{\theta_r}^{\theta_w} v d\theta} \Delta C = C_0 + \frac{\int_{\theta_r}^{\theta_w} v d\theta - \int_{\theta_r}^{\theta_c} v d\theta}{\int_{\theta_r}^{\theta_w} v d\theta} \Delta C \tag{3.18}$$

where

$$t_c = \frac{L}{v_c} \tag{3.19}$$

where $v_c$ is the velocity corresponding to water content $\theta_c$, which is equal to the celerity (Equation 3.14)

$$v_c = c(\theta_c) \tag{3.20}$$

Under the unit hydraulic gradient condition, the integrals in Equation 3.18 are equal to the specific discharge Equation 3.12, which are equal to the hydraulic conductivity, so that Equation 3.18 becomes

$$C(t_c) = C_0 + \left[1 - \frac{K(\theta_c)}{K(\theta_w)}\right] \Delta C \tag{3.21}$$

The computation of the concentration at time $t_c$ requires the computation of $\theta_c$ from the implicit equation obtained by combining Equation 3.22 and equation for celerity $c(\theta)$ from Table 3.1.

$$t_c = \frac{L}{c(\theta_c)} \tag{3.22}$$

For the modified Mualem-van Genuchten model, the value of $\theta_c$ corresponding to $t_c$ needs to be obtained numerically in an iterative manner. For the Brooks-Corey model this can be done explicitly. Substitution of the celerity equation for the Brooks-Corey model in Table 3.1 into Equation 3.22 and rearrangement of terms gives

$$\Theta_c = \frac{\theta_c - \theta_r}{\theta_s - \theta_r} = \left[\frac{\theta_s - \theta_r}{\alpha_K K_s} \frac{L}{t_c}\right]^{\frac{n_{BC}}{2+2n_{BC}}} \tag{3.23}$$

If the initial tracer concentration is zero, the breakthrough curve for the Brooks-

Corey model can be written explicitly as:

$$\frac{C(t_c)}{\Delta C} = \begin{cases} 0\ ; & t_c \leq \frac{L}{c(\theta_w)} \\ 1 - \frac{K_s}{K_w}\left[\frac{\theta_s - \theta_r}{\alpha_K K_s}\frac{L}{t_c}\right]^{\frac{3n_{\mathrm{BC}}+2}{2n_{\mathrm{BC}}+2}} ; & t_c > \frac{L}{c(\theta_w)} \end{cases} \tag{3.24}$$

where $L/c(\theta_w)$ is the first arrival time of the tracer, and the tailing is determined by the pore water velocity distribution.



The breakthrough curve for the Brooks-Corey model may be written as a function of the kinematic ratio $\alpha_K$ as:

$$\frac{C(t^*)}{\Delta C} = \begin{cases} 0\ ; & t^* <= \frac{1}{\alpha_K} \\ 1 - \left[\frac{1}{\alpha_K t^*}\right]^{\frac{a_K}{a_K - 1}} ; & t^* > \frac{1}{\alpha_K} \end{cases} \tag{3.25}$$

where $t^*$ is a dimensionless time, defined as:

$$t^* = \frac{\bar{v}}{L} t_c = \frac{K_w}{L(\theta_w - \theta_r)} t_c \tag{3.26}$$

For the Brooks-Corey model, substitution of the hydraulic conductivity function (from Table 3.1) into Equation 3.26, the dimensionless time can be formulated as a function of either soil water content or specific discharge:

$$t^* = \frac{K_s \Theta^{a_K - 1}}{L(\theta_s - \theta_r)} t_c = \frac{K_s}{L(\theta_s - \theta_r)} \left(\frac{K_w}{K_s}\right)^{1 - \frac{1}{a_K}} t_c \tag{3.27}$$

The kinematic ratio is a constant in the Brooks-Corey model (see Table 3.1), which means that the breakthrough curve as a function of dimensionless time $t^*$ in variably-saturated soil is independent of the specific discharge or effective saturation for the Brooks-Corey model.

### 3.2.5. DUAL-PERMEABILITY MODEL

Consider a dual-permeability system, which consists of two overlapping continua each with their own water retention and hydraulic conductivity function representing a matrix domain and a preferential flow domain [e.g., Romano et al., 2011; Durner, 1994; Köhne et al., 2002]. The preferential flow domain consists of pores with relatively large size (often taken as larger than 0.3 mm [Jarvis, 2007] in equivalent tube diameter) and low tortuosity, such as worm burrows, root channels, tension cracks, and inter-aggregate pores [Beven and Germann, 1982; Hendrickx and Flury, 2001]. The remaining micropores are classified as the matrix domain. In this section, equations are derived for the

average pore water velocity and celerity for a dual-permeability model under unit hydraulic gradient conditions.

The volumetric ratios of the preferential flow domain and the matrix flow domain sum up to 1:

$$w_f + w_m = 1 \tag{3.28}$$

where the subscripts $f$ and $m$ denote the preferential flow and matrix flow domain, respectively. The total water content and specific discharge in a dual-permeability model are calculated as the weighted averages of the two domains

$$\theta = w_f \theta_f + w_m \theta_m \tag{3.29}$$

$$q = w_f q_f + w_m q_m \tag{3.30}$$

The average velocity in the preferential flow and matrix domains are (see Equation 3.2):

$$\bar{v}_f = \frac{q_f}{\theta_f - \theta_{rf}} \; ; \quad \bar{v}_m = \frac{q_m}{\theta_m - \theta_{rm}} \tag{3.31}$$

where the $\theta_{rm}$ and $\theta_{rf}$ are the residual water content of the matrix and preferential flow domains, respectively. The celerity of each domain is:

$$c_f = \frac{\partial q_f}{\partial \theta_f} \; ; \quad c_m = \frac{\partial q_m}{\partial \theta_m} \tag{3.32}$$

Finally, the celerity of the dual-continuum pore system, the maximum velocity in the system, can be expressed as the maximum velocity in the preferential and matrix flow domain:

$$c = \max(c_f, c_m) \tag{3.33}$$

## 3.3. ANALYSIS

### 3.3.1. COMPARISON OF DIFFERENT MODELS AND SOILS

In this section, the velocity and celerity are compared for different soils. Parameter sets of 5 typical soils are presented in Table 3.2 taken from the UNSODA database [Leij, 1996; Van Genuchten et al., 1991]. The air entry pressure values in the modified Mualem-van Genuchten model are adopted from the Brooks-Corey model for all 5 soils and listed in the last column of Table 3.2. The pressure head, specific discharge, average pore velocity, celerity, and kinematic ratio are computed as a function of the effective saturation under the unit hydraulic gradient condition for all 5 soils (Figure 3.1).

The water retention curves (the logarithmic pressure head vs. the effective saturation) have distinct curvatures attributed to the different pore size distributions. The

Table 3.2: Standard parameter sets of 5 typical soils in Brooks-Corey model and modified van-Genuchten model

| | Brooks-Corey | | | | | Modified van-Genuchten | | | | | |
|---|---|---|---|---|---|---|---|---|---|---|---|
| Soil types | $K_s$ | $\theta_r$ | $\theta_s$ | $\alpha_{BC}$ | $n_{BC}$ | $K_s$ | $\theta_r$ | $\theta_s$ | $\alpha_{VG}$ | $n_{VG}$ | $h_s$ |
| Sand | 504.0 | 0.020 | 0.417 | 0.138 | 0.592 | 712.8 | 0.045 | 0.43 | 0.145 | 2.68 | 7.2 |
| Sandy loam | 62.16 | 0.041 | 0.412 | 0.068 | 0.322 | 106.1 | 0.065 | 0.41 | 0.075 | 1.89 | 14.7 |
| Loam | 16.32 | 0.027 | 0.434 | 0.090 | 0.220 | 24.96 | 0.078 | 0.43 | 0.036 | 1.56 | 11.1 |
| Clay Loam | 5.22 | 0.075 | 0.390 | 0.039 | 0.194 | 6.24 | 0.095 | 0.41 | 0.019 | 1.31 | 25.6 |
| Silty Clay Loam | 3.60 | 0.040 | 0.432 | 0.031 | 0.151 | 1.68 | 0.089 | 0.43 | 0.010 | 1.23 | 32.2 |

Note: the units of $K_s$ and $\alpha$ are cm/day and $cm^{-1}$. $h_s$ (cm) is the air entry pressure value of the Brooks-Corey model and the modified Mualem

Table 3.3: Kinematic ratio under low saturation condition ($\Theta < 0.5$)

| Soil types | Sand | Sandy loam | Loam | Clay Loam | Silty clay loam |
|---|---|---|---|---|---|
| Brooks-Corey model | 6.378 | 9.211 | 12.091 | 13.309 | 16.245 |
| Van-Genuchten model | 3.691 | 4.747 | 6.071 | 8.952 | 11.196 |

curve is much flatter for coarser soils than finer soils, as expected. The Brooks-Corey model, unmodified and modified Mualem-van Genuchten models have slightly different slopes near saturation. When approaching full saturation the slopes of the water retention curves for the Mualem-van Genuchten model (with zero air entry pressure) approach infinity, while the slopes of the Brooks-Corey model and the modified Mualem-van Genuchten model (Figure 3.1a) are near 0. These differences are attributed to the inclusion of an air entry pressure head [Van Genuchten et al., 1991].

The celerity, average pore water velocity, and specific discharge increase as the effective saturation increases. The range of values differs. The specific discharge $K/K_s$ ranges from 0 to 1 as expected. The average pore water velocity $\bar{v}/K_s$ is between 0 and 3 (because $\theta_s - \theta_r$ is around 0.35, see Table 3.2). The celerity $c/K_s$ ranges from 0 to 70. The kinematic ratio also ranges from 0 to 30, except for the unmodified Mualem-van Genuchten model under near-saturated condition. All four dimensionless variables reach their maximum value when the soil is saturated. The celerity can be over 20 times larger than the average velocity when the soil approaches saturation.

The celerity curves show different patterns for different soil types. Near saturation, the value of $c/K_s$ can reach above 50 for fine textured soils, while it reaches around 20 for coarse textured soils. On the contrary, when the effective saturation drops below 0.8-0.9, $c/K_s$ values are much smaller.

The relative hydraulic conductivity is below 0.5 for $\Theta = 0.85$ for all soil types. The value is highest for sand ($K/K_s = 0.5$ ) and the lowest for clay ($K/K_s = 0.2$ ), which means that more than 50% of the specific discharge flows through only 15 % of the pore space when flow is at saturation.

The slope of the celerity vs. the average pore water velocity is used as an additional indicator of the kinematic ratios as shown in Figure 3.2. The kinematic ratios for the

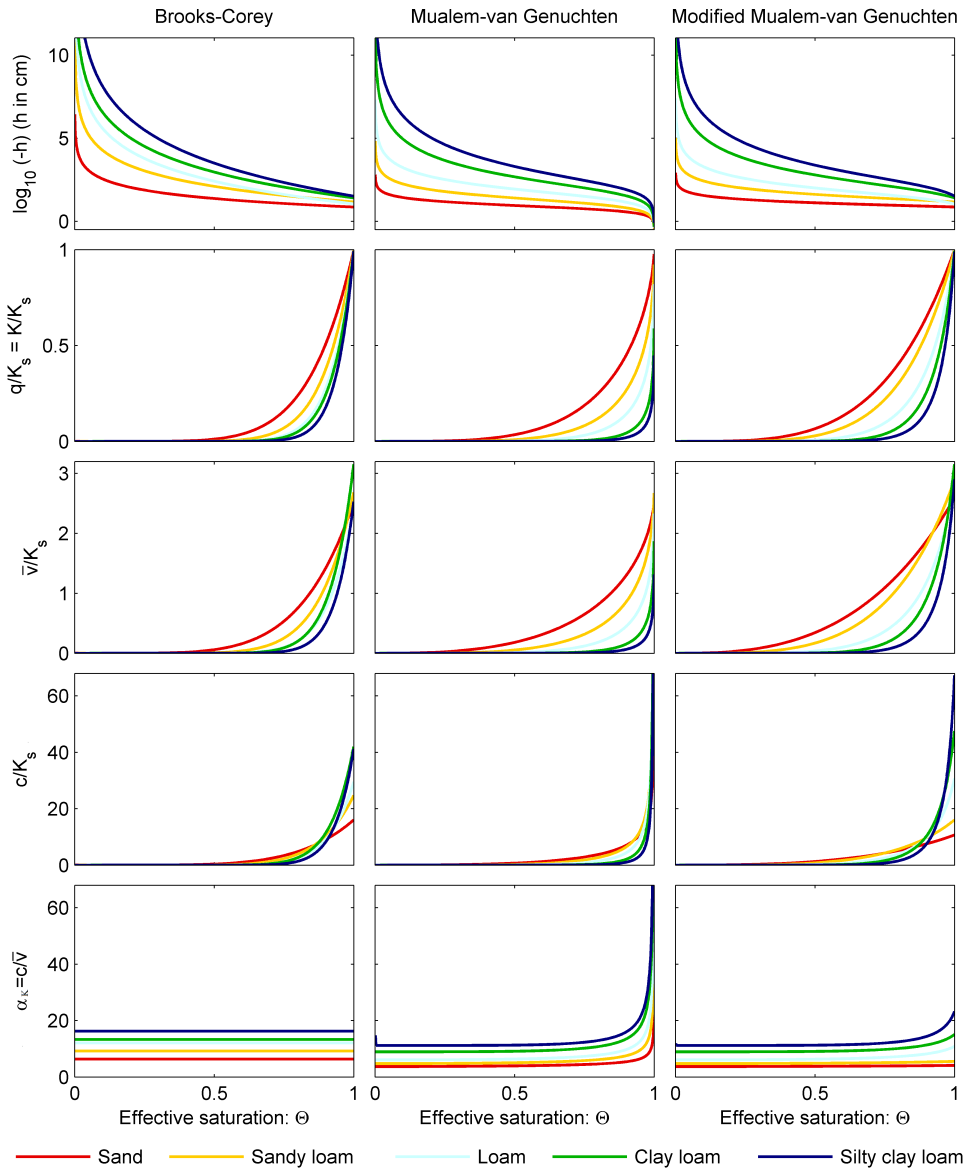


Figure 3.1: Pressure head, specific discharge, average velocity, celerity, and kinematic ratio as a function of effective saturation for 5 typical soils under unit hydraulic gradient conditions for three soil hydraulic models: Brook-Corey, Mualem-van Genuchten, and modified Mualem-van Genuchten model

Brooks-Corey model is independent of saturation for all the saturation range, while the kinematic ratio for the modified Mualem-van Genuchten function only weakly depends

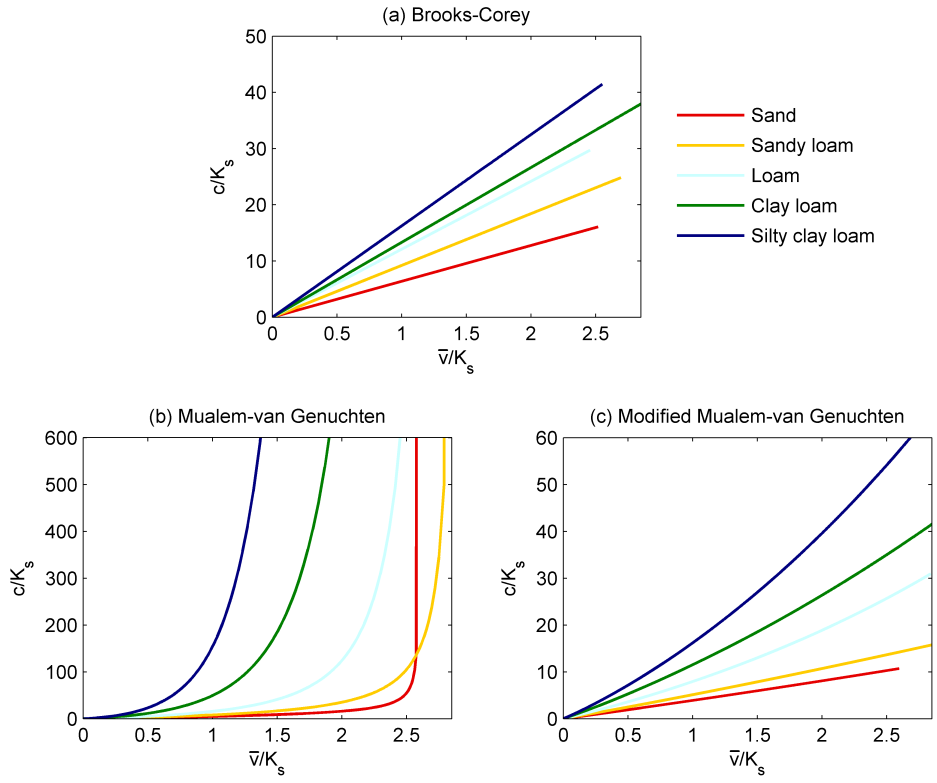


Figure 3.2: Relations between dimensionless celerity and dimensionless average pore water velocity for 5 typical soils under the Brook-Corey model, original and modified Mualem-van Genuchten model

on the saturation. Under low saturation range ($\Theta < 0.5$), the kinematic ratios of all three models are nearly constant (see Figure 3.1) with values listed in Table 3.3. Surprisingly, the kinematic ratios betweens the two models differ significantly for $\Theta < 0.5$ (Table 3.2). For the coarser soils considered (sand, sandy loam, loam) the celerity, and thus the maximum velocity, is almost twice as large in the Brooks-Corey model than in the Mualem-van Genuchten model. The kinematic ratios derived from the unmodified Mualem-van Genuchten model approach infinity near saturation, which is unrealistic.

### 3.3.2. BREAKTHROUGH CURVES

Breakthrough curves are generated for the five soils of Table 3.2 using the analysis presented in Section 3.2.4. All breakthrough curves in Figure 3.3 are for saturated conditions. Breakthrough curves are plotted for three soil hydraulic models, using an analytic approach for the Brooks-Corey model and a numerical approach for the unmodified and

modified van-Genuchten models. It is recalled that only advective transport is considered based on the pore bundle model, where water particles remain in the same pore group (and hence travel with the same velocity) for the entire length of the column. Outflow concentration is plotted vs. dimensionless time $t^*$ to eliminate the influence of different specific discharge values in various soils.

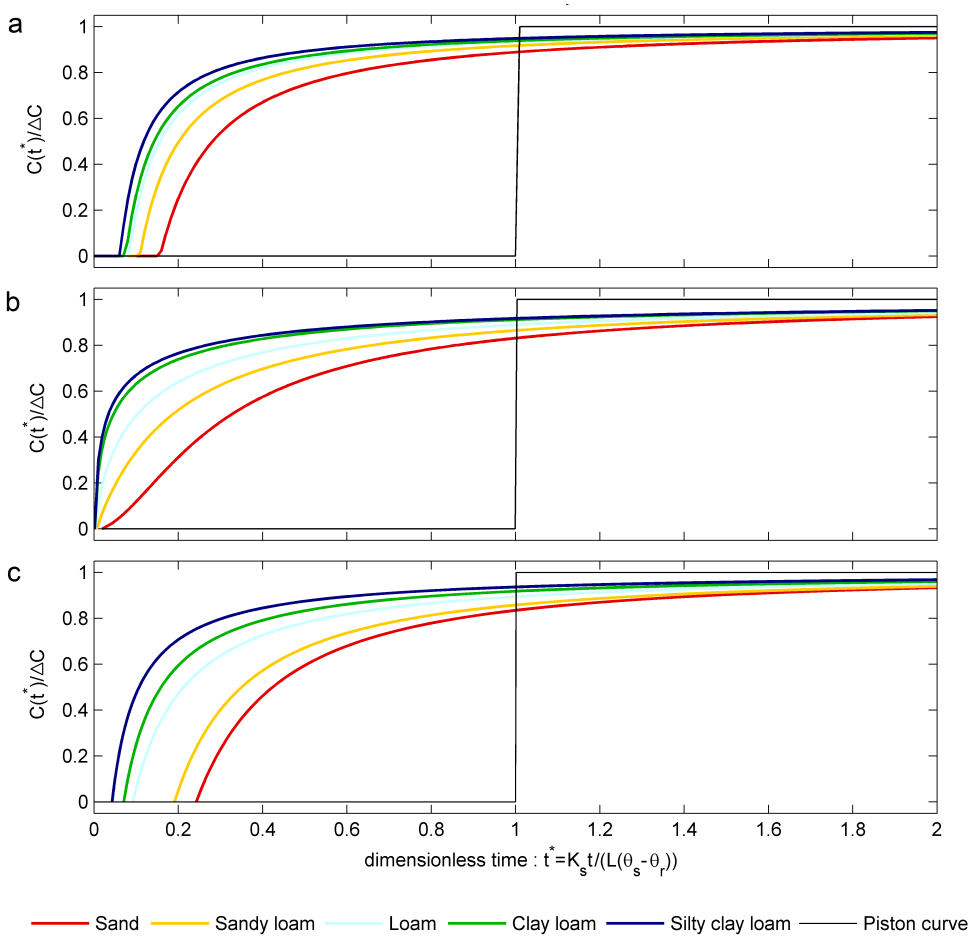


Figure 3.3: Breakthrough curves and the piston-shape breakthrough curves under the unit hydraulic gradient condition for 5 typical saturated soils in the Brook-Corey model, original and modified Mualem-van Genuchten.

The piston-shape breakthrough curves (black lines in Figure 3.3) are computed for tracer advection driven by flow with a uniform velocity distribution. The pore water velocity in all flow paths is equal to the average pore water velocity, and the kinematic ratio is equal to 1. The tracer concentration increases instantaneously from 0 to $\Delta C$ at

the dimensionless time $t^* = 1$.

The breakthrough curves of the different soil types consistently show an early first arrival time and long tailing. The dimensionless first arrival time can be determined as a reciprocal of the kinematic ratio. The kinematic ratio is lower in coarse-textured soil than in fine-textured soil, therefore the dimensionless first arrival time in fine-texture soil is earlier than in coarse-textured soil. The first arrival times computed with the Brooks-Corey and modified Mualem-van Genuchten models are significantly larger than computed with the original Mualem-van Genuchtem model for saturated conditions. The kinematic ratio under the original Mualem-van Genuchten model is an infinite value under saturated conditions, leading to a nearly-instant breakthrough of the tracer, which is unrealistic. At dimensionless time $t^* = 1$, the relative concentration is above 0.7 for all soil types and all soil hydraulic models. All breakthrough curves show very long tailing, caused by the low velocity in the smaller pore bundles.

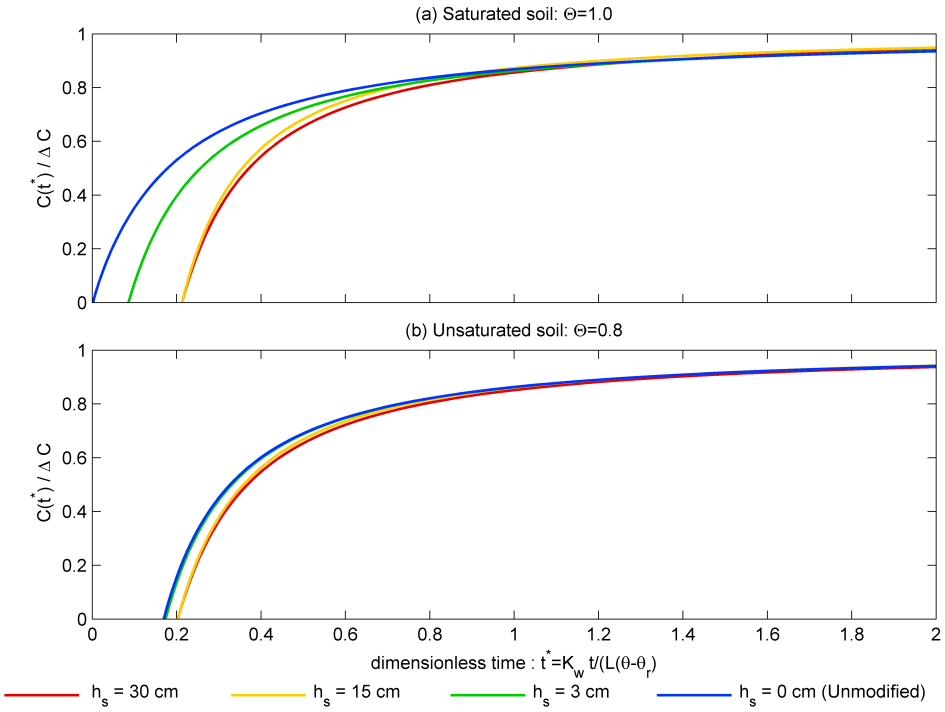


Figure 3.4: Effect of air entry pressure and effective saturation on breakthrough curves for sandy loam soil in unmodified and modified Mualem-van Genuchten.

In the Brooks-Corey model, the kinematic ratio is constant, and the breakthrough curves are independent of the effective saturation. In the modified Mualem-van Genuchten model, the shapes of the breakthrough curves are affected by the effective saturation

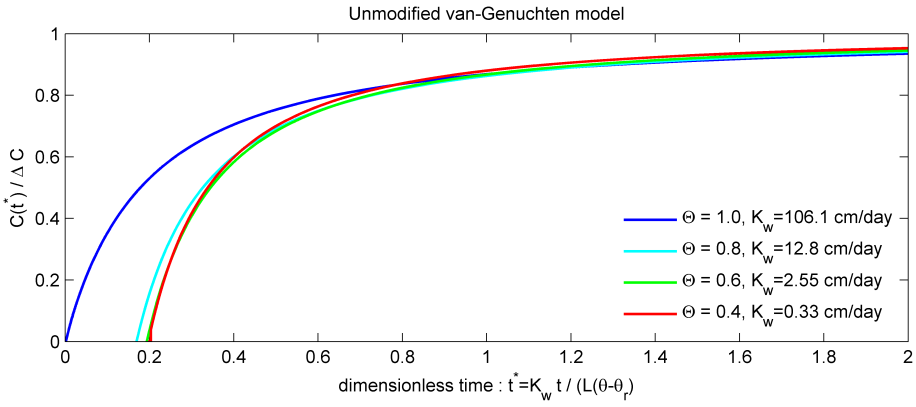


Figure 3.5: Effect of effective saturation on breakthrough curves for sandy loam soil for the unmodified Mualem-van Genuchten model.

and the value of the air entry pressure. The effect of the air entry pressure on the breakthrough curves for sandy loam soil under saturated and unsaturated ($\Theta = 0.8$) conditions is shown in Figure 3.4. Under saturated conditions (Figure 3.4a), the dimensionless first arrival time is zero for the unmodified Mualem-van Genuchten model ($h_s = 0$), and it approaches 0.2 when the air entry pressure is increased from 3 cm to 30 cm. In contrast, breakthrough curves do not depend significantly on the air entry pressure in unsaturated sandy loam (Figure 3.4b).

Breakthrough curves are shown for different effective saturation values for sandy loam for the unmodified Mualem-van Genuchten model in Figure 3.5. Except for the saturated case ($\Theta = 1.0$), the other three breakthrough curve are very similar.

### 3.3.3. DUAL-PERMEABILITY MODEL

In a dual-permeability model, the water content and hydraulic conductivity of the composite domain are bimodal functions of the pressure head [Durner, 1994]. Parameterization of bimodal soil hydraulic functions is difficult as the two conceptualized domains cannot be experimentally separated. Different parameter sets for dual-permeability models may produce almost the same water retention curves and soil hydraulic conductivity functions. This is sometimes referred to as equifinality. For example, Köhne et al. [2002] obtained 5 different parameter sets for dual-permeability model, which gave very similar fits of the data series of water retention and hydraulic conductivity. Two groups of parameters that produce almost the same composite water retention curves and hydraulic conductivity functions are selected in this analysis (Table 3.4), one with $w_f = 0.1$, and one with $w_f = 0.025$.

The water retention curve, hydraulic conductivity function, average pore velocity,

Table 3.4: Two parameter sets of the bimodal soil hydraulic function for a hypothetical soil that produce almost the same soil hydraulic functions

| | Matrix flow domain | | | | | Preferential flow domain | | | | |
|---|---|---|---|---|---|---|---|---|---|---|
| $w_f$ | $K_s$ | $\theta_r$ | $\theta_s$ | $\alpha_{VG}$ | $n_{VG}$ | $K_s$ | $\theta_r$ | $\theta_s$ | $\alpha_{VG}$ | $n_{VG}$ |
| 0.1 | 2.01 | 0.05 | 0.350 | 0.01 | 1.2 | 1000 | 0 | 0.6 | 0.1 | 2.5 |
| 0.025 | 1.9 | 0.0 | 0.36 | 0.01 | 1.2 | 3990 | 0 | 0.8 | 0.1 | 2.508 |

Note: the units of $K_s$ and $\alpha$ are m/day and $m^{-1}$, respectively.



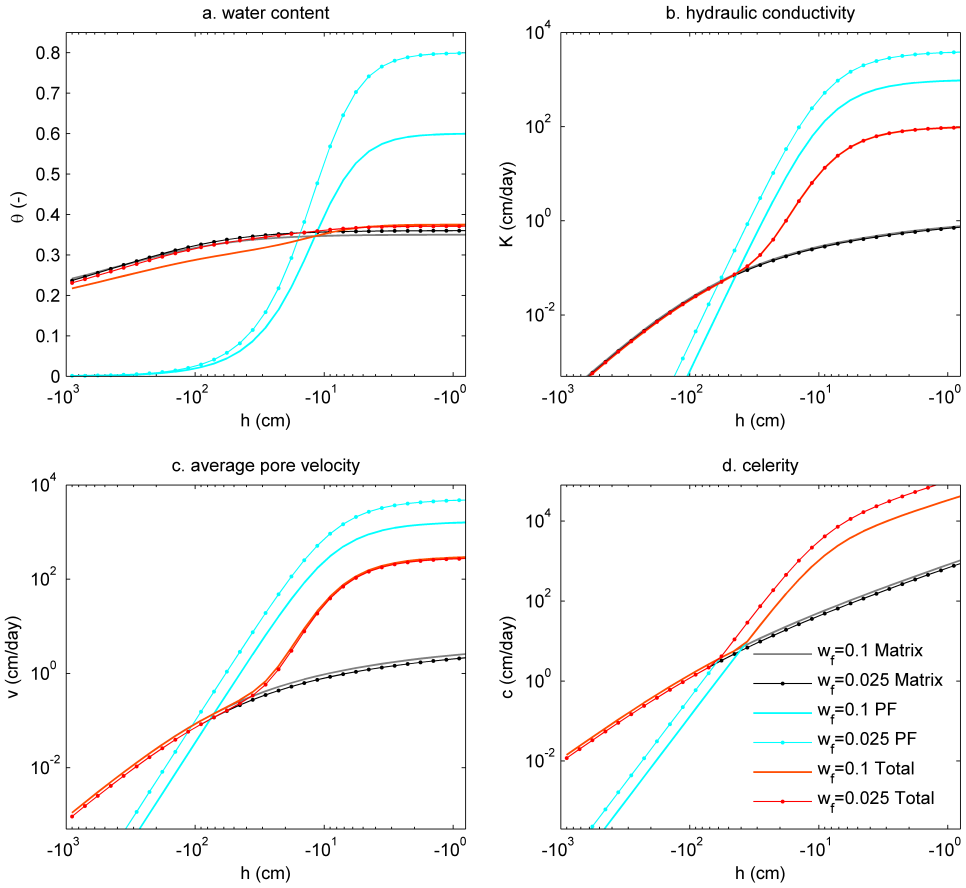


Figure 3.6: (a) water retention curve, (b) unsaturated hydraulic conductivity function, (c) average pore velocity, and (d) celerity function for matrix flow (Matrix), preferential flow (PF), and their total effect (total) for the two parameter sets of Table 3.4.

and celerity are shown for both parameter sets of Table 3.4 in Figure 3.6. The total water content vs. pressure head (shown as "Total" in Figure 3.6a) computed with the parameter sets agree well with each other. Moreover, the two parameter sets also result in nearly the same hydraulic conductivity and average pore water velocity of the total do-

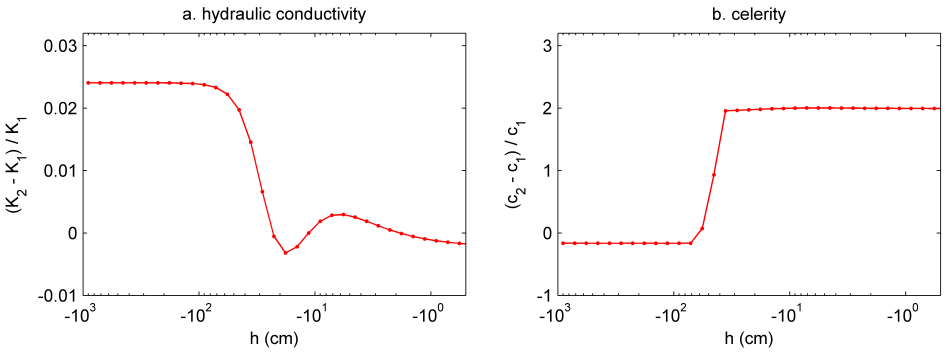


Figure 3.7: relative different of (a) unsaturated hydraulic conductivity, and (b) celerity of total soils under the the two parameter sets of Table 3.4.

main (see Figures 3.6b,c, the two red lines are indistinguishable). The higher hydraulic conductivity of the preferential flow domain of the second parameter set is compensated by a smaller volumetric fraction of $w_f$, which results in an equivalent amount of total hydraulic conductivity.

It is important to note that, the celerity of the two parameter sets differs significantly. The celerity $c(h)$ in the matrix domain is nearly the same for the two parameter sets. The celerity is controlled by the matrix flow when the pressure head is smaller than -35 cm. When the pressure head is larger than -35 cm, the celerity is controlled by the preferential flow with a much higher pore water velocity than the matrix flow.

The relative difference of the hydraulic conductivity and the celerity for the total domain is shown in Figure 3.7. For the two parameter sets, the relative difference of the hydraulic conductivity is less than 5% (Figure 3.7a). However, the celerity for the second parameter set ($w_f$=0.025) is approximately twice as large as with the first parameter set ($w$=0.1) (Figure 3.7b). This is an important results, as it can be decided which of the two parameter sets is the better one, if the celerity can be measured. The celerity can be measured with a tracer experiment by using a conservative tracer and measuring the first arrival time of the tracer.

## 3.4. PREDICTION OF THE MAXIMUM TRACER VELOCITY

Nimmo [2007] analyzed 64 field experiments and determined that the maximum tracer velocity varied within a small range, which could be predicted with by a simple model. The tracer experiments were conducted in various types of soil or bedrock with transport distances ranging from 0.3 to 1300 meter, and the maximum tracer velocity (with a 90% probability) ranged from 0.8 to 200 m/day. Nimmo [2007] proposed that the ratio of fastest tracer velocity $v_0$ over the effective precipitation rate $i_0$ (a spatially and temporarily averaged precipitation applied to the surface boundary) is essentially con-

stant. He determined that $v_0/i_0$ is approximately equaled to 18. The ratio, which has an order-of-magnitude accuracy, can be used to predict the fastest contaminant travel times. Nimmo [2007] suggested that the low variability of the ratio $v_0/i_0$ can be caused by a natural speed limit of the preferential flow in terms of the frictional forces and the water exchange between macropores and matrix.

The analysis of celerity in unsaturated soils, as presented in this chapter, can be compared to Nimmo's model. The ratio $v_0/i_0$ in Nimmo's paper has the same physical meaning as the ratio of $c/q$ that can be defined in this study. The value of $c/q$ is related to both kinematic ratio and soil water content as $c/q = c/(\bar{v}\theta) = \alpha_k/\theta$. The kinematic ratio of unsaturated flow based on the Brooks-Corey model is constant and ranges from 3 to 16 for the soils of Table 3.2. If assuming the soil moisture in natural system is within a range of 0.2-0.5 (effective saturation is within a range of 0.4-1.0), we can also derived the $c/q$ which is approximately ranging between 6 and 80. The geometric mean of $c/q$ is 23 based this rough estimation, which is close to the value of 18 from Nimmo's experimental finding.

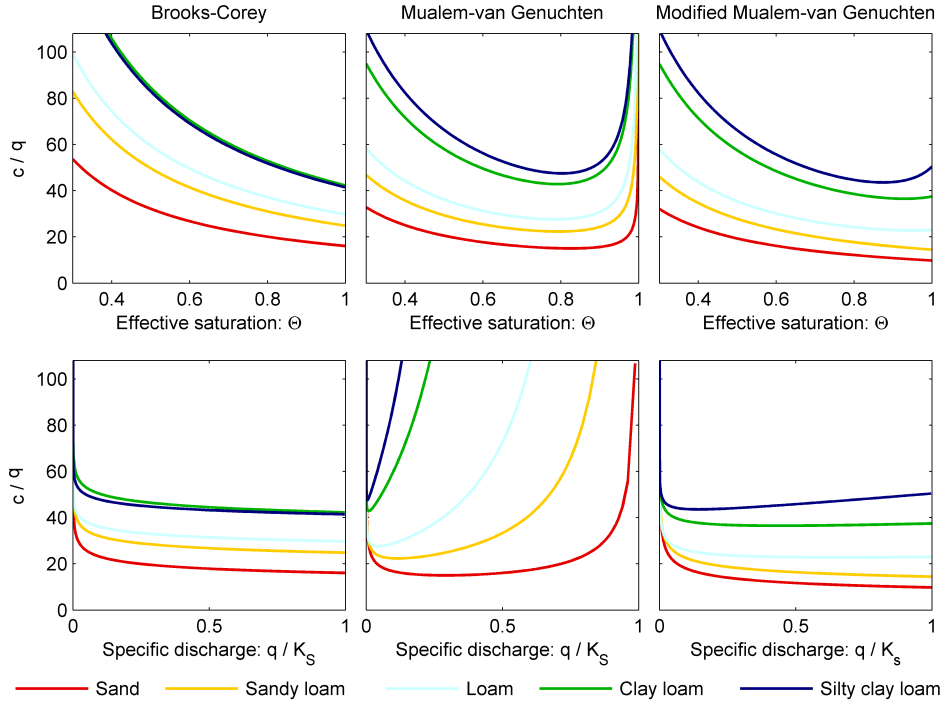


Figure 3.8: The relation between the ratio of $c/q$ with relative specific discharge $q/K_s$ and effective saturation $\Theta$

The ratio $c/q$ is computed for the 5 soils of Table 3.2. The ratio $c/q$ is plotted vs. the

effective saturation $\Theta$ in the first row of Figure 3.8. The value of $c/q$ decreases with $\Theta$ for the Brooks-Corey and the modified van Genuchten model. The value of $c/q$ approach infinity when the effective saturation decreases from 0.3 to 0, which is not shown here because the corresponding specific discharge is very small. Except for the unmodified van Genuchten model, the values of $c/q$ are fairly constant and only weakly depend on the specific discharge ($q/K_s$) as shown in the second row of Figure 3.8. The values roughly range from 10 to 50 for the Brooks-Corey and modified Mualem-van Genuchten models when the relative specific discharge $q/K_s$ is larger than 0.02. The geometric mean of $c/q$ is 22, which is consistent with the value of 18 from Nimmo's experimental finding.



## 3.5. CONCLUSIONS

In this study, a pore bundle model is applied to analyze the celerity in unsaturated soils. A mathematical derivation was presented showed that the celerity in unsaturated flow is the maximum velocity among all the water-filled flow paths, and the kinematic ratio is the ratio of the maximum velocity over the average velocity. The celerity function can be used to derive a breakthrough curve for advective tracer transport.

The soil hydraulic characteristics of five typical soil textures are analyzed by using the (modified) Mualem-van Genuchten and Brooks-Corey models with standard parameter sets. The results show that water in a small volumetric fraction (around 15%) of pores has a much higher velocity than the remaining pore volume. The first arrival time of a tracer is determined by the maximum pore water velocity, and the long tailing is caused by the flow in micropores with low velocities. The analysis of a bimodal soil hydraulic function shows that different parameter sets may results in similar water retention curves and soil hydraulic functions, but their celerity differs significantly. Finally, the ratio of celerity and specific discharge $c/q$ is fairly constant for specific soil texture, in accordance with published experiment findings.

# 4

# QUANTIFICATION OF THE INFLUENCE OF PREFERENTIAL FLOW ON SLOPE STABILITY USING A NUMERICAL MODELING APPROACH

*The effect of preferential flow on the stability of landslides is studied through numerical simulation of two types of rainfall events on a hypothetical hillslope. A model is developed that consists of two parts. The first part is a model for combined saturated/unsaturated subsurface flow and is used to compute the spatial and temporal water pressure response to rainfall. Preferential flow is simulated with a dual-permeability model consisting of a matrix domain coupled to a preferential flow domain. The second part is a soil mechanics model and is used to compute the spatial and temporal distribution of the local factor of safety based on the water pressure distribution computed with the subsurface flow model. Two types of rainfall events were considered: long-duration, low-intensity rainfall, and short-duration, high-intensity rainfall. The effect of preferential flow on slope stability is assessed through comparison of the failure area when subsurface flow is simulated with the dual-permeability model as compared to a single-permeability model (no preferential flow). For the low-intensity rainfall case, preferential flow has a positive effect on drainage of the hillslope resulting in a smaller failure area. For the high-intensity rainfall case, preferential flow has a negative effect on the slope stability as the majority of rainfall infiltrates into the preferential flow domain when rainfall intensity exceeds the infiltration capacity of the matrix domain, resulting in larger water pressure and a larger failure area.*

This chapter is based on:
Shao W, Bogaard T A, Bakker M, Greco R. Quantification of the influence of preferential flow on slope stability using a numerical modeling approach. Hydrology and Earth System Sciences, 2015, 19(5): 2197-2212, doi:10.5194/hess-19-2197-2015.

## 4.1. INTRODUCTION

Landslides are commonly triggered by rainfall events. Hydrological models may be integrated with slope stability analysis methods to calculate the factor of safety and predict the time and magnitude of landslides [Crosta and Frattini, 2008; Shuin et al., 2012; Aleotti and Chowdhury, 1999; Westen et al., 2006]. Combined hydro-mechanical models can roughly be divided into two types: simplified conceptual models [Montrasio and Valentino, 2008; Dai et al., 2002] and numerical models [Stead et al., 2001; Jing, 2003; Brinkgreve et al., 2010; Pastor et al., 2008; Konagai and Johansson, 2001], and have different levels of complexity depending on the scale and the research purpose.



The limit equilibrium method or infinite slope stability approach are frequently integrated with Richards' equation [Lanni et al., 2013; Ng and Shi, 1998; Godt et al., 2008; Shuin et al., 2012; Wilkinson et al., 2002; Talebi et al.; Greco et al., 2013] or the empirical infiltration model [Arnone et al., 2011; Simoni et al., 2008; Qiu et al., 2007] for landslide hazard evaluation. The limit equilibrium method and infinite slope approach assume or search for a potential failure surface. The factor of safety is defined as the ratio between the maximum retaining force and the driving force [Lanni et al., 2013; Lu et al., 2012]. Although the underlying assumptions of the slope failure mechanism have limitations [Huang and Jia, 2009; Griffiths et al., 2011], the simplified slope stability analysis method has low computational demand and is widely used for geotechnical analyses at the slope scale [Talebi et al.; Tsai and Yang, 2006; Abramson, 2002], watershed and catchment scale [Borga et al., 2002a; Baum et al., 2010; Wilkinson et al., 2002; Borga et al., 2002b].

The strength reduction method [Griffiths and Lu, 2005; Huang and Jia, 2009] or local factor of safety method [Lu et al., 2012] can result in similar factor of safety values and locations of the critical slip surface as the limit equilibrium method, while no assumption is needed about the critical failure surface [Griffiths and Lu, 2005; Hammouri et al., 2008; Kim et al., 1999]. The location, shape, and magnitude of the plastic deformation area are used to quantify the slip surface and factor of safety [Griffiths and Lane, 1999]. Geotechnical engineering software and numerical models – such as FLAC [Itasca, 2002], PLAXIS [Brinkgreve et al., 2010](based on the strength reduction method) – have been widely applied for slope stability analysis under the influence of transient hydrological conditions, such as rainstorms [Mukhlisin et al., 2008] and reservoir water level variations [Huang and Jia, 2009; Zhou et al., 2014]. The Darcy–Richards equation combined with pedotransfer functions is the most widely used approach in current software packages [Beven and Germann, 2013], but can not effectively simulate preferential flow resulting in rapid infiltration [Nieber and Sidle, 2010; Beven and Germann, 2013].

In highly heterogeneous slopes, preferential flow and transport can fundamentally influence subsurface flow [Jarvis, 2007; Hendrickx and Flury, 2001] and contaminant transport [Köhne et al., 2009; Allaire et al., 2009; Debieche et al., 2012; Zehe et al., 2001]. A chain of connected macropores is commonly found in various types of soils, includ-

ing forest soil and semiarid land [Uchida et al., 2001; Jarvis, 2007; Flury et al., 1994]. For example, an earthworm burrow can extend from the surface deep into the soil, as can decayed plant roots or soil cracks [Jarvis, 2007; Beven and Germann, 1982; Hendrickx and Flury, 2001]. The self-organizing preferential flow network will become active and hydraulically connected with an increase in soil saturation [Nieber and Sidle, 2010]. The saturated hydraulic conductivity of preferential flow paths is significantly larger than that of the soil matrix [Beven and Germann, 1982; Köhne et al., 2009]. A significant portion of subsurface stormflow [Uchida et al., 2004; Zhang et al., 2006; Beven, 1981] is transmitted via preferential flow paths [Nieber and Sidle, 2010]. Preferential flow through macropores, fractures, and other local high-permeability zones is extremely rapid, and contributes instantly to high pore-water pressures in deep soils [Jarvis, 2007].



Quantification of landslide triggering mechanisms is an essential step in landslide forecasting. Field studies have shown that preferential flow is one of the major mechanisms affecting the timing and location of landslides [Sharma and Nakagawa, 2010]. In forested hillslopes, minor preferential flow paths, such as soil pipes and macropores, are clearly associated with slope failure [Hencher, 2010; McDonnell, 1990; Uchida et al., 2001; Krzeminska et al., 2012; Debieche et al., 2012]. Besides the fact that internal erosion in preferential flow paths deteriorates the slope mass and reduces the soil shear strength, the occurrence of preferential flow can give rapid access to the deeper soil and groundwater system, reduce soil shear strength (due to pore pressure changes), and influence the timing and frequency of landslides [Köhne et al., 2009; Hendrickx and Flury, 2001].

Preferential flow and solute transport have been simulated at various scales including the scales of pores, soil columns, hillslopes, and catchments [Šimůnek et al., 2003; Gerke, 2006; Köhne et al., 2009] using increasingly sophisticated models such as the dual-porosity/dual-permeability model [Gerke and van Genuchten, 1993a; Jarvis et al., 1991; Larsbo and Jarvis, 2003], the multi-permeability model [Wu et al., 2004; Greco, 2002; Gwo et al., 1995], and the empirical model [Armstrong et al., 2000; Weiler, 2005; Vrugt et al., 2004; Mulungu et al., 2005]. The dual-permeability model is widely used because of its clear physical concept and powerful simulating ability [Roulier and Jarvis, 2003; Kodešová et al., 2005; Gerke and Köhne, 2004; Köhne et al., 2006; Christiansen et al., 2004; Weiler, 2005; Therrien and Sudicky, 2005; Vogel et al., 2000a]. The dual-permeability model assumes that the soil consists of two interacting, overlapping pore domains. The matrix domain with relatively low permeability represents the soil micropores where flow is governed by Richards' equation. The preferential flow domain represents the highly permeable preferential flow paths, such as macropores, fractures, cracks, or large pores between soil aggregate. Preferential flow is described by Richards' equation [Šimůnek et al., 2008; Gerke and van Genuchten, 1993a] or the gravity-driven kinematic wave equation [Larsbo and Jarvis, 2003; Jarvis et al., 1991; Greco, 2002]. The

water exchange between the two domains is driven by the pressure head difference between the two domains [Pirastru and Niedda, 2010; Gerke and van Genuchten, 1993b]. Dual-permeability models have proven to be effective for preferential flow simulation, but have not been incorporated into slope stability models.

The objective of this study is to quantify the temporal and the spatial effect of preferential flow on slope stability, and to analyze its underlying hydrological mechanisms using numerical experiments of rainfall-induced shallow landslides. This paper is organized as follows. First the subsurface dual-permeability hydrological model is described. The subsurface hydrological model is sequentially coupled with a soil mechanics model and a stress-field-based local factor of safety slope stability method (Section 4.2.2). The numerical experiments and parameterization are discussed in Section 4.3. The hydrological and geotechnical results are given in Section 4.4. The influence of preferential flow on subsurface hydrological processes and consequent slope stability is discussed in Section 4.5 by comparing the results of single and dual permeability models.



## 4.2. METHODS

### 4.2.1. SUBSURFACE FLOW MODEL

The single-permeability model is described by one Richards' equation to represent flow in a homogenous soil. The dual-permeability model divides the flow domain into two overlapping and interacting continua, where two coupled Richards' equations are used to describe the matrix flow and preferential flow [Gerke and van Genuchten, 1993a]:

$$\left[C_f + \Theta_f S_s\right] \frac{\partial h_f}{\partial t} = \nabla\left[K_f\left(\nabla h_f + \nabla z\right)\right] - \frac{\Gamma_w}{w_f} \tag{4.1}$$

$$\left[C_m + \Theta_m S_s\right] \frac{\partial h_m}{\partial t} = \nabla\left[K_m\left(\nabla h_m + \nabla z\right)\right] - \frac{\Gamma_w}{w_m} \tag{4.2}$$

where the subscript $f$ indicates the preferential flow domain and the subscript $m$ indicates the matrix domain. $C$ ($L^{-1}$)is the differential water capacity ($d\theta/\,dh$), $\Theta$ (–) is the effective saturation, $h$(L) is the pressure head, $t$ (T) is time, $z$ (L) is the vertical coordinate (positive upward), $K$ ($LT^{-1}$) is the isotropic hydraulic conductivity, $S_s$ ($L^{-1}$) is the specific storage, $w$ is the volumetric ratio of the preferential flow domain or the matrix domain over the total soil volume (–), and $\Gamma_w$ ($T^{-1}$) is the water exchange term between the two domains.

The Brooks–Corey function is used to describe the hydraulic properties of both the matrix andpreferential flow domains [Brooks and Corey, 1964]:

$$\Theta = \frac{\theta - \theta_r}{\theta_s - \theta_r} = \begin{cases} |\alpha_{BC} h|^{n_{BC}}, & \alpha_{BC} h < -1 \\ 1, & \alpha_{BC} h \geq -1 \end{cases} \tag{4.3}$$

$$K = K_s \Theta^{2/n_{\mathrm{BC}}+l_{\mathrm{BC}}+2} = K_s |\alpha_{\mathrm{BC}}|^{-2-n_{\mathrm{BC}}(l_{\mathrm{BC}}+2)} \tag{4.4}$$

$$C = -\frac{\mathrm{d}\theta}{\mathrm{d}|h|} = \begin{cases} \alpha_{\mathrm{BC}} n_{\mathrm{BC}} |\alpha_{\mathrm{BC}} h|^{-n_{\mathrm{BC}}}, & \alpha_{\mathrm{BC}} h < -1 \\ 0, & \alpha_{\mathrm{BC}} h \geq -1 \end{cases} \tag{4.5}$$

where $\theta$ ($\mathrm{L}^3\mathrm{L}^{-3}$) is the water content, subscripts $s$ and $r$ denote saturation and residual state, $K_s$ ($\mathrm{LT}^{-1}$) is the saturated hydraulic conductivity, and $\alpha_{\mathrm{BC}}$ ($\mathrm{L}^{-1}$), $l_{\mathrm{BC}}$ (-), $n_{\mathrm{BC}}$ (-), are fitting parameters.

The hydraulic interaction between the two domains can be calculated with a first order water exchange function[Ray et al., 1997]:

$$\Gamma_{\mathrm{w}} = \alpha_{\mathrm{w}} K_a \left(h_f - h_m\right) \tag{4.6}$$

where $\alpha_{\mathrm{w}}$ ($\mathrm{L}^{-2}$) is the effective water transfer coefficient, and the relative hydraulic conductivity $K_a$ ($\mathrm{LT}^{-1}$) is calculated by averaging the hydraulic conductivities of the two pore domains [Arora et al., 2011; Laine-Kaulio et al., 2014]:

$$K_a = \frac{K_f + K_m}{2} \tag{4.7}$$

The volumetric ratio of the preferential flow domain and matrix domain sum up to one:

$$w_f + w_m = 1 \tag{4.8}$$

The total water content of the soil is the weighted average of the water contents of the two domains:

$$\theta = w_f \theta_f + w_m \theta_m \tag{4.9}$$

The same holds for the total saturated hydraulic conductivity of the soil:

$$K_s = w_f K_{sf} + w_m K_{sm} \tag{4.10}$$

where $K_{\mathrm{sf}}$ and $K_{\mathrm{sm}}$ are saturated hydraulic conductivity of preferential flow domain and matrix domain, respectively.

Boundary conditions may be specified pressure head, specified flux, or mixed [Chui and Freyberg, 2009]. In the case of a dual-permeability model, specified flux $i$ (infiltration from rainfall) is divided between the matrix and preferential flow domains:

$$i = w_f i_f + w_m i_m \tag{4.11}$$

where $i_m$ and $i_f$ are boundary fluxes to the matrix and the preferential flow domains

($LT^{-1}$), respectively. The two domains have an equal opportunity to receive rainfall and are initially equal to rainfall intensity $R$ [Dusek et al., 2008]:

$$R = i = i_f = i_m \tag{4.12}$$

As the matrix domain has a larger volumetric ratio ($w_m > w_f$), the infiltration process is initially dominated by the matrix domain. Once the specified flux into the matrix is larger than its infiltration capacity, the boundary condition changes to specified pressure head and the specified flux for the preferential flow domain is increased to:

$$i_f = \frac{R - w_f i_m}{w_f} \tag{4.13}$$



Once the specified flux into the preferential flow domain is also larger than the infiltration capacity, the boundary conditions of both the matrix and the preferential flow domain are changed to a specified pressure head of zero and overland flow occurs.

### 4.2.2. SLOPE STABILITY ANALYSIS METHOD

The slope stability analysis is based on the local factor of safety approach [Lu et al., 2012]. The plane-strain linear elasticity model is used to calculate the stress [Abramson, 2002], which is governed by a momentum balance equation:

$$\nabla(\sigma) + \gamma \mathbf{b} = 0 \tag{4.14}$$

where $\sigma$ ($ML^{-1}T^{-2}$) is a stress tensor with three independent stress variables in two-dimensional space, $\gamma$ ($ML^{-2}T^{-2}$) is the bulk unit weight of the slope material, and **b** is the unit vector of body forces with two components. Neglecting the relative air pressure in Bishop's equation, the effective stress equation is:

$$\sigma' = \sigma - \chi p_{\mathrm{w}} \tag{4.15}$$

where $\sigma'$ is the effective stress, $p_{\mathrm{w}}$ ($ML^{-1}T^{-2}$) is the pore water pressure, and $\chi$ (-) is the matrix suction coefficient, which is usually approximated by the effective saturation [Lu et al., 2010].

The local factor of safety $F_{\mathrm{LFS}}$ (–) is defined as the "ratio of the Coulomb stress at the current state of stress to the Coulomb stress of the potential failure state under the Mohr-Coulomb criterion" [Lu et al., 2012]:

$$F_{\mathrm{LFS}} = \frac{\tau *}{\tau} \tag{4.16}$$

where $\tau^*$ is the limit Coulomb stress and $\tau$ is the actual shear stress ($ML^{-1}T^{-2}$).

Application of the Mohr-Coulomb failure criterion gives:

$$F_{\mathrm{LFS}} = \frac{2\cos\phi'}{\sigma'_1 - \sigma'_3}\left[c' + \frac{\sigma'_1 + \sigma'_3}{2}\tan\phi'\right] \tag{4.17}$$

where $c'$ is the effective cohesion ($\mathrm{ML^{-1}T^{-2}}$), $\phi'$(Deg) is the friction angle, $\sigma'_1$ and $\sigma'_3$ are the first and the third effective stress for the variably saturated soil ($\mathrm{ML^{-1}T^{-2}}$).

The influence of hydrology on slope stability is manifested in two ways. First, the unit weight function depends on the water content (Equation 4.9). Second, the effective stress depends on the pore water pressure. In the dual-permeability model, the pore water pressure of the preferential flow domain is used in the computation of the effective stress.

Figure 4.1 summarizes the structure of coupled dual-permeability and slope stability model. Two Richards' equations are coupled by the water exchange function. The hydrological results are sequentially coupled with a soil mechanics model without considering possible feedback of soil deformation on soil properties and the hydrological process.

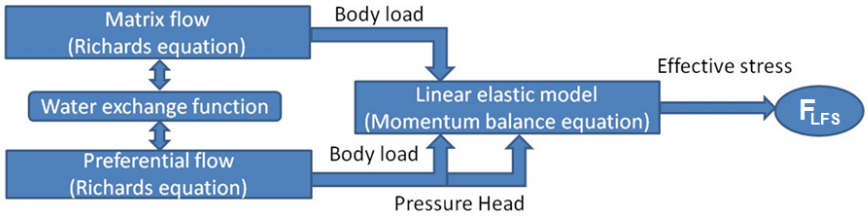


Figure 4.1: Structure of coupled dual-permeability model and soil mechanics model.

## 4.3. SETUP OF THE NUMERICAL EXPERIMENTS

### 4.3.1. SLOPE GEOMETRY

Consider a slope of 23 degrees consisting of fine-grained lithology such as clay shales with a more permeable weathered top soil layer [Bogaard, 2001; Berti and Simoni, 2012; Picarelli et al., 2006]; this is a typical slope that is vulnerable to failure. The slope is 6 meters high and 15 meters long and consists of two layers with a 2 meter thick homogeneous upper soil layer (see Figure 4.2).

The model domain is 42 m by 25 m to reduce the influence of boundary effects on hydrological and slope stability results. The computational mesh and the boundary conditions are shown in Figure 4.2. The boundary conditions of the subsurface flow model are atmospheric at the surface; the left-hand and bottom sides are no-flux boundaries. The right-hand side consists of a seepage boundary condition for the upper soil layer and

a specified pressure head to mimic a constant groundwater table for the lower layer. For the soil mechanics model, the surface is a free boundary, the bottom boundary (only horizontal displacements) and the left- and right-hand sides (only vertical displacements) are all roller boundaries.

Since the pressure head in the surface area can change drastically during rainfall, a very dense mesh was used near the surface to accurately model the transient hydrological conditions. The mesh density of the upper layer is approximately 0.25 m (vertical) by 0.5 m (horizontal). A coarser mesh was defined in the lower part of the slope as a less dynamic condition will occur here.



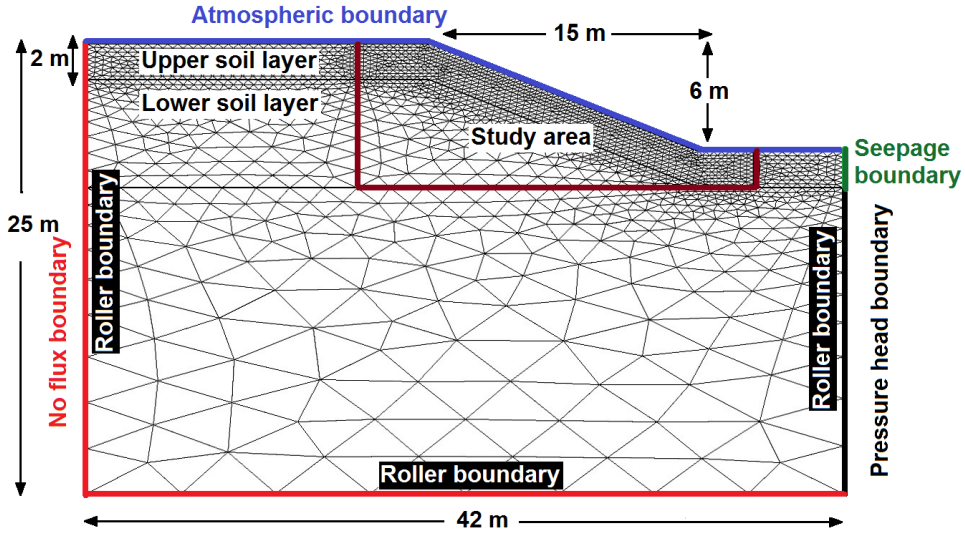


Figure 4.2: Structure of coupled dual-permeability model and soil mechanics model.

### 4.3.2. PARAMETERIZATION

The volumetric ratio of the preferential flow domain $w_f$ is 0.1; a typical range is 0.025 ~ 0.2 [Köhne et al., 2002]. The pore-size distribution of the preferential flow domain allows unsaturated infiltration before the matrix domain is saturated [Dusek et al., 2008]. A comparison is made between the hydrological results of the single-permeability and the dual-permeability models. The total weighted saturated hydraulic conductivity of the dual-permeability model is equal to the saturated hydraulic conductivity of the single-permeability model. The water exchange between the matrix and preferential flow domains depends on the hydraulic conductivity between the two domains $K_a$ and the water exchange coefficient $\alpha_w$ (Equation 4.6). Equilibrium between the preferential flow

and matrix domains is reached quicker for smaller values (closer to 1) of $K_{sf}/K_{sm}$ and larger values of $\alpha_w$. Moderate values are used for $K_{sf}/K_{sm}$ (100 in the upper layer and 5 in the lower layer) and for $\alpha_w$ (0.2 $m^{-2}$).

Table 4.1: Summary of parameters

| Symbol | Parameter name | Units | Upper layer (sandy loam) | Lower layer (clay) |
|---|---|---|---|---|
| $\theta_s$ | Saturated water content | (−) | 0.412 | 0.385 |
| $\theta_r$ | Residual water content | (−) | 0.041 | 0.09 |
| $K_s$ | Saturated hydraulic conductivity | (cm/h) | 2.59 | 0.06 |
| $K_{sf}$ | $K_s$ of preferential flow domain | (cm/h) | 23.76 | 0.214 |
| $K_{sm}$ | $K_s$ of matrix domain | (cm/h) | 0.2376 | 0.043 |
| $\alpha_w$ | Water exchange coefficient | ($m^{-2}$) | 0.2 | 0.2 |
| $\alpha_{BC}$ | Brooks-Corey fitting parameter | ($cm^{-1}$) | 0.068 | 0.027 |
| $n_{BC}$ | Brooks-Corey fitting parameter | (−) | 0.322 | 0.131 |
| $l_{BC}$ | Brooks-Corey fitting parameter | (−) | 1 | 1 |
| $\gamma_{dry}$ | Dry unit weight | ($kN/m^3$) | 15.5 | 15.5 |
| $E$ | Young's modulus | (MPa) | 10 | 10 |
| $\nu$ | Poisson's ratio | (−) | 0.35 | 0.35 |
| $\phi'$ | Friction angle | (deg) | 35 | 35 |

The soil hydraulic parameters are presented in Table 4.1. Preferential flow plays an important role in the upper soil layer where there is an abundance of macropores, but less so in the lower soil layer where macropores are almost non-existent [Bogner et al., 2013]. In other words, the volumetric percentage of preferential flow domain is still the same, but in the lower layer the saturated hydraulic conductivity of macropores are more similar to the pores of the matrix. The more permeable top layer is sandy loam and the fine-grained lower layer is clay; the soil hydraulic parameters are taken from the UNSODA database [Nemes et al., 2001; Leij, 1996].

Current laboratory practice for soil hydraulic testing cannot measure the parameters for two hydraulic functions and two water retention curves for one soil sample [Arora et al., 2011; Köhne et al., 2009]. There are two approaches to parameterize a dual-permeability model. The first approach determines the parameters from an infiltration experiment and inverse modeling, which results in a non-unique parameter set [Dusek et al., 2008; Köhne et al., 2002; Arora et al., 2011]. The second approach, which is adopted for this study, uses the same hydraulic parameters for both domains, except for the saturated hydraulic conductivities [Vogel et al., 2000a].

The parameters of the soil mechanics model are also shown in Table 4.1. In numerical modeling, effective cohesion $c'$ is scale dependent, and is usually defined as a linear function of the slope height to obtain identical values of the safety factor when applying it to different slope sizes [Griffiths and Lane, 1999; Lu et al., 2012]. In this study, two sets of cohesion values were selected; a homogeneous case where the effective cohesion of both layers is 5 kPa and a case where the effective cohesion of the upper layer is smaller

($c'_1$ = 3 kPa) than the lower layer ($c'_2$ = 6 kPa).

Two rainfall events are modeled: a low-intensity rainfall of 2 mm/h for 150 hours and a high-intensity rainfall of 20 mm/h for 15 hours. The initial condition is the steady pore water pressure distribution obtained from running the model with a daily rainfall of 1.64 mm/day (600 mm/year) for 10 years.

## 4.4. RESULTS

### 4.4.1. SUBSURFACE FLOW

A schematic diagram of the subsurface flow components in the study area is shown in Figure 4.3. Note that the study area is a small part of the model domain (Figure 4.2). The main fluxes are the infiltration from rainfall (blue), the inflow/outflow along the left side and bottom (black), the seepage outflow along the surface (red) and the outflow along the right boundary (green).

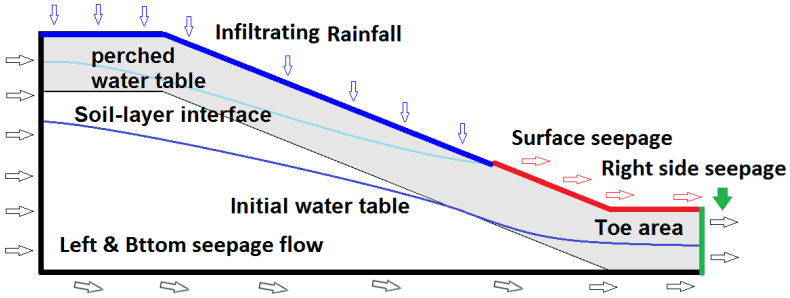


Figure 4.3: Flow component and water balance of study area

Hydrological results for the single- and dual-permeability models are shown in Figures 4.4 and 4.5, respectively. The graphs on the left are results for the long-duration, low-intensity rainfall case while the graphs on the right are results for the short-duration, high-intensity rainfall. Integrated fluxes, as shown in Figure 4.3, are reported in $m^2/h$.

For both models, all the rainfall infiltrates into the slope during the beginning of the rain event and infiltration decreases when rainfall exceeds infiltration capacity and part of the rainfall turns into overland flow. For the single-permeability model and low-intensity rainfall overland flow starts after 95 h (or 190 mm of rainfall) while for the high intensity rainfall overland flow starts after 8.5 h (or 170 mm of rainfall) (Figures 4.4a and b). In the dual-permeability model (Figure 4.5), the rainfall infiltration is divided over the two domains and additional rainfall infiltrates into the preferential flow domain when the matrix domain reaches infiltration capacity. Recall that the matrix domains is 90% of the domain, and the preferential flow domain is 10% of the domain. A smaller fraction of rainfall infiltrates into the preferential flow domain for the case of low-

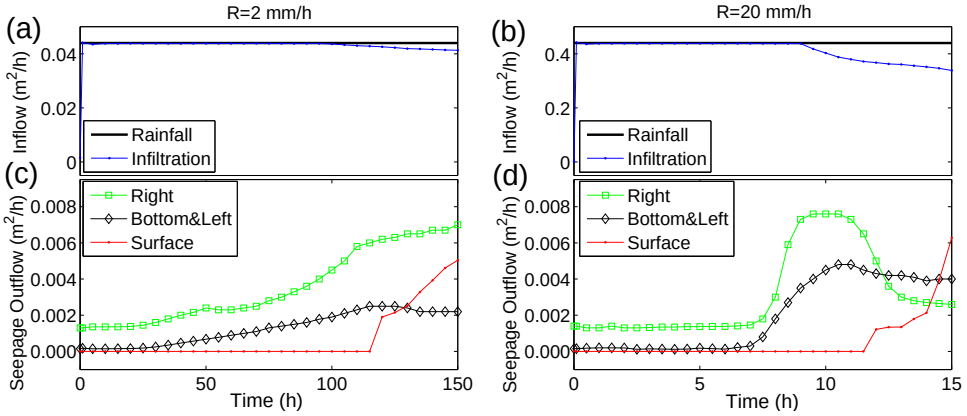


Figure 4.4: Integrated fluxes for single-permeability model and 2 mm/h (left) and 20 mm/h (right) rainfall. Rainfall and infiltration (a and b), and outflow at the right, outflow at the left and bottom, and outflow at the surface (c and d).

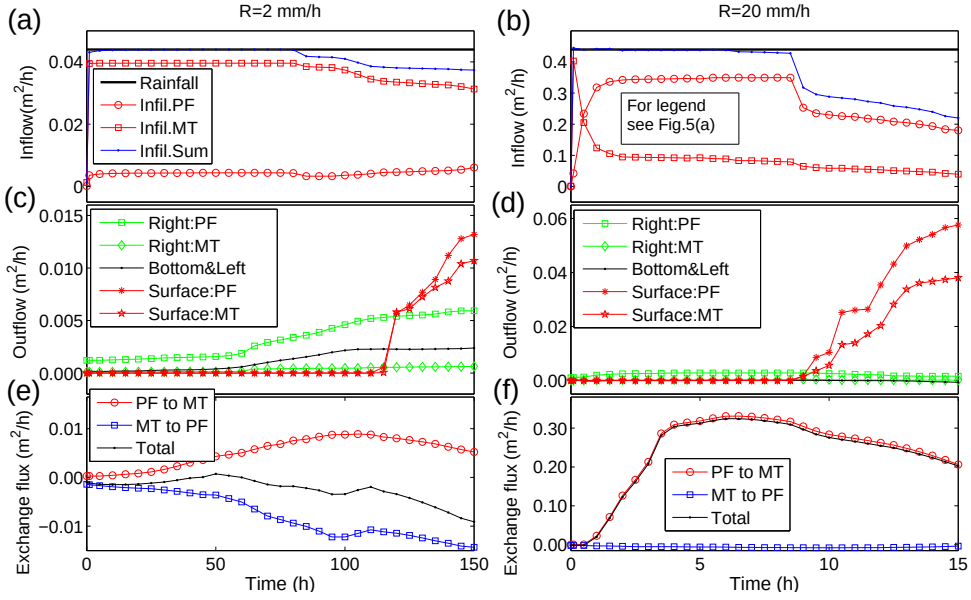


Figure 4.5: Integrated fluxes for dual-permeability model and 2 mm/h (left) and 20 mm/h (right) rainfall. Rainfall and infiltration (a and b), and outflow at the right, outflow at the left and bottom, and outflow at the surface (c and d), exchange between matrix domain (MT) and preferential flow domain (PF) (e and f) positive for flow from PF to MT and negative for flow from MT to PF.

intensity rainfall (10% ~ 15%) than for the case of high-intensity rainfall (50% ~ 85%). Overland flow starts after 80 h (or 160 mm of rainfall) for the low-intensity case and after

60 h (or 120 mm of rainfall) for the high-intensity case.

The seepage outflow increases along all three boundaries during the rainfall event (Figures 4.4c, 4.4d, 4.5c, 4.5d) and is smaller than the infiltration rate (storage is increasing). In the dual-permeability model and the low-intensity rain, outflow along the surface boundary starts after 115 h (or 230 mm of rainfall) while for the high-intensity rain outflow starts after 9 h (or 180 mm rainfall). The outflow rate along the surface boundary depends on the groundwater level in the upper layer. In the dual-permeability model, the outflow along the right boundary is approximately 10 times larger for the preferential flow domain than for the matrix domain, which is consistent with their volumetric ratio and their saturated hydraulic conductivity ratio. The water exchange between the two domains in the dual-permeability model is shown in Figures 4.5e and 4.5f. For the low-intensity rainfall case, the water exchange from the preferential flow domain to the matrix domain increases during the first 100 h and then decreases, while the water exchange from the matrix domain to the preferential flow domain is almost always increasing (more negative). For the high-intensity rainfall case, the water exchange from the matrix to the preferential flow domain is negligible, while the water exchange from the preferential flow domain to the matrix domain reaches more than 0.3 $m^2$/h, which is similar to the infiltration into the preferential flow domain. After five hours, approximately 75% of infiltration into the matrix domain is water exchange from the preferential flow domain (Figure 4.5f) and 25% infiltration from the surface boundary (Figure 4.5b).

### 4.4.2. WATER BALANCE

The integrated rainfall and water storage for the study area are shown for both models in Figure 4.6. The water balance is obtained by integrating all flow components along the boundaries of the study area. The numerical water balance errors are between 2% and 3%.

For all cases, the storage increase flattens out when the inflow decreases (Figures 4.4 and 4.5). For the high-intensity rainfall, the dual-permeability model stores 8% less water than the single-permeability model. The total storage after 150 h of low-intensity rainfall is less than after 15 h of high-intensity rainfall, probably caused by the longer time that water can drain from the study area under low-intensity rain.

For the dual-permeability model, the water exchange has a significant influence on the storage change in each domain. For the low-intensity rainfall, the storage in the preferential flow domain doesn't increase much after 6 hours (Figure 4.6). For the high-intensity rainfall, the storage in the preferential flow domain increases rapidly over the first 3 hours as very little water infiltrates into the matrix domain due to the low infiltration capacity of the matrix. After 3 hours, the preferential flow domain has almost reached full saturation and the large pressure difference between the preferential flow domain and matrix domain causes extensive water exchange (Figure 4.5f).

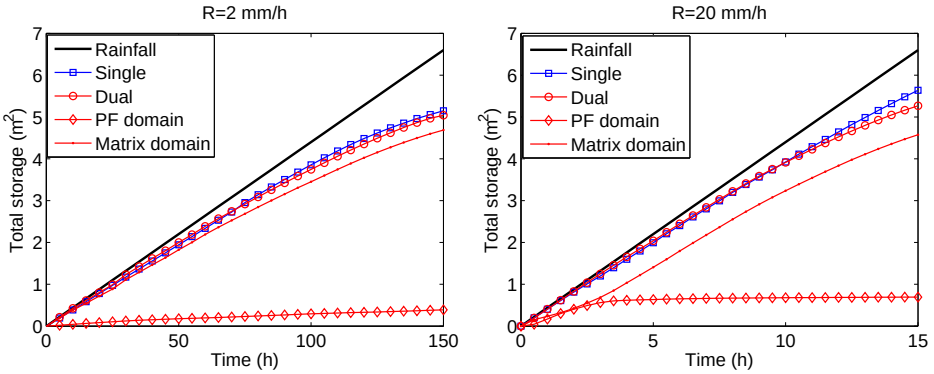


Figure 4.6: Storage increase of single-permeability model and dual-permeability model



### 4.4.3. WATER CONTENT

The water content distribution in the study area is shown in Figure 4.7 for both the single-permeability model (left-hand panels) and the dual-permeability model (center and right-hand panels). The water exchange rate between the matrix and preferential flow domains of the dual-permeability model is shown in Figure 4.8. The infiltration process of the dual-permeability model differs significantly from that of the single-permeability model.

The initial water content distribution in the matrix and preferential flow domains is similar for both models. During the rainfall events, the wetting front in the single-permeability model develops parallel to the surface and propagates downward. This holds for both low and high rainfall intensities (Figure 4.7 left-hand column). The wetting front generally reaches the groundwater table at the toe of the slope first, after which the infiltrated water continuously enlarges the saturated area.

In the dual-permeability model, the combined effects of the preferential flow and the matrix flow show a more complicated response. For the low-intensity rainfall, infiltration is dominated by matrix flow, as 90% of the subsurface consists of the matrix. Because the rainfall intensity is lower than the saturated conductivity of the matrix domain, rainfall never exceeds infiltration capacity (Figure 4.5a), so that 90% of the rainfall infiltrates into the matrix domain and 10% of the rainfall infiltrates into the preferential flow domain. The pressure are different between domains, that directly cause the water exchange at the matrix wetting front (Figures 4.5e and 4.8a ). At first, water quickly reaches the soil layer interface by preferential flow where it transmits to the matrix, although this exchange flux is very small (Figures 4.5e and 4.8a). After sufficient time (70 hours), a much stronger matrix flow (taking about 80% of the infiltrated rainfall) reaches the soil layer interface and generally reverses the water exchange direction (Figure 4.5e).

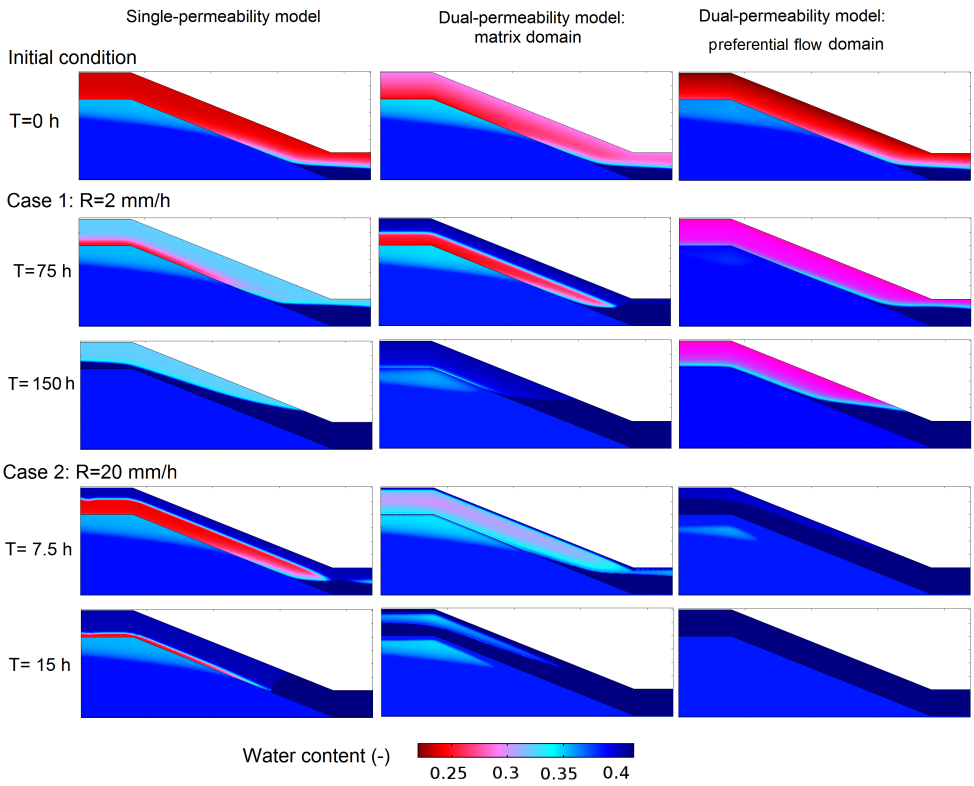


Figure 4.7: Water content distribution

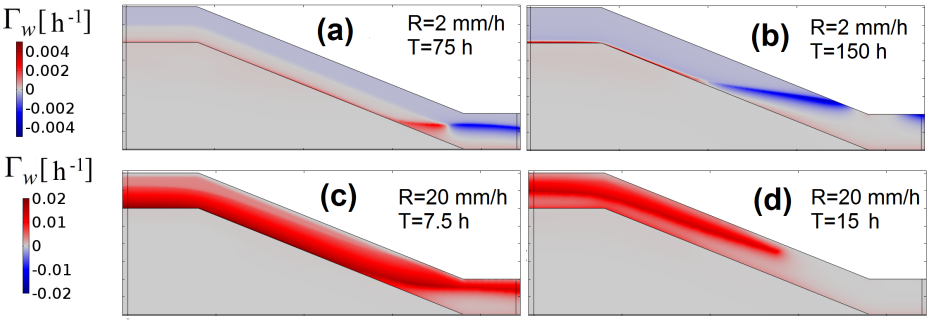


Figure 4.8: Water exchange rate distribution Positive values (blue) mean water exchange from preferential flow domain to matrix, negative values (blue) mean water exchange from matrix to preferential flow domain.

Overall, water exchange during low-intensity rainfall in the study area is dominated by flow from the matrix to the preferential flow domain (Figures 4.8 a-b).

For the high-intensity rainfall, the rainfall intensity is 8.4 times the matrix saturated hydraulic conductivity. The percentage of infiltration into the matrix domain decreases from 90% to 50% within the first half hour, and continues to decrease to less than 20% after 1.5 h. In contrast, the percentage of rainfall that infiltrates into the preferential flow domain increases from 10% to over 80% after 2 h. Water in the preferential flow domain quickly reaches the deeper soil layer and forms a perched groundwater table (Figure 4.7), where a significant amount of water infiltrates into the matrix (Figure 4.5f).

### 4.4.4. SLOPE STABILITY

The local factor of safety is computed based on the computed water pressure distribution (Figure 4.7). The distribution of the local factor of safety is shown in Figure 4.9 for the initial condition and after 150 h (low-intensity rainfall) and 15 h (high-intensity rainfall) for both the single-permeability model and the dual-permeability model and for the case with different cohesion values for the upper and lower layers. The case with equal cohesion values is not shown because the potential failure areas are very small.



A local factor of safety below 1.0 indicates a potential failure area. The area with a $F_{\text{LFS}}$ below 1 was determined every time interval (5 h in case 1, and 0.5 h in case 2) and is shown by the black line in Figure 4.9. Slope stability is related to both the specific weight of the wet soil and the pore water pressure in the soil. The specific weight changes due to changes in water storage are relatively small, but changes in water pressure have a significant effect on slope stability, especially in the area of the perched water table.

The size of the potential failure area is plotted vs. the cumulative rainfall in Figure 4.10 for the two different rainfall events and two sets of cohesion values. The results for the same cohesion values ($c'_1 = c'_2 = 5$ kPa) are shown in Figure 4.10a. For the low-intensity rainfall, the failure area is very small and is approximately the same for both permeability models. For the high-intensity rainfall, the failure area in the single-permeability model is larger than for the low-intensity rainfall, but the trend is similar. The failure area in the dual-permeability model is significantly larger. Failure starts after 60 mm rainfall, and the failure area continues to grow during the rainfall infiltration process.

The results for different cohesion values ($c'_1$=3 kPa, $c'_2$=6 kPa) are shown in Figure 4.10b. For the low-intensity rainfall, the failure area is 0.7 m$^2$ in the single-permeability model after 20 mm of cumulative rainfall. The size of this area shows almost no increase until approximately 220 mm of cumulative rainfall, when the groundwater table starts to rise (Figure 4.7). The failure area of the dual-permeability model is 40% smaller than that of the single-permeability model as the preferential flow domain drains more water into the matrix domain. For the high-intensity rainfall, the failure area of the dual-permeability model is larger than of the single-permeability model, as for the case with equal cohesion values. The failure areas of both models increase fairly quickly to 2 m$^2$, or 5% of the upper layer in the study area. The failure area increases to 5 m$^2$ in the dual-

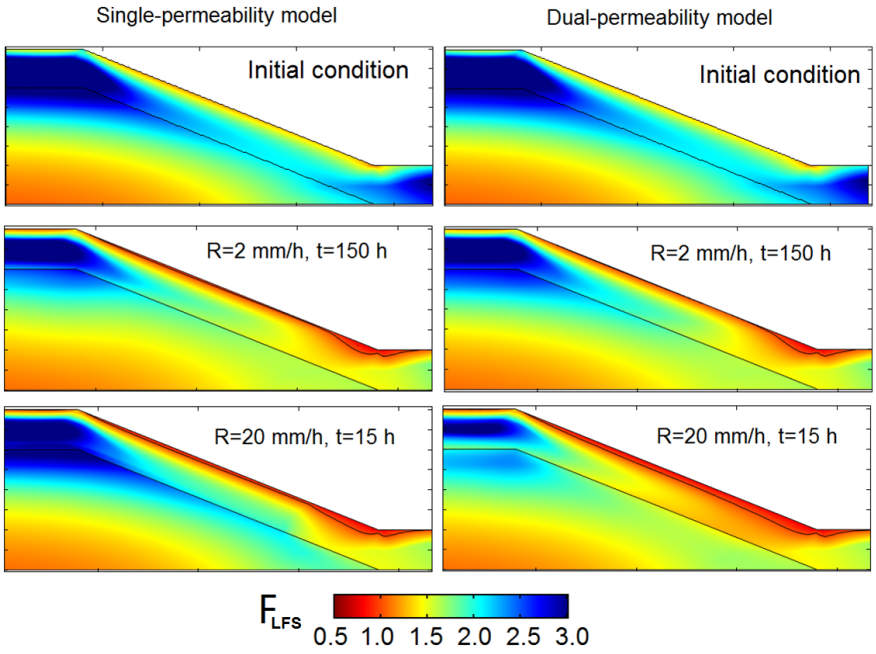


Figure 4.9: Water exchange rate distribution Positive values (blue) mean water exchange from preferential flow domain to matrix, negative values (blue) mean water exchange from matrix to preferential flow domain.

permeability model and to 3 $m^2$ in the single-permeability model.

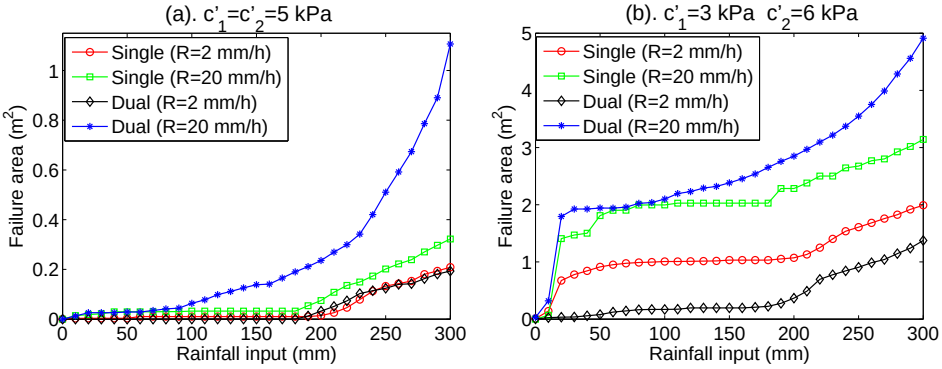


Figure 4.10: Water exchange rate distribution Positive values (blue) mean water exchange from preferential flow domain to matrix, negative values (blue) mean water exchange from matrix to preferential flow domain.

## 4.5. DISCUSSION

The slope stability result are directly related with subsurface hydrological results. For the low-intensity rainfall, the failure area for the single-permeability model is very similar in size and location to the dual-permeability model as the location of the water table is very similar in both models (Figure 4.7). The initial condition of the dual-permeability model is slightly more stable than that of the single-permeability model, since the preferential flow domain has a higher drainage capacity and, consequently, a lower pore water pressure. In the case of low-intensity rainfall, the matrix flow dominates the groundwater recharge and, consequently, the slope instability. Furthermore, the pore water pressure in the preferential flow domain is very low due to its strong drainage capacity. As a result, the failure area calculated by the dual-permeability model under low-intensity rainfall is slightly smaller than that calculated by the single-permeability model (Figure 4.10a). The location of the failure area is similar in the single- and the dual-permeability domain (Figure 4.9).



For the high-intensity rainfall, the failure area is significantly larger for the dual-permeability model than for the single-permeability model as the perched water table in the preferential flow domain is much more extensive in the dual-permeability model as compared to the single-permeability model (Figure 4.7). The regular wetting front of the single-permeability model does not reach the interface between soil layers, and the failure area is limited to the toe of the slope. For the dual-permeability model, the high-intensity rainfall results in a rapid infiltration through preferential flow, which quickly reaches the interface between soil layers, and increases the degree of saturation and pressure head of the deeper soil. Positive pore water pressure occurs in the preferential flow domain before the entire slope is fully saturated, and produces a larger failure area than in the equivalent single-permeability model.

The role of preferential flow in hydrology focuses mainly on the rapid vertical infiltration of water and contaminant [Christiansen et al., 2004; Kodešová et al., 2005; Laine-Kaulio et al., 2014], or the rapid discharge in hillslope and catchment hydrological studies on discharge generation [Zhang et al., 2006; Mulungu et al., 2005]. A physically based numerical model can be used to investigate the hydrologic response under predefined conditions. Prior to this study, a systematic evaluation of the influence of preferential flow on slope stability using a fully coupled dual-permeability and slope stability model has not been carried out. In this section, the underlying approximations of the numerical model are explored and the influence of the chosen parameter sets on the model outcome is discussed. The numerical experimental results are compared with field studies and other published numerical experiments.

### 4.5.1. CONTINUUM MODEL

Soil heterogeneity is one of the most difficult problems in both hydrology and soil mechanics studies. As an alternative to the continuum approach used here, preferential flow may be simulated by explicitly including fissures, pipes, or fracture networks in discrete (or discontinuous) model. Several field studies [Hencher, 2010] and numerical experiments [Tsutsumi and Fujita, 2008; Chang et al., 2014] have focused on the investigation and simulation of pipe flow (in soil) and fracture flow (in rock). In order to accurately describe the geometry of the preferential flow paths, the high-resolution macropore image reconstruction approach [Hu et al., 2014] or the statistical approach [Köhne et al., 2009] may be applied. Numerical simulation of these natural macropore networks require large amounts of geometry information [Nieber and Sidle, 2010] and computational time and are consequently limited to small-scale studies with a limited number of pipes [Tsutsumi and Fujita, 2008] or cracks [Moonen et al., 2008].



The dual-permeability model is a useful tool to simulate subsurface stormflow and solute transport in a forested hillslope when the parameterization is able to capture the hydraulic characteristics of each domain [Laine-Kaulio, 2011; Laine-Kaulio et al., 2014]. As the dual-permeability model describes the subsurface as a continuum of two linked domains, it is suitable for heterogeneous slopes with a high density of preferential flow paths and not for slopes with only a few large fissures or cracks [van der Spek et al., 2013].

In this paper, flow in both domains is described with the Darcy-Richards' equation, which is valid when the macropores have a relatively small size, and the macropore flow is still viscous [Köhne and Mohanty, 2005; Laine-Kaulio et al., 2014]. When fluid velocities are high and flow becomes turbulent, Darcy's equation is not valid [Nield and Bejan, 2006; Beven and Germann, 2013] as may be the case in large cracks or fissures under near-saturated or ponded infiltration [Beven and Germann, 1982]. The existence of pore necks and dead ends in preferential flow paths reduce the occurrence of turbulent flow [Jarvis, 2007].

### 4.5.2. COUPLING TERM IN DUAL-PERMEABILITY MODEL

In the dual-permeability model, the two domains are in general not at equilibrium. The water exchange is governed by two parameters: the water exchange coefficient and the average hydraulic conductivity between the two domains (Equation 4.6). The average hydraulic conductivity in turn is a function of the hydraulic conductivities of the two domains, which are a function of the pressure head. The larger the product, the quicker the two domains equilibrate. Estimation of the water exchange coefficient from physical measurements is very difficult. The most widely used equation is [Gerke and van Genuchten, 1993b]:

$$\alpha_{\mathrm{w}} = \frac{\beta}{d^2}\gamma_w \tag{4.1}$$

where $\beta$ is a scaling factor, $d$ is half the representative distance between two macropores, and $\gamma_w$ is a geometry-dependent shape factor that equals 3 for rectangular slabs and 15 for spheres [Ray et al., 1997]. Parameter values for the water exchange term used in several studies are summarized in Table 4.2. Vogel et al. [2000a] and Gerke and Köhne [2004] conceptualize the preferential flow domain as rectangular matrix blocks arranged as parallel slabs. A reduction factor of 0.01 or 0.001 was used to significantly reduce the water exchange between the two domains, because the hydraulic conductivity at the matrix/fracture interface was conceptualized to be controlled by relatively impermeable coatings that are composed of minerals and organic matter [Ray et al., 2004; Gerke and Köhne, 2002]. Köhne and Mohanty [2005] conceptualize the tadual domain as a hollow cylindrical matrix that is filled with coarse sand in the middle to mimic the macropore domain. Arora et al. [2011] based their parameters on a high density of macropore columns, and they calculated $K_a$ by averaging the hydraulic conductivities of the two pore domains (as adopted in this paper; see Equation 4.7). Arora et al. [2011] and Köhne and Mohanty [2005] did not consider the influence of coatings on the permeability, nor was this done in this study.



It may be seen from Table 4.2 that the magnitude of the product $\alpha_{\mathrm{w}} K_{sa}$ is similar for all studies, even though some of the other values (notably the ratios $K_{sa}/K_{sm}$ and the values of $\alpha_{\mathrm{w}}$ differ by several orders of magnitude. As such, the water exchange between all these models is likely similar.

Table 4.2: parameters setting of water exchange coefficients in different literatures.

| Parameter | 2D synthetic slope[1] | Bokhorst clay soil[2] | Macropore: coarse sand[3] | Macropore in sandy loam[4] | This study[5] |
|---|---|---|---|---|---|
| $w_f$ | 0.05 | 0.05 | 0.009675 | 0.00033 | 0.1 |
| $K_{sf}/K_{sm}$ | 1000 | 100 | 3878 | 63.6 | 100 |
| $K_{sa}/K_{sm}$ | 0.01 | 0.001 | 1 | 32.1 | 50.5 |
| $K_{sm}$(cm/h) | 0.012 | 0.1 | 0.056 | 0.13 | 0.238 |
| $d$(cm) | 1 | 1 | 11 | 1.89 | – |
| $\gamma_w$ | 0.4 | 0.4 | 0.4 | 0.001 | – |
| $\beta$ | 3 | 15 | 1.0685 | 0.67 | – |
| $\alpha_{\mathrm{w}}$(cm$^{-2}$) | 1.2 | 6 | $2.5\times10^{-3}$ | $1.8\times10^{-4}$ | $2.0\times10^{-5}$ |
| $\alpha_{\mathrm{w}} K_{sa}$(cm$^{-1}$h$^{-1}$) | $1.4\times10^{-4}$ | $6.0\times10^{-4}$ | $2.0\times10^{-4}$ | $7.8\times10^{-4}$ | $2.4\times10^{-4}$ |

Note: the parameter sets in Table 4.2 are taken from [1] Vogel et al. [2000a]; [2] Gerke and Köhne [2004]; [3] Köhne and Mohanty [2005]; [4] Arora et al. [2011]; and [5] this study.

### 4.5.3. COMPUTATION OF EFFECTIVE STRESS

In the dual-permeability model, the pore water pressure of the matrix and the preferential flow domains are different and water flows from the domain with a higher pressure to the domain with a lower pressure. Recently, van der Spek et al. [2013] show that in the case of varved clays with a low hydraulic conductivity of the soil matrix and a low density

of fissures, the time delay between water entering the fissure network and an increase in pressure in the matrix is relatively large. This study concerns a system with a very high density of macropores and consequently the numerical simulations show only a small time delay for the pressure propagation from the preferential flow domain to the matrix domain. The pore water pressure of the preferential flow domain is used for the effective stress calculation in the slope stability analysis, but failure time and area are only slightly different when the matrix pore water pressure is used for the slope stability analysis. Field evidence [Uchida et al., 2001] and numerical experiments [Nieber and Sidle, 2010; Lanni et al., 2013] suggest that individual preferential flow networks are hydraulically connected, and that the high pore water pressure build-up in the preferential flow paths is directly correlated with slope failure.



### 4.5.4. IMPLICATIONS OF PREFERENTIAL FLOW FOR HAZARD ASSESSMENT

This study is not the first to address the influence of preferential flow on subsurface flow and slope stability. Preferential flow has an effect on infiltration and drainage fluxes and as such influences the triggering factors for rainfall-induced landslides. Moreover, storage capacity relates to the pore distribution in a soil and controls the antecedent condition or the cause of landslide occurrence. The complexity hides in the combination of rainfall characteristics and soil hydraulic properties, together with the physiographic properties like slope, soil thickness, bedrock topography and so on, which determine the resultant pore water pressure response. The model runs and analyses show that rainfall intensity needs to be related to both the soil infiltration rate of the matrix domain and the preferential flow domain. Natural hillslopes show a bimodal response depending on the rainfall intensity which cannot be simulated with a single-permeability model with effective soil hydraulic parameters.

Parameterization of a dual-permeability model is difficult in practice [Laine-Kaulio et al., 2014]. Therefore the use of single-permeability models with effective soil hydraulic parameters prevails in regional hazard assessment [Zhou et al., 2014]. Rainfall-intensity duration plots for regional hazard assessment are well established and abundantly used but do not include soil and hydrological information [Guzzetti et al., 2007]. They empirically relate precipitation intensity and duration to observed landslides. The inclusion of more detailed hydrometeorological information in these analyses is ongoing. Recently, von Ruette et al. [2014] showed the importance of spatially and temporally heterogeneous rainfall on the initiation of landslides. In a synthetic study they showed that spatially distributed rainfall resulted in an increase of the number of shallow landslides as compared to uniform or intermittent rainfall (short periods with higher rainfall intensities but spatially homogeneous). They concluded that “low-rainfall intensities (below soil infiltration capacity) and long durations resulted in more infiltration, lower stream discharge, and more saturations and thus failure”. This is in full agreement with the re-

sults for low rainfall intensities in this study. Generally speaking, this holds for every case where infiltration capacity of the matrix remains higher than the rainfall intensity even in the presence of preferential flow paths. For low intensity rainfall, the water pressure increase simulated with a single-permeability model is generally larger than with a dual-permeability model as drainage by the preferential flow paths is underestimated. Soil drainage is a typical threshold process of the soil to get rid of its high pore water pressure and in this way stabilizes the slope. Consequently, the stability is slightly underestimated with a single-permeability model for low intensity rainfall.

The reverse is true, however, for high rainfall intensities, when the matrix reaches infiltration capacity early on. In these cases the preferential flow system dominates because water that cannot infiltrate into the matrix domain infiltrates into the preferential flow domain instead, resulting in a large pressure increase with a negative effect on slope stability. A much smaller pressure increase is simulated with a single-permeability model for the same high intensity rainfall. Consequently, the stability is overestimated with a single-permeability model even when equivalent parameters are used.



## 4.6. CONCLUSION

An coupled dual-permeability and slope stability model was developed to simulate the influence of preferential flow on subsurface hydrology and consequent slope failure area. The dual-permeability model is able to simulate both preferential flow and matrix flow. The slope failure area was determined with a local factor of safety analysis. Numerical experiments were carried out to study the effect of rainfall events on slope stability with both a single-permeability (no preferential flow) and a dual-permeability model. A 23 degree slope consisting of two soil layers was used in the study. The upper layer is sandy loam and the bottom layer is clay. Both the case where the cohesion of the two layers are equal, and the case where the cohesion of the upper layer is smaller than the lower layer were simulated. Two types of rainfall events were considered low-intensity, long duration rainfall, and high-intensity short duration rainfall; the total amount of water of both rainfall events was equal. The effect of preferential flow on slope stability was studied by comparing the failure area obtained with a single-permeability model and a dual-permeability model for the same rainfall event.

For low intensity rainfall, the failure area of both models is similar when the cohesion of the upper and lower layers is equal, but the failure area is significantly larger in the single-permeability model as compared to the dual-permeability model when the cohesion of the upper layer is lower than the cohesion of the lower layer. During low intensity rainfall, preferential flow has a positive effect on slope stability as it drains water from the matrix domain and decreases the water pressure.

For high intensity rainfall, the failure area of the dual-permeability model is significantly larger than the single-permeability model whether the cohesion values of the two

layers are equal or not. During high intensity rainfall, the rainfall intensity is larger than the infiltration capacity of the matrix domain so that most of the rainfall infiltrates into the preferential flow domain. As a result, the water pressure increases very quickly in the preferential flow domain resulting in a much larger failure area than is the case for the single-permeability model.

In summary, the coupled dual-permeability and slope stability model is an effective tool to better understand the influence of preferential flow on slope stability. Preferential flow has a positive effect on slope stability during low intensity rainfall and a negative effect on slope stability during high intensity rainfall.

# 5

# COUPLING A 1D DUAL-PERMEABILITY MODEL WITH AN INFINITE SLOPE STABILITY APPROACH TO QUANTIFY THE INFLUENCE OF PREFERENTIAL FLOW ON SLOPE STABILITY

*In this study, a 1D hydro-mechanical model was developed by coupling a dual-permeability model with an infinite slope stability approach to investigate the influence of preferential flow on pressure propagation and slope stability. The dual-permeability model used two modified Darcy-Richards equations to simultaneously simulate the matrix flow and preferential flow in a slope. The simulated pressure head was sequentially coupled with the soil mechanics model. The newly-developed numerical model was codified with the Python programming language, and benchmarked against the HYDRUS-1D software. The benchmark example proved that the proposed model is able to simulate the non-equilibrium phenomenon in a heterogeneous soil. We further implemented the model to conduct a synthetic experiment designing a slope with heterogeneous soil overlying an impermeable bedrock as a combined analysis of hydrology and slope stability, the results shows that the occurrence of preferential flow can reducing the time and rainfall amount required for slope failure. The proposed model provides a relatively simple and straightforward way to quantify the effect of preferential flow on the pressure propagation and landslide-triggering in heterogeneous hillslope.*

This chapter is based on:
Shao W, Bogaard T A, Su Y, Bakker M,. Coupling a 1D dual-permeability model with an infinite slope stability approach to quantify the influence of preferential flow on slope stability. Procedia Earth and Planetary Science, **16**, 128—136 (2016)

## 5.1. INTRODUCTION

Rainfall-induced shallow landslides are among one of the most frequent natural hazards in mountainous areas [Westen et al., 2006; Guzzetti et al., 1999; Rosso et al., 2006]. Slope instability is often initiated by a fast pore-water pressure response to precipitation or snow-melt events that reduces the suction stress and shear strength of the slope [Rosso et al., 2006; Ng and Pang, 2000]. Therefore, quantification of pressure propagation in a subsurface hydrological system is critical to simulate the timing and location of rainfall-triggered landslides [Ng and Pang, 2000; Berti and Simoni, 2012; Iverson, 2000].

In response to rain-pulses, the pressure propagation in a saturated soil is nearly-instant due to a low compressibility of the saturated soil [Berti and Simoni, 2012; Iverson, 2000]. While, in an unsaturated soil, fast pore water response might be related with preferential flow bypassing the adjacent soil matrix, directly reaching the groundwater table [Uchida et al., 2001, 2004; Hencher, 2010; Sidle et al., 2001]. Preferential flow paths, such as cracks, macropores, fissures, pipes, etc., are common features in highly-heterogeneous soils [Uchida et al., 2001, 2004; Sidle, 2006; Hencher, 2010; Nieber and Sidle, 2010; Krzeminska et al., 2012, 2013; Beven and Germann, 2013]. Increasingly sophisticated models have been developed for simulating preferential flow in various environmental systems [Nieber and Sidle, 2010; Krzeminska et al., 2012; Šimůnek et al., 2003; Köhne et al., 2009]. The widely-used dual-permeability models conceptualize the soil as two porous domains that interact hydrologically: the more permeable domain with associated larger porosity represents the macropores, fractures, fissures, and cracks; and the less permeable domain with lower porosity represents the soil matrix [Gerke and van Genuchten, 1993a; Šimůnek et al., 2003; Christiansen et al., 2004; Köhne et al., 2006, 2009].

Yet, most of the hydro-mechanical models calculate the pore water pressure based on a single-permeability assumption, and the effects of preferential flow on pressure wave propagation and landslide-triggering under high-intensity rainstorms are rarely quantified. Therefore, the objective of this paper is to describe a hydro-mechanical model, which couples a 1D dual-permeability model simulating infiltration and lateral flow along a slope gradient with an infinite slope stability approach. Such direct coupling of dual-permeability hillslope hydrological model and slope stability calculation allows to quantify the influence of preferential flow on slope stability under different boundary conditions. First we present the model set up, then we use a synthetic numerical experiment for model validation. Thereafter, we investigate pressure propagation and landslide-triggering under the influence of preferential flow in a pre-defined heterogeneous hillslope.

## 5.2. MODEL DESCRIPTION AND NUMERICAL IMPLEMENTATION

### 5.2.1. STEADY INITIAL PRESSURE DISTRIBUTION

In a conceptualized 2D hillslope, the groundwater table at lower part of the slope is higher, which is therefore highly correlated with the slope failure. Here, we adopt a widely-used approach to estimate the groundwater table at the lower part of the slope that further can assist in specifying an initial pressure distribution along a vertical profile of the slope [Montgomery and Dietrich, 1994; Rosso et al., 2006].

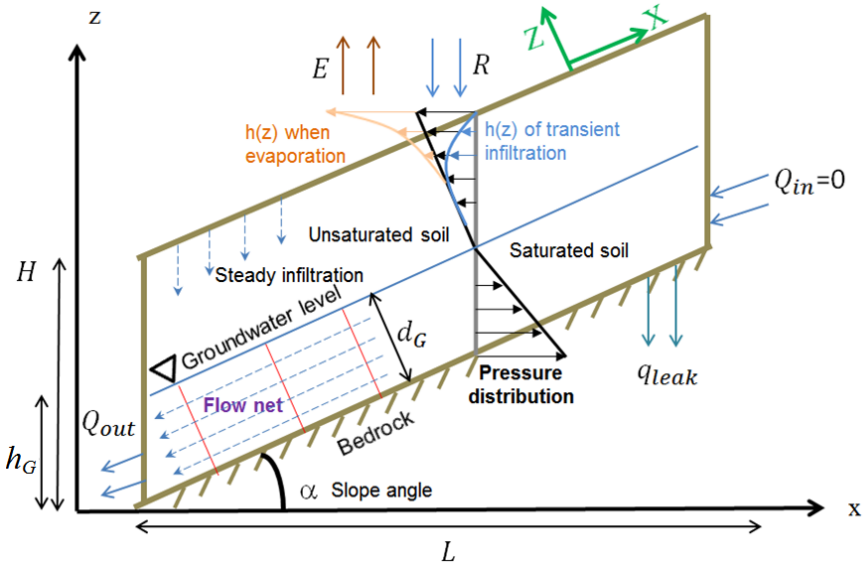


Figure 5.1: Schematic of the slope with a plane geometry.

Considering a long-term lateral steady flow parallel to the slope (Figure 5.1), the water table height at the slope bottom $h_G$ can be expressed as [Rosso et al., 2006]:

$$h_G = \frac{L(R-E) - Q_{leak}}{K \sin\alpha} \tag{5.1}$$

where $\alpha$ (Deg) is the slope angle, $K$ ($LT^{-1}$) is the hydraulic conductivity of the soil material, $L$ (L) is the length of a slope, $R$ and $E$ ($LT^{-1}$) are the flow rate of rainfall and evaporation, and $Q_{leak}$ ($L^2T^{-1}$) is the groundwater leakage. Assuming a leakage flow $q_{leak}$ ($LT^{-1}$) normal to the bottom boundary of the slope, the specific discharge $q$ ($LT^{-1}$) in the normal direction (Z) of the slope can be expressed by Darcy's Law [Iverson, 2000]:

$$q(Z)\big|_{Z<h_G} = -K_s\left(\frac{\partial h(Z)}{\partial Z} + \cos\alpha\right) = -q_{leak} \tag{5.2}$$

where $h$ (L) is the pressure head, $K_s$ ($LT^{-1}$) is the saturated hydraulic conductivity. Equa-

tion 5.2 implies that an extra elevation head of gravitational gradient (sin $\alpha$ in Equation 5.1) drives a parallel saturated flow in the hillslope (cos $\alpha$ in Equation 5.2). As a result, the water pressure head distribution can be derived as:

$$h(Z)|_{Z<d_G} = (d_G - Z)\left[\cos\alpha - \frac{q_{leak}}{K_s}\right] \tag{5.3}$$

Furthermore, the pressure distribution at a vertical coordinate system can be written as:

$$h(z)|_{z<h_G} = (h_G - z)\left[\cos^2\alpha - \frac{q_{leak}}{K_s}\cos\alpha\right] \tag{5.4}$$

where $z$ (L) is the vertical coordinate (positive upward).

For hydrostatic conditions, the initial pressure head distribution can approximately be specified with a linear distribution following Equation 5.4 for the vertical soil profile.

5

### 5.2.2. TRANSIENT PRESSURE RESPONSE

In a hillslope, the transient pressure response to rain-pulses can be simulated by the modified Darcy-Richards equation that was originally proposed as a single-permeability model [Baum et al., 2010]. Here we extend it to a modified dual-permeability model to simulate matrix flow as well as preferential flow:

$$C_f\frac{\partial h_f}{\partial t} = \frac{\partial}{\partial z}\left[K_f\left(\frac{1}{\cos^2\alpha}\frac{\partial h_f}{\partial z} + 1\right)\right] - \frac{\Gamma_w}{w_f} \tag{5.5}$$

$$C_m\frac{\partial h_m}{\partial t} = \frac{\partial}{\partial z}\left[K_m\left(\frac{1}{\cos^2\alpha}\frac{\partial h_m}{\partial z} + 1\right)\right] + \frac{\Gamma_w}{w_m} \tag{5.6}$$

$$\Gamma_w = \alpha_w\frac{K_m(h_f) + K_m(h_m)}{2}(h_f - h_m) \tag{5.7}$$

where the subscript $f$ indicates the preferential flow domain, the subscript $m$ indicates the matrix domain, $t$ (T) is time, $\theta$ ($L^3L^{-3}$) is the water content, $d\theta/dh$ ($L^{-1}$) is the differential water capacity, $h$ (L) is the pressure head, $K$ ($LT^{-1}$) is the unsaturated hydraulic conductivity, $w$ (-) is the volume fraction of the preferential flow domain or the matrix domain, $\alpha_w$ ($T^{-2}$) is the water exchange coefficient, and $\Gamma_w$ ($T^{-1}$) is the water exchange term [Gerke and van Genuchten, 1993b; Arora et al., 2011].

The Mualem-van Genuchten model is used to describe the hydraulic properties of both the matrix and the preferential flow domains [Van Genuchten, 1980]:

$$\Theta = \frac{\theta - \theta_r}{\theta_s - \theta_r} = \begin{cases} \left[1 + |\alpha_{VG}h|^{n_{VG}}\right]^{-m_{VG}}, & h < 0 \\ 1, & h \geq 0 \end{cases} \tag{5.8}$$

$$K = K_s\Theta^{0.5}\left[1 - \left(1 - \Theta^{1/m_{VG}}\right)^{m_{VG}}\right]^2 \tag{5.9}$$

$$C = -\frac{\mathrm{d}\theta}{\mathrm{d}|h|} = \begin{cases} m_{\mathrm{VG}} n_{\mathrm{VG}} \alpha_{\mathrm{VG}} (\theta_s - \theta_r) \Theta^{1/m_{\mathrm{VG}}} \left(1 - \Theta^{1/m_{\mathrm{VG}}}\right)^{m_{\mathrm{VG}}}, & h < 0 \\ S_s, & h \geq 0 \end{cases} \tag{5.10}$$

where $\Theta$ (-) is the effective saturation; $\theta$ ($\mathrm{L}^3\mathrm{L}^{-3}$) is the volumetric water content with subscript $r$ and $s$ denote the residual and saturated state, $\alpha_{\mathrm{VG}}$ ($\mathrm{L}^{-1}$) , $n_{\mathrm{VG}}$ (-), and $m_{\mathrm{VG}}$ (-) are fitting parameters; $S_s$ ($\mathrm{L}^{-1}$) denotes the specific storage; and $K_s$ ($\mathrm{LT}^{-1}$) is the saturated hydraulic conductivity.

### 5.2.3. SURFACE BOUNDARY CONDITION FOR DUAL-PERMEABILITY MODEL

The boundary conditions of the Darcy-Richards equation could be specified for pressure head, flux, or mixed [Shao et al., 2015, 2014]. The specified infiltration flux $i$ ($\mathrm{LT}^{-1}$) on a dual-permeability soil surface is divided into the two constituting domains:

$$i = w_f i_f + w_m i_m \tag{5.11}$$

where $i_m$ and $i_f$ are specified boundary fluxes on the surface of the matrix domain and the preferential flow domains respectively.

We assume the preferential flow not to be triggered at the beginning of a rainfall event, and consequently, the infiltration process starts in the matrix domain only:

$$R = i = w_m i_m \tag{5.12}$$

In case the specified flow at the matrix surface exceeds its infiltration capacity, the boundary condition of the matrix domain changes to a specified pressure head. Hereafter, the infiltration-excess water at that time-step will be reallocated to the surface boundary of preferential flow domain:

$$i_f = \frac{R - w_m i_m}{w_f} \tag{5.13}$$

Once the specified flux into the preferential flow domain is larger than its infiltration capacity, the boundary conditions of both domains are changed to the specified pressure head corresponding to the surface water ponding depth.

### 5.2.4. INFINITE SLOPE STABILITY APPROACH

Using an infinite slope stability approach to formulate the factor of safety $F_s$ (-), it is expressed as a ratio of resisting force to gravitationally driving force with three terms[Lu

and Godt, 2008]:

$$F_s(z_H) = \underbrace{\frac{\tan\phi'}{\tan\alpha}}_{\text{friction angle term}} + \underbrace{\frac{c'}{G\sin\alpha\cos\alpha}}_{\text{cohesion term}} - \underbrace{\frac{\sigma^s}{G}\frac{\tan\phi'}{\sin\alpha\cos\alpha}}_{\text{suction stress term}} \tag{5.14}$$

$$G = \int_{z_H}^{H} \left[\gamma_s + \gamma_w\theta\right]\, dz \tag{5.15}$$

$$\sigma^s = \chi p_w = \chi\gamma_w h \tag{5.16}$$

where $z_H$ (L) is the depth that below the soil surface; $c'$($ML^{-1}T^{-2}$) is effective cohesion; $\phi'$(deg) is friction angle; $G$ ($ML^{-1}T^{-2}$) is weight of soil; $\sigma_s$ ($ML^{-1}T^{-2}$) is suction stress; $p_w$ ($ML^{-1}T^{-2}$) is pore water pressure; and $\chi$(-) is matrix suction coefficient, which can be approximated by the effective saturation[Lu et al., 2010].

5

### 5.2.5. NUMERICAL IMPLEMENTATION

The dual-permeability model is numerically solved by an author-developed script under Python 2.7 programming environment, in which the algorithms use implicit finite difference method and Picard iteration technique in each time step [van Dam and Feddes, 2000]. During simulation, the tolerable error of water content is set to 0.0001, and the time step is dynamic in the range of 0.015 - 2 min, ensuring the numerical accuracy and computational efficiency. The hydrological results are sequentially coupled with the soil mechanical calculations as follows: i) the soil moisture distribution (Equation 5.15) determines the unit self-weight of soil; ii) the effective saturation and the pore water pressure (Equation 5.16) influence the suction stress and consequently the shear strength. The dual-permeability model simulates the non-equilibrium phenomenon of different water contents, pore water pressures, and flow velocities between the two domains [Shao et al., 2014, 2015]. The total water content and effective saturation can be evaluated by the weighted average of two domains. In this study, the pore water pressure in the preferential flow domain is assumed to be the “effective pressure head” for calculating the slope stability analysis [Shao et al., 2014, 2015]. However, in Section 5.4 we show and discuss the differences of simulated slope stability using the pressure head from either the matrix domain or preferential flow domain.

## 5.3. BENCHMARK WITH HYDRUS-1D

### 5.3.1. PARAMETERIZATION

Two synthetic numerical examples that can be simulated with dual-permeability model in HYDRUS-1D, are used as benchmark case to demonstrate the ability, accuracy and effectiveness of our hydrological code for modeling non-equilibrium flow. We use a 10

hours infiltration experiment in a sandy-loam soil column with dual-permeability hydraulic properties. The soil is conceptualized with two domains, in which the preferential flow and matrix flow co-exist. Two water retention curves and two soil hydraulic conductivity functions of the Mualem-van Genuchten model are specified in Table 5.1 following the approach of Köhne et al. [2002]. The water exchange coefficient $\alpha_w$ is set to as a moderate value of 0.01 $cm^{-2}$ to be able to obtain a non-equilibrium phenomenon with a clear difference in water exchange between two domains.

Table 5.1: Soil hydraulic parameters for the dual-permeability model

| Sandy loam (depth:1m) | $w$ (-) | $\theta_r$ ($cm^3/cm^3$) | $\theta_s$ ($cm^3/cm^3$) | $K_s$ (cm/day) | $\alpha_{VG}$ ($cm^{-1}$) | $n_{VG}$ (-) | $l_{VG}$ (-) | $\alpha_w$ ($cm^{-2}$) |
|---|---|---|---|---|---|---|---|---|
| matrix domain | 0.9 | 0.0 | 0.446 | 2.78 | 0.008 | 1.485 | 0.5 | 0.001 |
| PF domain | 0.1 | 0.0 | 0.76 | 296 | 0.188 | 1.269 | 0.5 | 0.001 |

Note: "PF domain" denote the preferential flow domain



### 5.3.2. INFILTRATION UNDER UNIT HYDRAULIC GRADIENT CONDITION

The first synthetic numerical experiment considers an infiltration experiment in a sandy-loam soil column with an infinitely-deep groundwater level. First, the initial condition of dual-permeability model is specified with a unit hydraulic gradient of a uniform pore water pressure distribution with a value of -2 m in both the matrix domain and the preferential flow domain. Second, the specified upper boundary is a constant pressure head of -0.001 m, and the specified lower boundary is gravitational drainage.

Figure 5.2 shows the infiltration development in 2-hour time step profiles of simulated water content, pressure head, and water exchange fluxes in two domains. Figure 5.2c shows the total water content as a weighted average, and Figure 5.2f shows the water exchange rate between two domains. Under a surface ponding condition, the wetting front in preferential flow domain is much faster than that in matrix domain, which causes the non-equilibrium phenomenon in terms of different water contents and pressure heads between two domains. The pressure head difference between the two domains drives the water exchange fluxes.

Figure 5.2f shows the water exchange rates calculated by HYDRUS-1D are slightly larger than that calculated by Python code, and thus leading to a slightly slower wetting front in preferential flow domain compared with Python code (Figure 5.2a,c). While those differences are nearly-negligible, we can conclude that the simulated results obtained by our Python code showed good agreement with the HYDRUS-1D simulations.

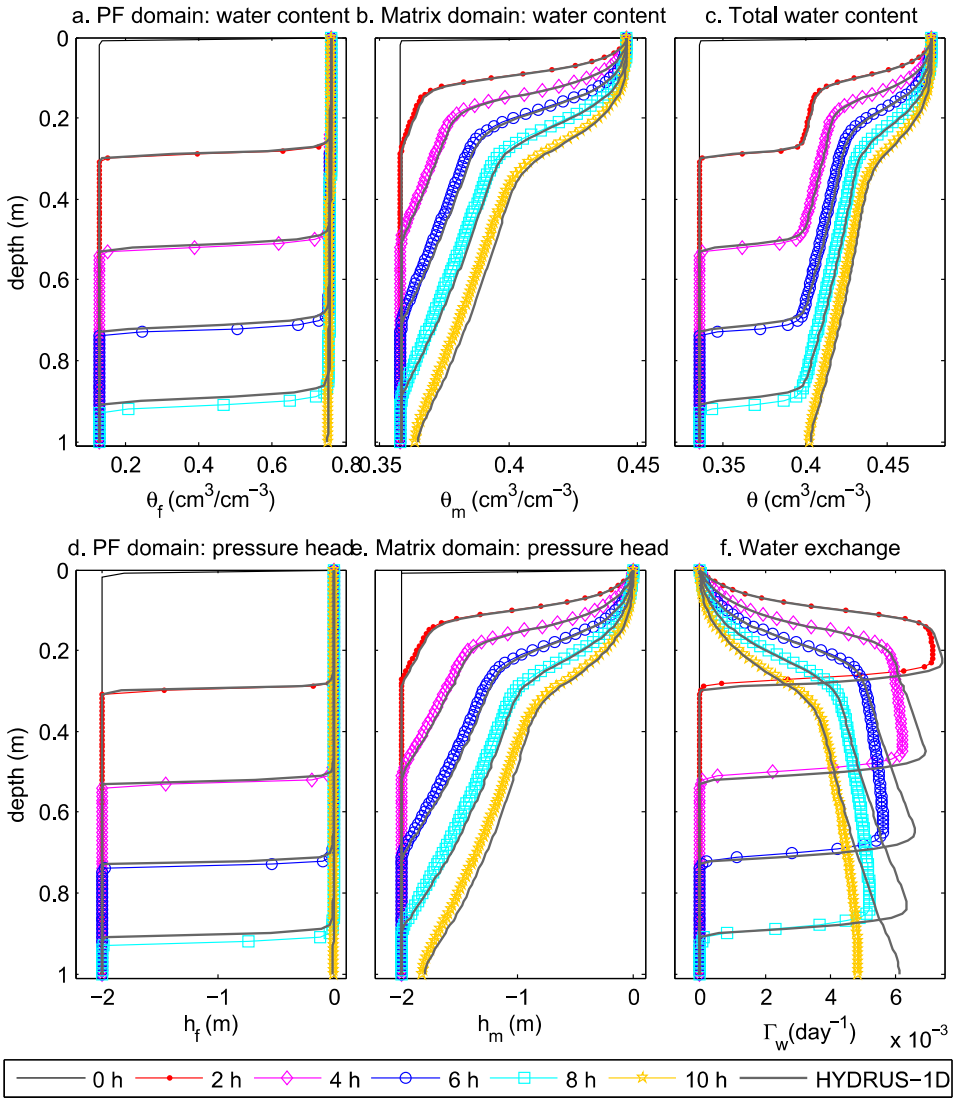


Figure 5.2: Benchmark the simulated hydrology results between Python code and HYDRUS-1D: ponding infiltration (at upper boundary) under unit hydraulic condition (initial condition) with a free drainage condition (lower boundary)

### 5.3.3. INFILTRATION UNDER HYDROSTATIC PRESSURE CONDITION

The second synthetic numerical experiment considers the infiltration occurs in soil column with a high groundwater level, specifically located at 80 cm depth below the soil

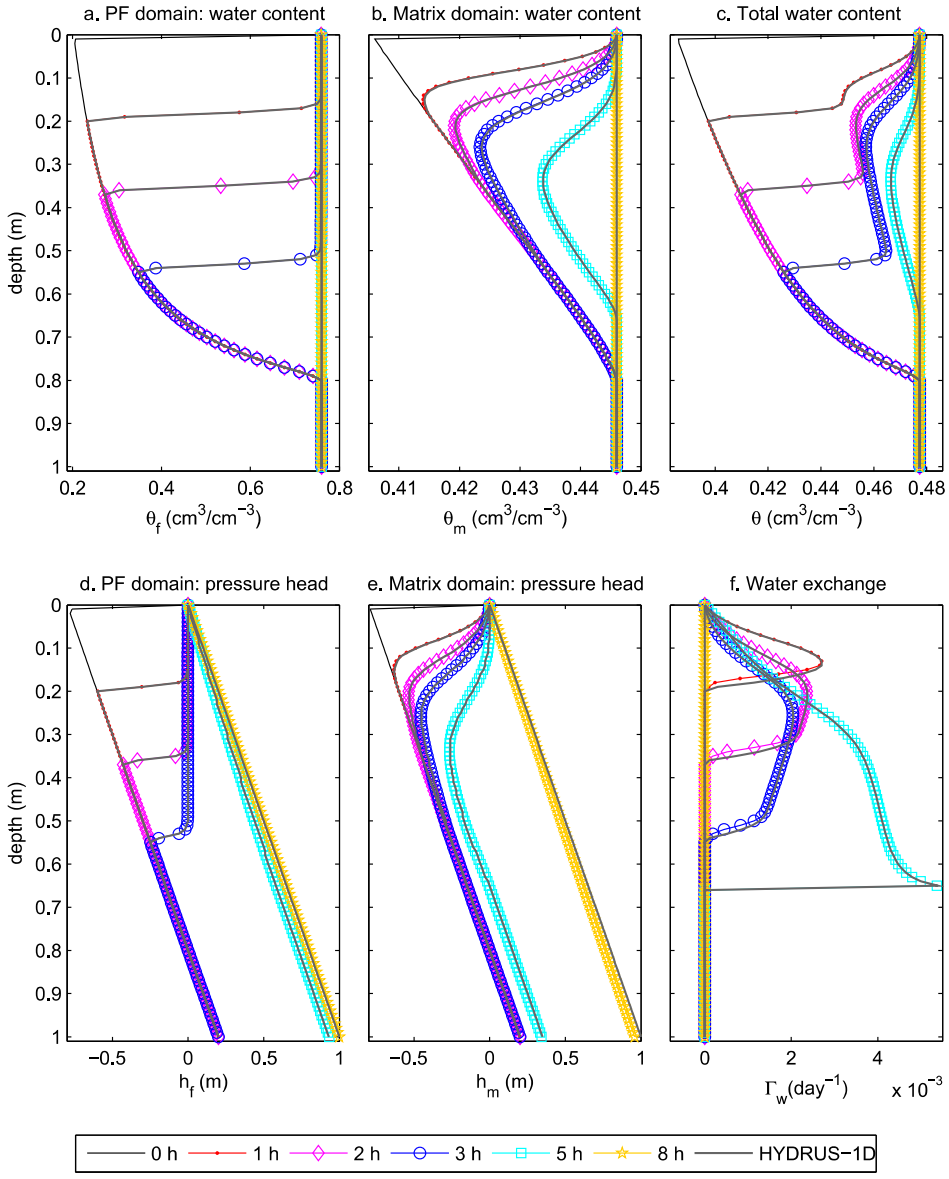


Figure 5.3: Benchmark the simulated hydrology results between Python code and HYDRUS-1D: ponding infiltration (at upper boundary) under hydrostatic pressure condition (initial condition) with a free drainage condition (lower boundary)

surface. The initial condition of dual-permeability model is therefore specified with a hydrostatic pressure distribution: the pressure heads in both the matrix domain and the

preferential flow domain linearly increase from -0.8 m (at soil surface) to 0.2 m (at 1 m depth of lower boundary).The specified upper boundary set as a constant pressure head of -0.001 m , while the specified lower boundary is defined as no-flow boundary condition. Following HYDRUS-1D, we additionally adopt a simulation strategy specifying the water exchange rate as zero for the area where the matrix and preferential flow domains are both reaching saturation.

Figure 5.3 shows results of simulated water content, pressure head, and water exchange fluxes for second benchmark example. The initial pressure and antecedent soil moisture of second numerical experiment are relatively larger than the first numerical experiment. The wetting front in preferential flow domain starts reaching the groundwater table after approximately 4 h. Consequently, at 5 h the pressure differences between two domains are significant, which causes the highest water exchange rate in the direction from preferential flow domain to matrix domain. At 8 h, both domains reach the fully saturated conditions (Figure 5.3b), since then the pressure heads of both two domains reach an equilibrium state, following a linear distribution. Overall, the results show the simulated results by Python code agree well with that from HYDRUS-1D, and identifiable differences from two models are the water exchange rate (Figure 5.3e).



Overall, the two benchmark numerical experiments demonstrate that the Python code can provide correct numerical solution of pressure response. In a hillslope, a fraction of slope gradient is driving saturated slope parallel flow which can influence pressure build-up at vertical direction. The following analysis will focus on the combined soil hydrology and slope stability analysis in a hillsolpe by using the modified dual-permeability model codified with the Python script.

## 5.4. EXAMPLE OF COMBINED HILLSLOPE HYDROLOGY AND SOIL MECHANICS ANALYSIS

In this section we present the results of combined hillslope hydrology and slope stability analysis for a synthetic slope that has dual-permeability hydraulic features. We used a 100 m long slope with 1.5 m thick clay soil overlying an impermeable bedrock, and the slope angle is set to 30°.

Table 2 shows the soil hydraulic parameters. Furthermore, we specify the soil mechanics parameters as follows: the dry bulk density is 1.62 kg/$m^3$, the friction angle is 25°, and the effective cohesion is 6 kPa. For specifying the initial condition, the water storage variation is neglected. Thus, the initial groundwater table of the hillslope is influenced by lateral drainage, which is mainly controlled by topography (slope angle and thickness), soil hydraulic properties (hydraulic conductivity), and long-term meteorological conditions (rainfall and evaporation). For instance, if we consider a net rainfall of 1000 mm/year, the initial groundwater table estimated with Equation 5.1 is approximately 54 cm above the bedrock. Hereafter, the initial pressure distribution in two do-

mains can be specified as the steady state pressure profiles following Equation 5.4. In our simple synthetic experiment, the rainfall event is set as a constant 10 mm/h with a duration of 10 hours (Figure 5.4a), and such a short-term rainfall is sufficient to induce transient pressure response and landslide in the defined hillslope.

Table 5.2: Soil hydraulic parameters for the dual-permeability model

| Sandy loam (depth:1m) | $w$ (-) | $\theta_r$ ($cm^3/cm^3$) | $\theta_s$ ($cm^3/cm^3$) | $K_s$ (cm/day) | $\alpha_{VG}$ ($cm^{-1}$) | $n_{VG}$ (-) | $l_{VG}$ (-) | $\alpha_w$ ($cm^{-2}$) |
|---|---|---|---|---|---|---|---|---|
| matrix domain | 0.9 | 0.05 | 0.35 | 2.01 | 0.01 | 2.5 | 0.5 | 0.006 |
| PF domain | 0.1 | 0.0 | 0.60 | 1000 | 0.10 | 1.2 | 0.5 | 0.006 |

Note: "PF domain" denote the preferential flow domain

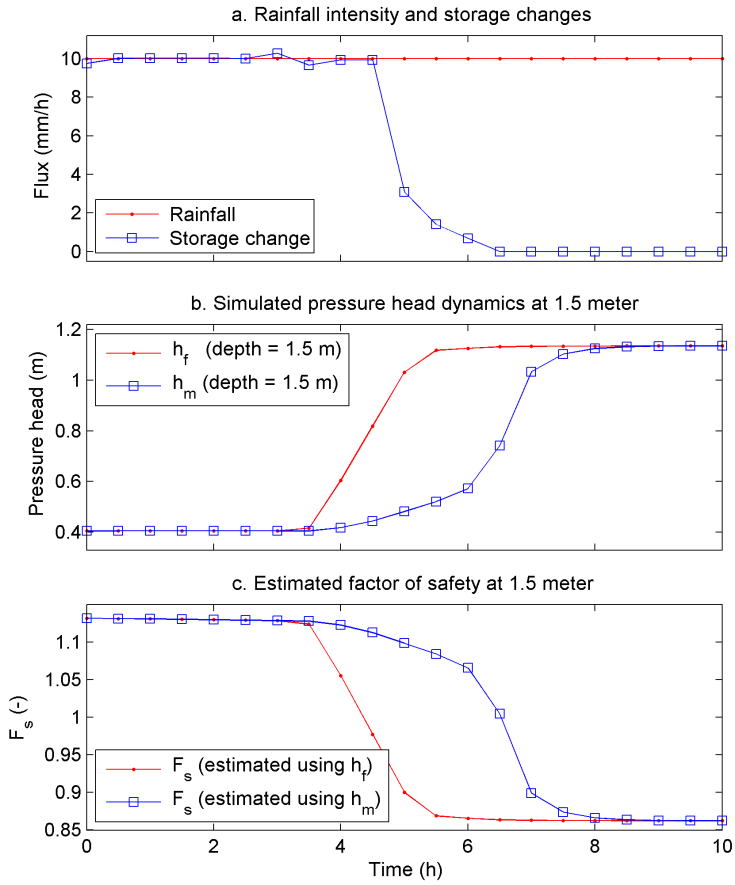


Figure 5.4: The simulated soil hydrology and slope stability results

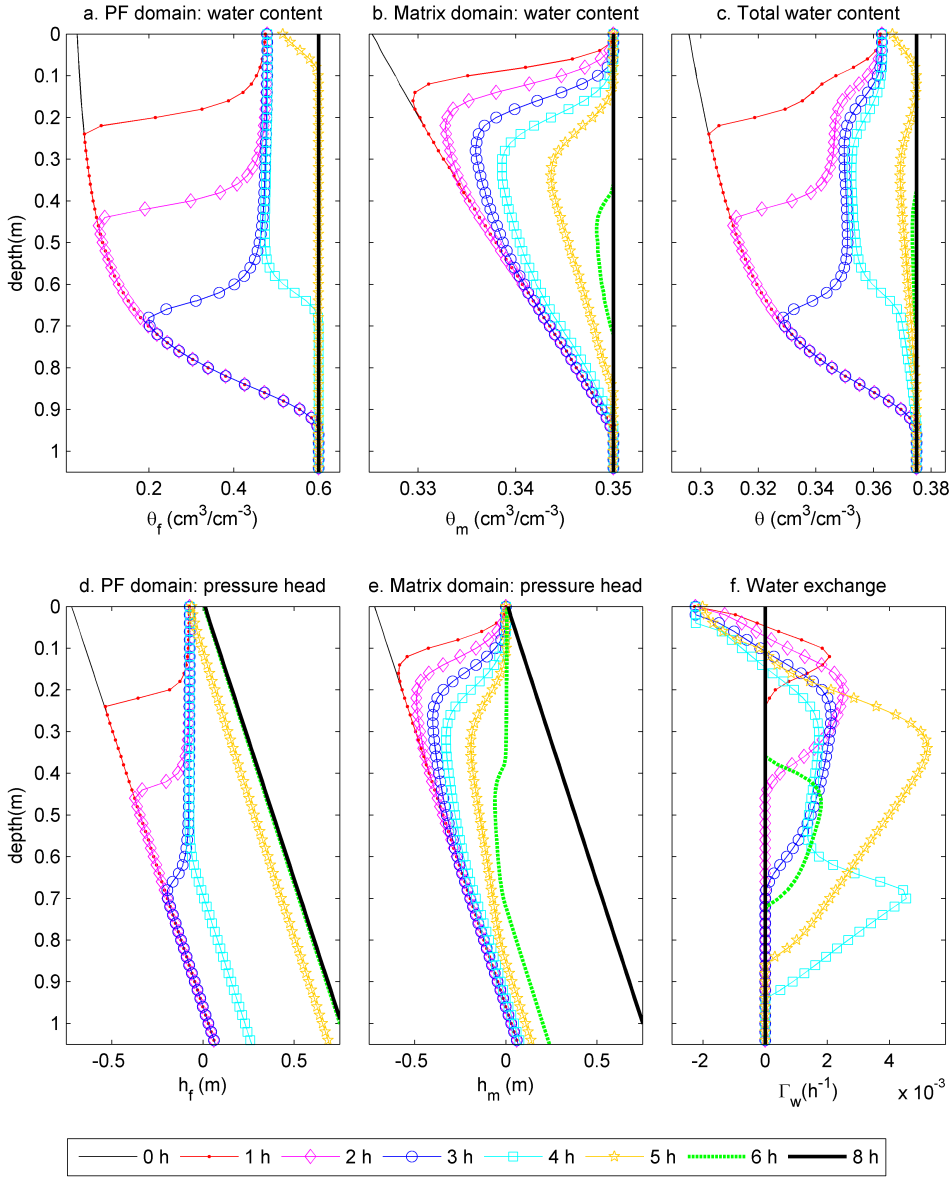


Figure 5.5: The simulated soil hydrology results under Experiment 2 with a 10 mm/h rainfall

The simulated water storage changes, and pressure head at 1.5 m depth of the two domains are given in Figure 5.4. The mass-balance error is less than 2 % during the first 5 hours, after which the soil profile is approaching full-saturation and the storage varia-

tion is approaching zero (Figure 5.4a). The dual-permeability model simulates pressure heads for both domains (Figure 5.4b). In Figure 5.4c we provide the calculated factor of safety using either $h_f$ or $h_m$ to demonstrate the influence on slope stability of the selection of the pore water pressure information: from the matrix or from the preferential flow domain. The factor of safety calculated with $h_f$ shows a 2-hour earlier failure time than that calculated with $h_m$ (Figure 5.4c).

Figure 5.5 shows the detailed hydrological results of the numerical simulations. As the rainfall intensity is larger than the infiltration capacity of the matrix domain, a saturated wetting front in matrix domain develops (positive pressure head, Figures 5.5 b,e). However, the rainfall intensity is not sufficient to cause a ponding infiltration in the preferential flow domain. The wetting front in the preferential flow domain remains unsaturated, and consequently the pressure head in preferential flow domain is lower than that in matrix domain (Figures 5.5a, d). Therefore, water exchange occurs form the matrix towards preferential flow domain in the shallow surface soil (0-10 cm) (Figure 5.5f).

After 3 hours, as the wetting front progressed faster in the preferential flow domain, water reaches the lowest part of the soil matrix via the preferential flow, so by-passing the soil matrix and directly reaching the deep soil. The pressure response in preferential flow is much quicker than that in matrix domain, and the preferential flow develops a perched groundwater table after sufficient amount (36 mm) of rainfall. Consequently, the pressure head of preferential flow in deeper soil is larger than that of matrix flow domain, which drives a positive water exchange flow transferring water from the preferential flow domain to the matrix domain (Figure 5.5f: 4-6 h). Finally, the pressure head of the two domains will reach an equilibrium condition after 8 hours (Figures 5.5 d, e).



## 5.5. CONCLUSIONS

This study proposed a 1D hydro-mechanical model that integrated a modified dual-permeability model with infinite slope stability approach, which can quantify the influence of preferential flow on pressure propagation and slope failure initiation under different slope angles in a fast and relatively simple way. The model was tested with two numerical examples. The first experiment was attempted to benchmark the newly-developed model against the HYDRUS-1D software, and showed that the programmed Python code provides a reliable and fast numerical solution to simulate the combined matrix flow and preferential flow as well as the complex subsurface flow processes, such as non-equilibrium flow and bypass flow. Secondly, we report on a synthetic numerical experiment for combined hillslope hydrology and soil mechanics analyses, which highlighted the soil hydrological conditions which control water and pressure wave propagations in the case of a dual-permeability subsurface. In conclusion, the proposed model is a useful tool for coupling the dual-permeability model and slope stability analysis, and can further provide detail on the importance of preferential flow in pressure wave

propagation and thus slope stability assessment. The planned future work includes the extension of the dual-permeability model to simulate complex hydrological systems under the influence of evaporation, transpiration, interception, surface runoff, etc.

# 6

# ANALYZING THE INFLUENCE OF PREFERENTIAL FLOW ON PRESSURE PROPAGATION AND LANDSLIDE TRIGGERING OF THE ROCCA PITIGLIANA LANDSLIDE

*The fast pore water pressure response to rain events is an important triggering factor for slope instability. The fast pressure response may be caused by preferential flow that bypasses the soil matrix. Currently, most of the hydro-mechanical models simulate pore water pressure using a single-permeability model, which cannot quantify the effects of preferential flow on pressure propagation and landslide triggering. Previous studies showed that a model based on the linear-diffusion equation can simulate the fast pressure propagation in near-saturated landslides such as the Rocca Pitigliana landslide. In such a model, the diffusion coefficient depends on the degree of saturation, which makes it difficult to use the model for predictions. In this study, the influence of preferential flow on pressure propagation and slope stability is investigated with a 1D dual-permeability model coupled with an infinite-slope stability approach. The dual-permeability model uses two modified Darcy-Richards equations to simultaneously simulate the matrix flow and preferential flow in hillslopes. The simulated pressure head is used in an infinite-slope stability analysis to identify the influence of preferential flow on the fast pressure response and landslide triggering. The dual-permeability model simulates the height and arrival of the pressure peak reasonably well. Performance of the dual-permeability model is as good as or better than the linear-diffusion model even though the dual-permeability model is calibrated for two single pulse rain events only, while the linear-diffusion model is calibrated for each rain event separately.*

This chapter is based on:
Shao W, Bogaard T A, Bakker M,. Analysing the influence of preferential flow on pressure propagation and landslide triggering of Rocca Pitigliana landslide. Journal of Hydrology (in print)

## 6.1. INTRODUCTION

Landslides are severe geologic hazards in mountainous areas [Westen et al., 2006; Guzzetti et al., 1999]. The potential triggering factors for landslides include geological activities (e.g., earthquakes), hydrological effects (e.g., rain storms and snowmelt), weathering processes, and human activities [Chang et al., 2014]. The stabilizing factor in a potential landslide is the shear strength, which is a function of cohesion, frictional force, and pore water pressure. A landslide may be triggered when the gravitational driving force is larger than the resistance force [Rosso et al., 2006]. Rainfall is one of the most important triggering factors of landslides. Rainfall has two effects on the slope stability. First, rainfall infiltration increases the pore water pressure, which reduces the effective shear strength. Second, a larger water storage increases the weight of a slope, influencing the gravitational driving force and resistant forces [Asch et al., 1999]. Many studies found that landslide occurrence is statistically correlated with the intensity and amount of rainfall [Guzzetti et al., 2007]. The prediction of the timing of rainfall-triggered landslides requires a hydro-mechanical model that integrates the theories of both subsurface hydrology and soil mechanics [Griffiths and Lu, 2005; Rahardjo et al., 2012].



In many hydro-mechanical models, soil moisture dynamics and pressure propagation are simulated with the Darcy-Richards equation [Greco et al., 2013; Baum et al., 2010; Lu et al., 2012; Shao et al., 2015]. Hydrological results are used as input for a soil mechanics model that calculates the effective stresses and displacements with a momentum-balance equation combined with stress-strain constitutive relations (e.g., linear-elastic, elasto-plastic). Finally, the slope stability analysis can be analyzed with a shear strength reduction method or a limit-equilibrium approach [Griffiths and Lu, 2005; Lu et al., 2012]. Several software packages have been developed for the combined analysis of seepage and soil mechanics, such as FLAC [Itasca, 2002], PLAXIS [Brinkgreve et al., 2010], ANSYS [Stolarski et al., 2011], COMSOL [Shao et al., 2015], and SEEP/W, SLOPE/W and SIGMA/W [Rahimi et al., 2010]. The implementation of a 2D/3D numerical model might still be difficult mainly because of the extensive geotechnical investigations that are needed for model set-up and parameterization [Rosso et al., 2006]. The 1D limit-equilibrium approach (the infinite-slope stability approach) is an attractive and simple alternative that may be coupled with a hydrological model to predict the timing and location of rainfall-induced shallow landslides in mountainous areas [Lu and Godt, 2008; Baum et al., 2010; Talebi et al.; Krzeminska et al., 2013].

Preferential flow paths such as macropores, pipes, fractures, and inter-aggregate pores in a hillslope influence both the subsurface hydrology and soil mechanics [Brunsden, 1999]. The influence of preferential flow on pore water pressure propagation and landslide-triggering can be characterized by two mechanisms: enhanced drainage and fast pressure buildup [Bogaard and Greco, 2016; Shao et al., 2015; Uchida et al., 2001, 2004; Krzeminska

et al., 2012; Hencher, 2010; Sharma and Nakagawa, 2010]. Drainage enhancement has a positive effect on slope stability as high-permeable preferential flow paths can facilitate pressure dissipation and reduce the pressure buildup [Krzeminska et al., 2012; Pierson, 1983]. Fast pressure buildup has a negative effect on slope stability as preferential flow can bypass the soil matrix, resulting in more rapid and deeper water movement and pressure response [Hendrickx and Flury, 2001; Beven and Germann, 1982, 2013; Nimmo, 2012]. The pore water pressure in the preferential flow paths may be larger than in the surrounding matrix, especially when the cavities of preferential flow paths are filled with water or blocked during a rainfall event.

Most of the subsurface hydrological models currently employed in slope stability analysis are based on a single-permeability formulation to simulate subsurface flow and do not consider the effects of preferential flow on subsurface hydrology and soil mechanics [Nieber and Sidle, 2010; Beven and Germann, 2013; Uchida et al., 2004; Hencher, 2010]. Hydro-mechanical models need to become multi-continuum models to account for the influence of preferential flow [Vogel et al., 2000a], such as dual-porosity/dual-permeability models [Gerke and van Genuchten, 1993a; Larsbo and Jarvis, 2003], or multi-permeability models [Wu et al., 2004; Greco, 2002; Gwo et al., 1995]. A dual-permeability model conceptualizes the soil porous medium into two interacting and overlapping continua [Šimůnek et al., 2008; Gwo et al., 1995; Simunek et al., 2005; Laine-Kaulio et al., 2014]: a matrix domain with a relatively low permeability that represents the soil micropores, and a preferential flow domain with a relatively high permeability that represents the preferential flow paths. Preferential flow and matrix flow can be simulated simultaneously with two Darcy-Richards equations combined with a water-exchange function [Gerke and van Genuchten, 1993a; Šimůnek et al., 2008]. Shao et al. [2015] applied a 2D dual-permeability model with a hydro-mechanical model for a hypothetical case. No real-world cases have been published where the effects of preferential flow on pressure propagation and landslide-triggering under high intensity rainstorms are quantified with a numerical modeling approach.

The linear-diffusion model is a linearization of the Darcy-Richards equation to approximate the pressure propagation in soils that are fully saturated or near saturation [Iverson, 2000]. The linear-diffusion model has been applied to simulate the observed pressure responses in different landslides [Iverson, 2000; Reid, 1994; D'Odorico et al., 2005] including the Rocca Pitigliana landslide located roughly 50 km south of Bologna [Berti and Simoni, 2012, 2010]. In the latter reference, the authors conclude that the linear-diffusion model was capable of simulating the observed pore water pressure response when the hydraulic diffusivity was treated as a calibration parameter. The measured water pressure response for each rainfall event could only be simulated reasonably well when a different diffusion coefficient was determined through calibration for each

rainfall event. Berti and Simoni [2010] discussed the importance of preferential flow in the Rocca Pitigliana landslide, but did not include it in their model.

In this study, the influence of preferential flow on flow and stability of the Rocca Pitigliana landslide is analyzed and quantified using a 1D coupled dual-permeability hydrology and slope stability model. Results are compared with field observations and with the outcomes of the linear-diffusion model of Berti and Simoni [2010].

## 6.2. FIELD SITE

The Rocca Pitigliana landslide is located roughly 50 km south of Bologna, Italy. Only the essential features of the field site are summarized here; a detailed description can be found in Berti and Simoni [2012]. The slope consists of three main lithostratigraphic units (Figure 6.1): unweathered clay-shale bedrock, a sandy soil above the main scarp, and a clay soil at the toe of the main scarp. Most slope failures develop in the clay soil, which is a landslide deposit consisting of weathered clay-shale with a thickness of 2–4 m and a fairly uniform slope of 15°–20°.



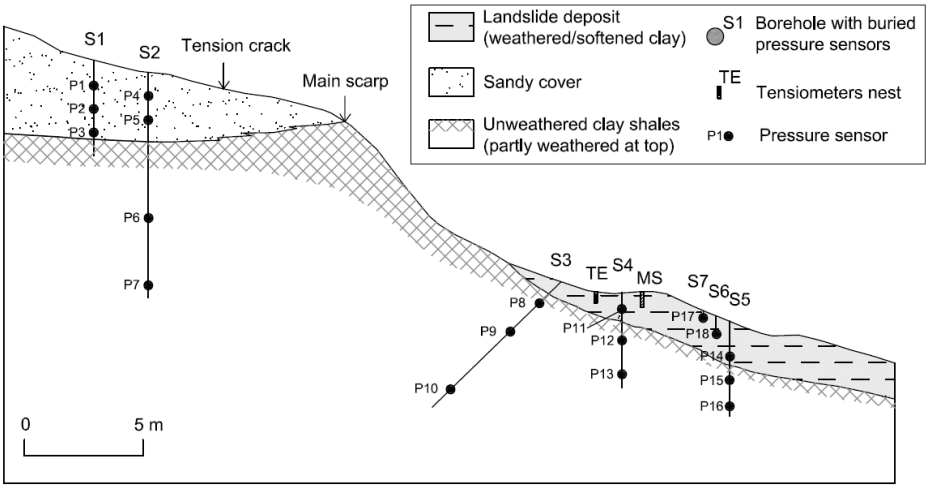


Figure 6.1: Schematic map of a cross section of the Rocca Pitigaliana monitoring system [Berti and Simoni, 2010].

Landslides are periodically reactivated with different velocities in response to rainstorms or snow-melting events. The landslide mass can move slowly with typical velocities of a millimeter up to a centimeter per year. Rapid increase of pore water pressure can be the most important triggering factor for the reactivation of a large part of the landslide.

Five nests of closed pressure sensors were installed at the top and bottom of the

slope, in the sandy and clay covers respectively. The closed pressure sensors were placed in small cotton bags filled with clean fine sand and placed on top of a 20 cm thick layer of sand at the desired depth in the clay cover. Sand was added around and above the sensor to act as a porous filter for accurate measurements with minimal time delay (Berti and Simoni 2010). Three years of pore water pressure dynamics are available.

The rainfall pattern in the study area follows a typical seasonal distribution. Many rainy periods occur during the wet season from late October to May. The dry season is from June to September and may include intermittent storms. Soil moisture measurements indicate that the near-surface clay soil layer (10 – 20 cm depth) experiences a significant variation in water content during evaporation and precipitation events. The water table is close to the ground surface and fluctuates seasonally from tens of centimeters to approximately 1 m below surface. The available water storage in the 2 m thick clay cover varies from 0 mm to approximately 20 mm. During the 3-year monitoring period, most rain-events resulted in pore water pressure increases in the clay cover on the order of 10 to 80 cm, but no clear pore water pressure responses in the underlying clay-shale bedrock were observed, aside from the long-term seasonal fluctuations. Among the 4 sensors buried in the clay cover landslide material (P11, P14, P17, P18) , the pressure head recorded by sensors P11 and P14 have clear responses to more than 70% of the rainfall events [Berti and Simoni, 2012]. The pressure responses in P11 and P14 were selected in this study to facilitate the model comparison with the results of Berti and Simoni [2010].



The hydraulic characteristics of the landslide material are affected by discontinuities and heterogeneities in grain-size and porosity. Saturated hydraulic conductivities were measured with 32 Guelph-Permeameter tests, and showed a wide variability from $5 \times 10^{-4}$ m/s to $1 \times 10^{-9}$ m/s [Berti and Simoni, 2010]. The measured maximum value of the hydraulic conductivity is likely the result of tension cracks, macropores, and the opening of fissures. The clay-shale bedrock has a higher density than the overlying clay, and its saturated hydraulic conductivity is usually lower than $3 \times 10^{-8}$ m/s with an average value of $1 \times 10^{-8}$ m/s. The mean porosity of the clay soil is 0.38, based on 41 samples.

Field investigations in the study area showed that preferential flow paths exist in the clay landslide cover. The clay soil is expansive, and consequently horizontal shrinkage and swelling will easily generate tension cracks that may act as preferential paths. Preferential flow can also occur in other types of macropores, e.g., worm burrows, root channels, and inter-aggregate pores. In the Rocca Pitigliana landslide, there are clear fast pressure response patterns, which are controlled by the large number of tension cracks that exist under low soil moisture conditions in both summer and fall.

## 6.3. LINEAR-DIFFUSION MODEL

Berti and Simoni [2010] used an analytical solution of the linear-diffusion equation as proposed by Iverson [2000] to simulate the pressure propagation in the Rocca Pitigliana landslide. The linear-diffusion equation is a linearized form of the Darcy-Richards equation,

$$\frac{\partial h}{\partial t} = D_0 \cos^2\alpha \frac{\partial^2 h}{\partial z^2} \tag{6.1}$$

where $h$ (L) is the pressure head, $z$ (L) is the vertical coordinate (positive upward), $t$ (T) is time, $\alpha$ is the slope angle, and $D_0$ ($L^2\ T^{-1}$) is the diffusion coefficient. The diffusion coefficient is constant under saturated conditions, but varies under unsaturated conditions. Berti and Simoni [2010] linearized the diffusion equation by using a constant value for $D_0$ for each rain event analyzed.

The linear-diffusion model was able to reproduce the pressure response in the Rocca Pitigliana landslide reasonably well, but uncertainty in parameter estimation is high [Berti and Simoni, 2010]. Berti and Simoni [2010, 2012] found that the diffusion coefficient depends on both the influence of small unsaturated layers and the variation of the soil skeleton stiffness. Consequently, the diffusion coefficient was treated as a model parameters rather than a physical parameter and was calibrated for each rain event. The variation in the values of the calibrated diffusion coefficient can be indicative of the influence of the initial soil moisture conditions and the existence of fissures and cracks [Berti and Simoni, 2012]. In the following, it is proposed to use a modified dual-permeability model combined with a fixed set of parameters to simulate the soil moisture dynamics and pressure response in the Rocca Pitigliana landslide.

## 6.4. 1D DUAL-PERMEABILITY MODEL

Consider a 1D dual-permeability model simultaneously simulating matrix flow and preferential flow in a variably saturated soil. Flow in both the preferential flow domain and the matrix domain is governed by the Darcy-Richards equation

$$C_f \frac{\partial h_f}{\partial t} = \frac{\partial}{\partial z}\left[K_f\left(\frac{1}{\cos^2\alpha}\frac{\partial h_f}{\partial z} + 1\right)\right] - \frac{\Gamma_w}{w_f} \tag{6.2}$$

$$C_m \frac{\partial h_m}{\partial t} = \frac{\partial}{\partial z}\left[K_m\left(\frac{1}{\cos^2\alpha}\frac{\partial h_m}{\partial z} + 1\right)\right] + \frac{\Gamma_w}{w_m} \tag{6.3}$$

where the subscripts $f$ and $m$ denote the preferential flow and matrix flow domain, respectively, $C$ ($L^{-1}$) is the differential water capacity $d\theta/dh$, $K$ ($LT^{-1}$) is the hydraulic conductivity, $w$ (-) is the volumetric fraction, and $\Gamma_w$ ($T^{-1}$) is the water exchange rate between the two domains [Gerke and van Genuchten, 1993b; Arora et al., 2011],

$$\Gamma_w = \alpha_w K_a \left(h_f - h_m\right) \tag{6.4}$$

where $\alpha_w$ ($T^{-2}$) is the water exchange term, $K_a$ ($LT^{-1}$) is the mean value of the hydraulic conductivity between the two domains

$$K_a = \frac{K_m\left(h_f\right) + K_m\left(h_m\right)}{2} \tag{6.5}$$

The Mualem-van Genuchten model is used to describe the hydraulic properties of both the matrix and preferential flow domains [Van Genuchten, 1980]:

$$\Theta = \frac{\theta - \theta_r}{\theta_s - \theta_r} = \begin{cases} \left[1 + |\alpha h|^n\right]^{-m}, & h < 0 \\ 1, & h \geq 0 \end{cases} \tag{6.6}$$

$$K = K_s \Theta^{0.5}\left[1 - \left(1 - \Theta^{1/m}\right)^m\right]^2 \tag{6.7}$$

$$C = \begin{cases} mn\alpha\left(\theta_s - \theta_r\right)\Theta^{1/m}\left(1 - \Theta^{1/m}\right)^m, & h < 0 \\ S_s, & h \geq 0 \end{cases} \tag{6.8}$$

where $\Theta$ (-) is the effective saturation, $\theta$ (-) is the volumetric water content, subscript $r$ and $s$ denote the residual and saturated state, respectively, $S_s$ ($L^{-1}$) denotes the specific storage, and $K_s$ ($LT^{-1}$) is the saturated hydraulic conductivity. $\alpha$ ($L^{-1}$) , $n$ (-), and $m$ (-) are fitting parameters.

The specified infiltration flux $i$ ($LT^{-1}$) at the soil surface is divided over the two domains such that

$$i = w_f i_f + w_m i_m \tag{6.9}$$

where $i_m$ and $i_f$ are the specified fluxes at the surface of the matrix domain and the preferential flow domains, respectively.

It is assumed that preferential flow is not triggered at the beginning of a rain event, so that infiltration starts in the matrix domain

$$i_m = \frac{R}{w_m} \tag{6.10}$$

where $R$ ($LT^{-1}$) is rainfall. The infiltration capacity is the product of the saturated hydraulic conductivity and the pressure head gradient at the soil surface. When the specified flow at the surface of the matrix domain exceeds the infiltration capacity, the boundary condition of the matrix domain changes to a specified pressure head (corresponding to the surface water ponding depth) and the infiltration-excess water is reallocated to the preferential flow domain

$$i_f = \frac{R - w_m i_m}{w_f} \tag{6.11}$$

Once the specified flux into the preferential flow domain is larger than its infiltration capacity, the boundary conditions of both domains are changed to the specified pressure head corresponding to the surface water ponding depth. The maximum ponding depth was set to 1 cm in this study; surface water ponding over 1cm becomes overland flow, which will occur only under heavy rainfall.

The initial pore water pressure distribution is hydrostatic and is computed with the analytical solution for hydrostatic conditions on a hillslope (Lu and Godt 2008, Iverson 2000), which is appropriate as the groundwater table is close to the soil surface at the study site for the entire year. The initial pressure head is given by

$$h(z) = \left(z_g - z\right)\left[\cos^2\alpha - \frac{q_{leak}}{K_s}\cos\alpha\right] \tag{6.12}$$

where $z_g$ is the elevation of the groundwater table, and $q_{leak}$ ($\mathrm{LT}^{-1}$) is the specified groundwater flux that leaks out of the bottom of the clay layer and into the underlying bedrock.



## 6.5. INFINITE-SLOPE STABILITY MODEL

The factor of safety $F_s$ (-) for an infinite slope may be expressed as the ratio of the resisting force to the gravitational driving force and consists of three terms [Lu and Godt, 2008]:

$$F_s(z) = \underbrace{\frac{\tan\phi'}{\tan\alpha}}_{\text{friction angle term}} + \underbrace{\frac{c'}{G\sin\alpha\cos\alpha}}_{\text{cohesion term}} - \underbrace{\frac{\sigma_s}{G}\frac{\tan\phi'}{\sin\alpha\cos\alpha}}_{\text{suction stress term}} \tag{6.13}$$

where $c'(\mathrm{ML}^{-1}\mathrm{T}^{-2})$ is the effective cohesion, and $\phi'$ is the friction angle. $G$ ($\mathrm{ML}^{-1}\mathrm{T}^{-2}$) is the weight of the soil column defined as

$$G = \int_z^0 \left[\gamma_s + \gamma_w\theta\right]\, dz \tag{6.14}$$

where $\gamma_s$ and $\gamma_w$ are the specific weight of the solids and water ($\mathrm{ML}^{-2}\mathrm{T}^{-2}$), respectively, and surface level is at $z = 0$. $\sigma_s$ ($\mathrm{ML}^{-1}\mathrm{T}^{-2}$) is the suction stress, defined as

$$\sigma_s = \chi p_w = \chi\gamma_w h \tag{6.15}$$

where $p_w$ ($\mathrm{ML}^{-1}\mathrm{T}^{-2}$) is the pore water pressure and $\chi$(-) is the matrix suction coefficient, which is approximated by the effective saturation [Lu et al., 2010].

## 6.6. NUMERICAL IMPLEMENTATION

The dual-permeability model is solved numerically with an implicit finite difference method implemented using the Python programming language. Picard iteration is used for each time step [van Dam and Feddes, 2000]. During simulation, the error tolerance of the water content was 0.0001. The time step is adapted in the range of 0.015 – 2 min to ensure numerical accuracy.

The hydrological results are used as input for the soil mechanical calculations. The soil weight was determined from the soil moisture distribution (Equation 6.14) and the suction stress and shear strength were computed from the pore water pressure and effective saturation. It is an unresolved issue in slope stability analysis whether $h_f$ or $h_m$ should be used for the calculation of the suction stress with Equation 6.15. This aspect will be analyzed and discussed in the next few sections.

## 6.7. PARAMETERIZATION

The thickness of the landslide is set equal to the upper 2 m of the clay cover. One hundred cells of 2 cm are used. The slope of the landslide is $\alpha = 20°$. The soil hydraulic parameters for the dual-permeability model are based on Berti and Simoni (2010, 2012). Preferential flow plays an important role in the upper part of the soil layer where macropores and fissures are abundant, whereas macropores are almost non-existent in the lower part of the soil layer. The saturated hydraulic conductivity $K_{sf}$ of the preferential flow domain is represented with an exponential function to simulate this variation

$$K_{sf}(z) = K_{sm} \exp(\beta(z + H)) \tag{6.16}$$

where $H = 2$ m is the thickness of the clay cover and parameter $\beta$ is chosen as $\beta = 3.454$ $m^{-1}$ so that $K_{sf}$ is equal to $K_{sf}(z = 0) = 1000 K_{sm}$ at the soil surface, and exponentially decreases to $K_{sm}$ at the bottom of the model ($z = -H$). The leakage into the bedrock is simulated as a constant flux of $q_{\text{leak}} = 1.5 \times 10^{-8}$ m/s for both domains. This value falls within the range of values estimated by Berti and Simoni [2010].

The volumetric fraction of the preferential flow domain $w_f$ is set to 0.05, so that the volumetric fraction of the matrix domain $w_m$ is 0.95 [Köhne et al., 2002]. The residual water content is set to 0.09 for both domains based on the UNSODA database [Nemes et al., 2001; Leij, 1996]. The measured porosity is 0.38, which is interpreted as the combined saturated water content for the entire domain, and the saturated water contents of the matrix and preferential flow domains are estimated as 0.37 and 0.57, respectively. The Van Genuchten shape parameter $n$ was set to 1.2 and 2.0 for the matrix domain and for the preferential flow domain, respectively, based on the values suggested by Köhne et al. [2002]. The Van Genuchten shape parameter $\alpha$ for the two domains was set to 2.5

and 5.0, respectively, to ensure that the water storage deficit varies from 0 to 20 mm. The water exchange coefficient $\alpha_w$ strongly influences the simulated pressure response in the two domains and is obtained through calibration to the measured pressure dynamics under single-pulse rainfall events (see Section 7.8).

The following parameters are used for the soil mechanics model. The friction angle is $\phi' = 25°$, the cohesion is $c' = 3.5$ kPa, the specific storage is $S_s = 0.001$ m$^{-1}$, the specific weight of dry soil is $\gamma_d = 16.2$ kN/m$^3$, and the specific weight of water is $\gamma_w = 9.8$ kN/m$^3$. The value for cohesion is a representative value for clay; all other values are taken from Berti and Simoni [2010].

## 6.8. MODEL CALIBRATION CRITERIA

The model performance is evaluated by comparing the simulated and observed pressure heads ($h_s$ and $h_o$ ) using the Nash-Sutcliffe coefficient $E_f$ [Nash and Sutcliffe, 1970] :

$$E_f = 1 - \frac{\sum(h_o - h_s)^2}{\sum(h_o - \bar{h}_o)^2} \tag{6.17}$$

where $\bar{h}_o$ is the average observed head. The Nash-Sutcliffe coefficient ranges from $-\infty$ to 1, where 1 indicates a perfect match and 0 means that the model does not do better than the average observed head.



After a rainfall event, the groundwater level recedes slowly back to the pre-event level (the recession period), which is caused by vertical leakage to the bedrock, the evaporation flux, and lateral drainage. The analysis focuses on the fast pore water pressure response (rise and recession) under short-term rainfall events, so the evaporation flux are neglected. The recession curves of pore water pressure during the recession periods can be characterized by an exponential function as:

$$h(t - t_0) = h_0 \exp[-(t - t_0)/\lambda] \tag{6.18}$$

where $h_0$ and $t_0$ are the head and time at the start of the recession, respectively, and $\lambda$ is the depletion factor (T) [e.g., Krzeminska et al., 2014].

## 6.9. CALIBRATION ON PRESSURE RESPONSE TO SINGLE-PULSE RAINFALL

The measured and simulated pressure heads in the matrix and preferential flow domains are compared for two single-pulse rain events that took place in the dry season (Figure 6.2). The comparison is for sensor P11 at 0.7 m depth (Figure 6.1). The first event occurred on 28 July 2003 with a total rainfall of 11 mm in 10 h. The initial groundwater table

was located at 0.7 m below the surface. In the first 4 h, 9 mm of rainfall was recorded, followed with 2 mm in 2 h. This 11 mm rainfall is insufficient to fully saturate the soil profile according to the measured pressure response. The second event occurred on 23 October 2005 with a total rainfall of 8 mm in 3 hours, which was sufficient to cause full saturation due to the wetter initial soil moisture condition of the slope.

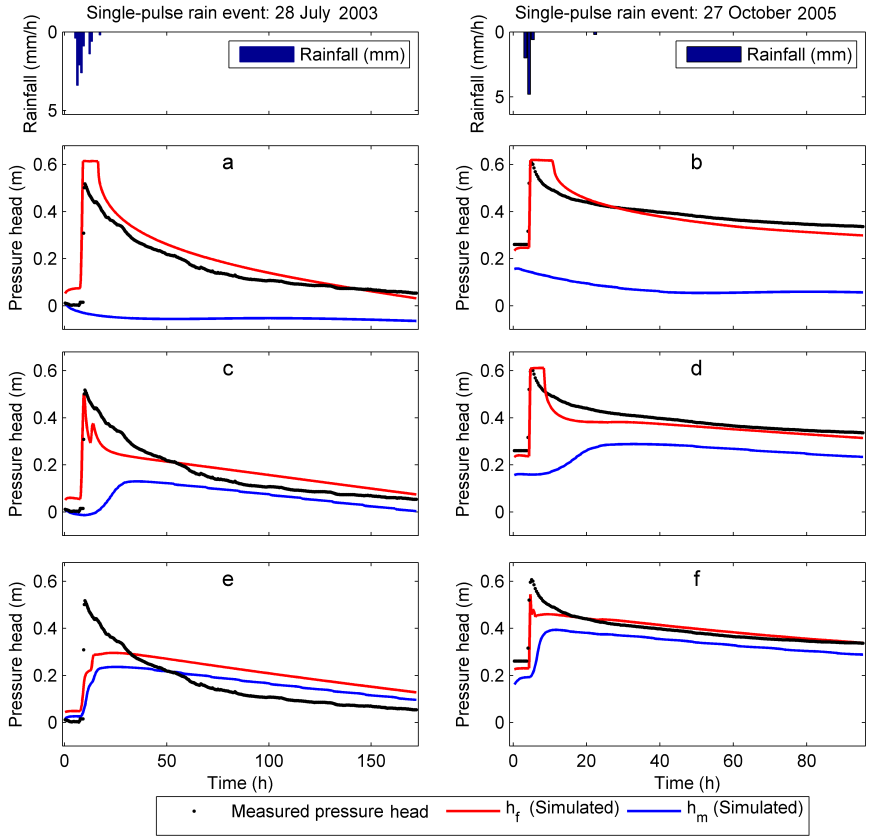


Figure 6.2: Measured and simulated pressure head at 0.7 m depth (sensor P11) in response to two single-pulse rain fall events. The water exchange coefficient is 6 $m^{-2}$ (Figures a,b), 60 $m^{-2}$ (Figures c,d), and 600 $m^{-2}$ (Figures e,f)

The observed and simulated pressure heads for three water exchange coefficients are shown in Figure 6.2. A higher water exchange coefficient represents a stronger hydraulic interaction between the two domains, while a lower water exchange coefficient represents a nearly independent pressure response in the two domains. The two domains have limited hydraulic interaction for the lowest water exchange coefficient of $\alpha_w = 6$ $m^{-2}$ (Figure 6.2a, b), the recession of the head in the preferential flow domain

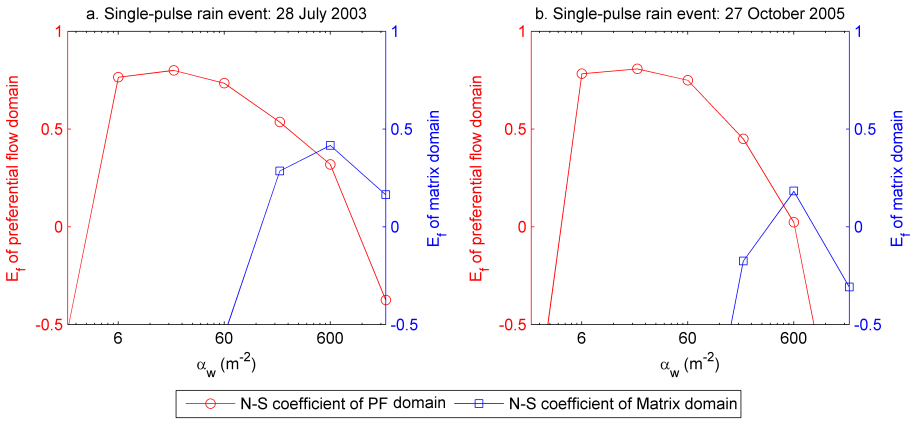


Figure 6.3: Nash-Sutcliffe coefficient vs. the water exchange coefficient for the rainfall events at (a) 8 September, 2003 and (b) 23 October, 2005.

is too slow, and the simulated heads in the matrix domain are unrealistic as they show almost no response to rainfall. The pressure heads are quite similar in both domains for the highest water exchange coefficient of $\alpha_w = 600$ m$^{-2}$ (Figure 6.2e, f), but they deviate significantly from the measurements. The most reasonable result if obtained for the intermediate value of the water exchange coefficient of $\alpha_w = 60$ m$^{-2}$ (Figure 6.2c, d), where the head in the preferential flow domain is a reasonable match of the observed pressure response, and the response in the matrix domain is realistic.

The Nash-Sutcliffe coefficient of the simulated pressure heads is shown as a function of the water exchange coefficient in Figure 6.3; both the head in the preferential flow domain and in the matrix domain are used to compute a Nash-Sutcliffe coefficient. Reasonably high Nash-Sutcliffe coefficients are obtained only for the head in the preferential flow domain and not for the head in the matrix domain. Good model performance is obtained for both rainfall events for water exchange coefficients between 6 and 60 m$^{-2}$, which gives Nash-Sutcliffe coefficients for the head in the preferential flow domain between 0.7 and 0.8.

The recession of the simulated pressure head after a rainfall event in the preferential flow domain is compared to the observed recession for different water exchange coefficients (Figure 6.4). The vertical axis of Figure 6.4 is log-scaled such that, according to Equation 6.18, the recession should be a straight line. A larger depletion factor $\lambda$ means a slower recession and vice versa. The model with a water exchange coefficient of 60 m$^{-2}$ simulates the recession best.

Based on the results of Figures 6.2-6.4, the water exchange coefficient is set to 60 m$^{-2}$ in the remainder of the study as this value gives a reasonable match between the head

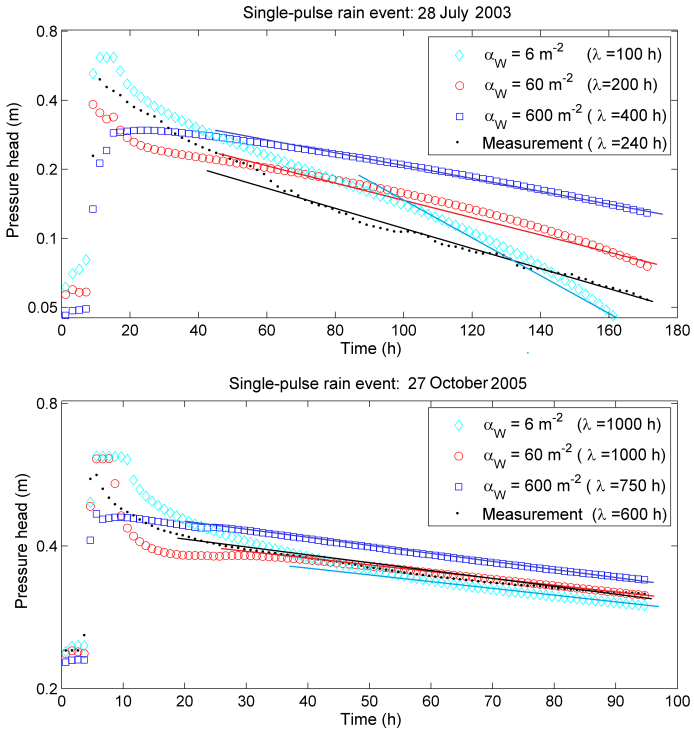


Figure 6.4: Measured recession (sensor P11) and recession of pressure head in preferential flow domain (0.7 m depth) for rainfall event (a) 28 September, 2003 and (b) 23 October 2005. Vertical axis has log scale.

in the preferential flow domain and the observed head for both rainfall events, a realistic variation of the head in the matrix domain, and an acceptable recession of the head in the preferential flow domain as compared to the observed recession.

## 6.10. HYDROLOGIC RESPONSE TO SINGLE-PULSE RAINFALL EVENTS

The simulated water content and pressure head in the preferential flow and matrix domains, and the water exchange between the two domains is shown in the first 80 cm below the surface for the rain event of 28 July, 2003 (Figure 6.5). The initial water exchange between the two domains is negligible (Figure 6.5f), although the initial pressure head in the preferential flow domain is slightly higher than in the matrix domain.

All the rainwater infiltrates into the matrix domain during the first hour, as shown by an increase in water content and pressure head in Figures 6.5b and 6.5c, respectively. Preferential flow became significant after 2 h (purple line in Figure 6.5a). The complex behavior of the water exchange is shown in Figure 6.5f. Near the soil surface, the pres-

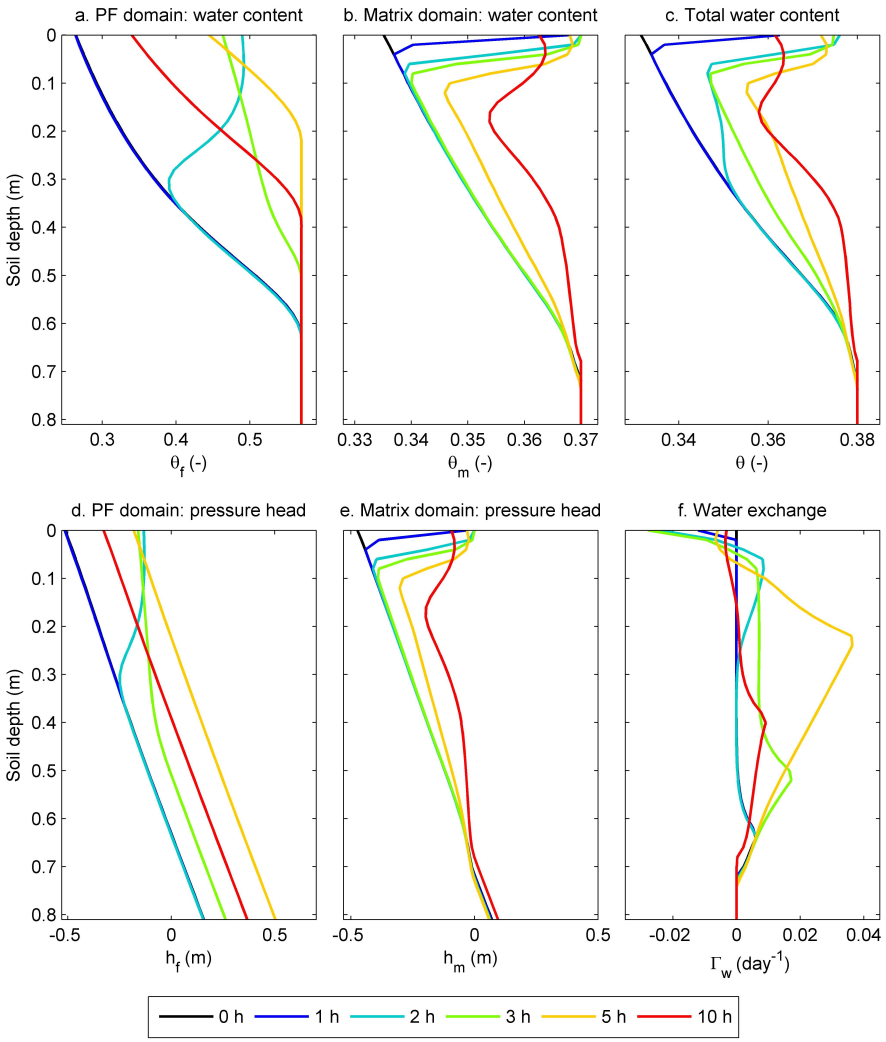


Figure 6.5: Simulated vertical profiles for the first 10 hours of the rain event of 28 July 2003: water content in (a) the matrix domain, (b) the preferential flow domain, and (c) the total domain; pressure head in (d) the matrix domain and (e) the preferential domain; (f) water exchange rate according to Equation 6.4 (positive is from preferential flow domain to the matrix domain).

sure head in the matrix domain is larger than that in preferential flow domain and the direction of the water exchange is from the matrix to the preferential flow domain. The highest water exchange rate occurred after 5 hours when the preferential flow domain was saturated up to 0.2 m depth. After the rain event (10 h), the pressure in the preferential flow domain started to decrease quickly, while the recession of the pressure in the

the matrix domain is much slower.

## 6.11. HYDROLOGICAL RESPONSE TO MULTI-PULSE RAINFALL EVENTS AND RESULTING SLOPE STABILITY

Multi-pulse rainfall events are typical for the summer season. The calibrated values of the single-pulse rain events are used. Two multi-pulse rainfall events are considered. The first event started on 8 September, 2003, and lasted 50 h. The event consisted of 3 rain pulses. The rainfall amounts were 17 mm (duration $T_r = 3$), 2 mm ($T_r = 4$ h), and 6 mm ($T_r = 2$ h), respectively. The second event started on 22 September, 2003, and consisted of 2 rain pulses. The rainfall amounts were 11 mm ($T_r = 10$ h) and 22 mm ($T_r = 3$ h), respectively. The initial groundwater table was approximately at 80 cm below the surface for the first event, and 70 cm below the surface for the second event.

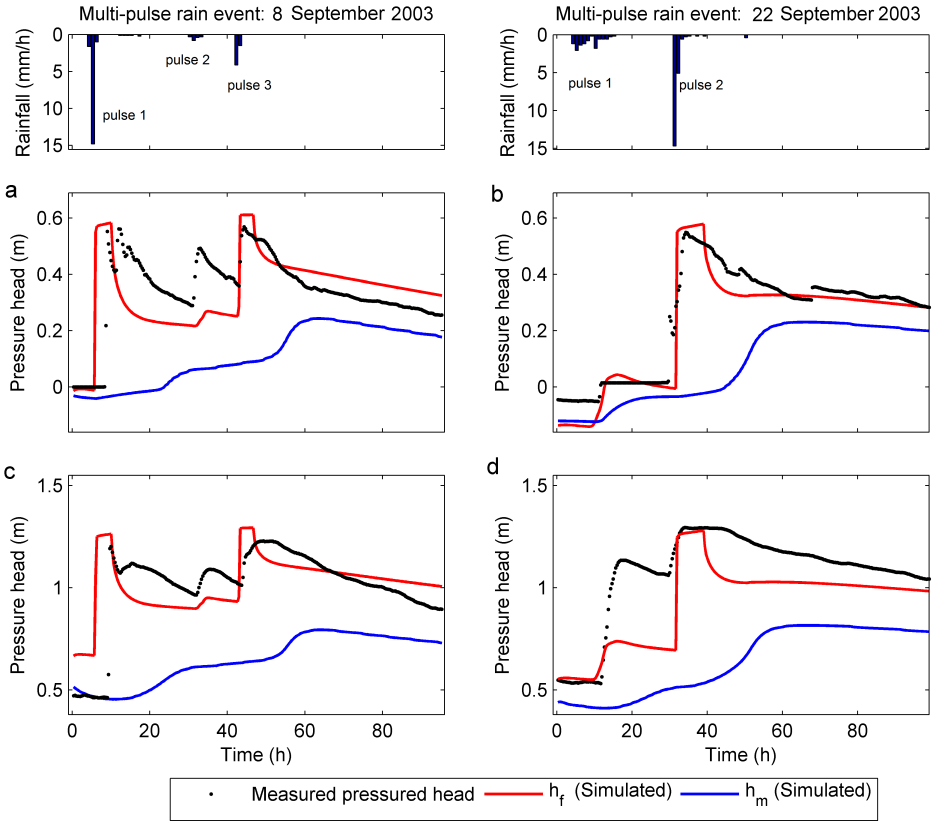


Figure 6.6: Measured and modeled pressure heads at sensor P11 (0.7 m depth, Figures a,b) and sensor P14 (1.5 m depth, Figures c,d) in response to two multi-pulse rainfall events.

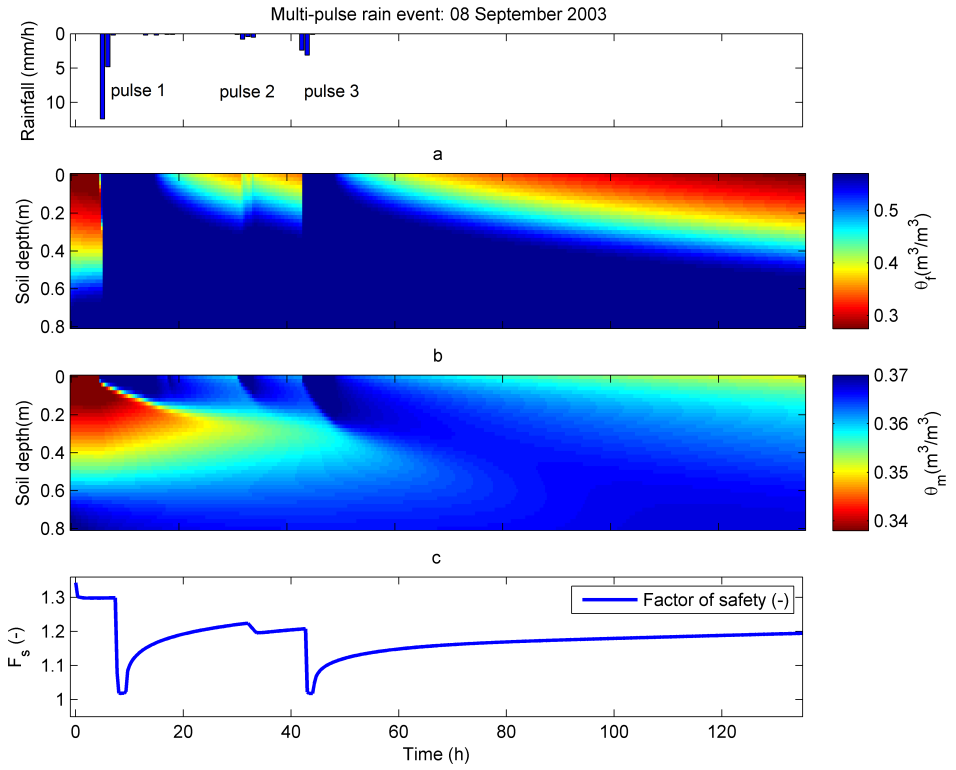


Figure 6.7: Simulated soil water content in (a) preferential flow domain and (b)matrix domain, and (c) factor of safety at 1.5 m depth under the multi-pulse rain event starting on 8 September, 2003.

The measured and simulated pressure responses of the two multi-pulse rainfall events are shown in Figure 6.6 at 0.7 m depth (sensor P11, Figures 6.6a and 6.6b) and 1.5 m depth (sensor P17, Figures 6.6c and 6.6d). It is observed that the first rain pulse during the rain event starting on 8 September 2003 saturated the clay cover in a few hours, which resulted in a rapid observed pressure response to the rain-pulses at $t$ = 35 h and $t$ = 50 h. The first rain pulse (11 mm) of the rain event starting on 22 September 2003 raised the groundwater table from 0.8 m to 0.65 m below the surface, but the measured pressure head in sensor P14 (1.5 m depth) increased to 1.2 m at $t$ = 20 h. The pressure head in sensor P14 increased to 1.3 m at $t$ = 30 h due to the second rain pulse. Overall, the simulated pressure heads in the preferential flow domain show reasonable agreement with the measured values, although the second peak is missed for the event starting on 8 September, 2008. The simulated pressure head in the matrix domain deviates significantly from the measured pressure heads and shows a delayed response.

Soil moisture profiles during the multi-pulse rainfall event starting on 8 September

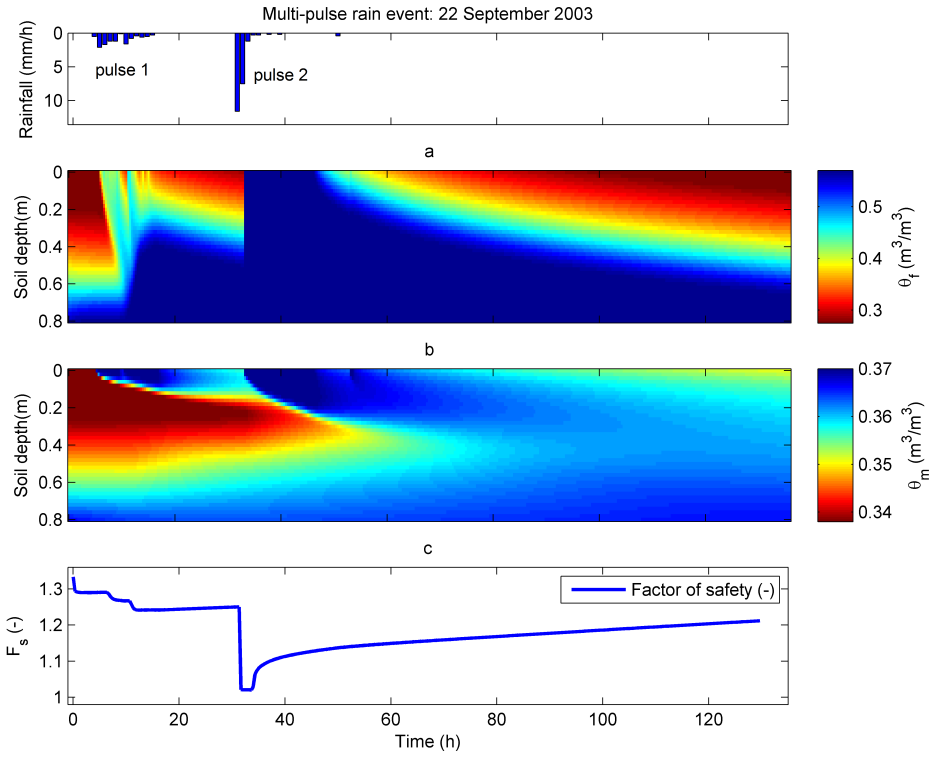


Figure 6.8: Simulated soil water content in (a) preferential flow domain and (b) matrix domain, and (c) factor of safety at 1.5 m depth under the multi-pulse rain event starting on 22 September, 2003

2003 are presented in Figures 6.7a and b to analyze the wetting front propagation in both domains. The factor of safety for a slip surface located at 1.5 meter depth is presented in Figure 6.7c. The model results show that the first rain pulse of 17 mm in 2 hours saturated the preferential flow domain (Figure 6.7a), while the wetting front propagation in the matrix domain was much slower (Figure 6.7b). The rain pulse increased both the pressure head and water content and reduced the factor of safety from 1.36 to 1.02 (Figure 6.7c). The second rain pulse had a low intensity (< 1 mm/h) and induced a wetting front in the matrix domain, while the effect on the pressure response in the preferential flow domain and estimated factor of safety was negligible, although the measured pressure head increased significantly. The difference between the measured pressure response and the simulated response in the preferential flow domain may be caused by an underestimation of water exchange flux from the matrix domain to the preferential flow domain. Alternatively, the measured pressure response may be correlated more significantly to the pressure head in the matrix domain for small rainfall events. The third

rain-pulse of 6 mm in 2 h caused wetting fronts in both domains, which resulted in lower slope stability for a short period.

Soil moisture profiles during the multi-pulse rainfall event starting on 22 September 2003 are presented in Figures 6.8a and b. The factor of safety for a slip surface located at 1.5 meter depth is presented in Figure 6.8c. The first pulse of 11 mm with an intensity of less than 2 mm/h did not saturate the slope, but caused an increase of pore water pressure and water content in both domains. After 10 hours, the factor of safety had dropped from 1.32 to 1.22. A second rain-pulse of 22 mm in 2 hours took place about 40 h later. This large amount of rainfall saturated the slope fully, and the factor of safety at 1.5 m depth dropped as low as 1.05.

## 6.12. PRESSURE RESPONSE DURING THE EARLY WINTER SEASON

The simulations described in the previous deal with summer and early fall conditions in which, for example, desiccation cracks are clearly visible. A winter season event was analyzed to assess the performance of the dual-permeability model under wetter initial conditions. The evaporation rate is low during the wet season, the clay soil is nearly saturated, and desiccation cracks are essentially absent. Under these conditions, it may be expected that the pore pressure response is controlled by matrix flow. A period of 21 days is simulated from 21 December 2003 to 11 January 2004, during which the pressure response was not affected by frozen soil or snow cover. The measured rainfall and measured and simulated pressure response at 70 cm depth are shown in Figure 6.9.

The initial pressure head at 70 cm depth is approximately 45 cm, which implies the slope is close to full saturation. During the 21-day period, the total rainfall is 66 mm, consisting of 3 rain pulses of 4.3 mm (6 h), 57.8 mm (80 h), and 3 mm (8 h). The intermittent recession periods are 180 h and 35 h, respectively.

The measured pressure head reaches a peak of 62 cm after the first and second rain pulse (Figure 6.9). The matrix domain and preferential flow domain are both initially near saturation, which implies similar pressure responses in both domains. The measured pressure response to the first rain pulse is nearly instantaneous, while the measured pressure response to the second rain pulse shows a considerable time delay. The first peak was captured well by the dual-permeability model, but the model overestimates the pressure response of the second rain pulse, and its timing is 30 h early. Following the rain pulses, the measured pressure recession is described reasonably well by the pressure of the preferential flow domain, although the flattening of the recession in the middle stage of the recession was not simulated accurately.

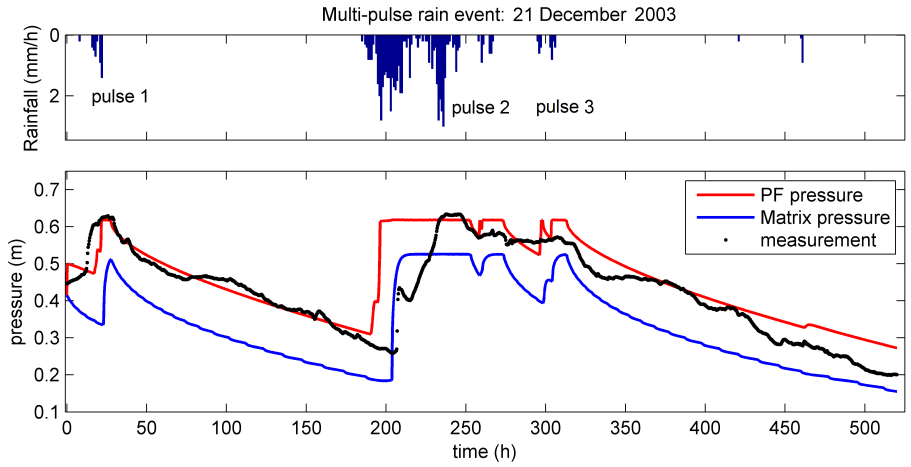


Figure 6.9: Comparison between measured and simulated pressure head in the clay cover (at depth 70 cm measured by P11 sensor) using dual-permeability model during the selected early winter period of 2003.

## 6.13. COMPARISON WITH THE LINEAR-DIFFUSION MODEL



Performance of the linear-diffusion model of [Berti and Simoni, 2010] and the dual-permeability model presented here are compared in Table 3 through evaluation of the Nash-Sutcliffe coefficient at a depth of 70 cm. The performance is quite good for both models during the two single-pulse events used for calibration of the dual-permeability model. The diffusion coefficient $D_0$ is calibrated separately for each rain event for the linear-diffusion model. The calibrated values of $D_0$ range from $3.5 \cdot 10^{-6}$ to $7.0 \cdot 10^{-5}$ $m^2/s$. A linear-diffusion model with one value for the calibrated diffusion coefficient for all events gave unsatisfactory results in a prior study [Berti and Simoni, 2010]. Recall that for the dual-permeability model the exchange coefficient $\alpha_w$ was calibrated on the data of the first two single-pulse events, after which all parameters were fixed for the other multi-pulse rain events. Performance of the dual-permeability model for the three multi-pulse events gave two low and one high Nash-Sutcliffe coefficient.

Table 6.1: Nash-Sutcliffe coefficient of the pressure head at 70 cm depth and the calibrated value of the diffusion coefficient for the linear-diffusion model

| Event | Dual-permeability | Linear-Diffusion |
|---|---|---|
| 28-Jul-2003 | 0.669 (Calibration) | 0.680 (Calibrated $D_0$=$3.0 \times 10^{-5}$ $m^2/s$) |
| 27-Oct-2005 | 0.772 (Calibration) | 0.878 (Calibrated $D_0$=$7.0 \times 10^{-5}$ $m^2/s$) |
| 08-Sep-2003 | 0.105 (Validation) | 0.512 (Calibrated $D_0$=$6.0 \times 10^{-5}$ $m^2/s$) |
| 22-Sep-2003 | 0.882 (Validation) | 0.369 (Calibrated $D_0$=$2.0 \times 10^{-5}$ $m^2/s$) |
| 28-Dec-2003 | 0.386 (Validation) | -0.572 (Calibrated $D_0$=$3.5 \times 10^{-6}$ $m^2/s$) |

Table 6.2: Difference in peak height and arrival, and the estimated depletion factor for dual-permeability model (Dual), linear-diffusion model (Diff), and measurements (Meas)

| Rain Event | | Peak height (m) | | Peak arrival (h) | | Depletion factor (h) | | |
|---|---|---|---|---|---|---|---|---|
| Date | Pulse | Dual | Diff | Dual | Diff | Meas | Dual | Diff |
| 28/7/2003 | Single | -0.02 | -0.13 | -0.3 | 5 | 200 | 270 | 352 |
| 27/10/2005 | Single | 0.02 | 0.01 | -0.3 | 1 | 670 | 740 | 725 |
| 8/9/2003 | First | 0.02 | -0.2 | -2 | -1.7 | 100 | 260 | 60 |
| 8/9/2003 | Second | -0.25 | 0.1 | 1.3 | 2 | 110 | 235 | 50 |
| 8/9/2003 | Third | 0.03 | 0.03 | -1 | 0.3 | 190 | 310 | 185 |
| 22/9/2003 | First | 0.02 | 0.4 | 1 | 7 | 1270 | 600 | 100 |
| 22/9/2003 | Second | 0.03 | -0.03 | -2 | 8 | 250 | 500 | 140 |
| 28/12/2003 | Second | -0.01 | -0.08 | -30 | 50 | - | - | - |
| 28/12/2003 | Third | 0.05 | -0.02 | -10 | 20 | 400 | 555 | 2500 |

Comparison between the measured and simulated pressure heads at 70 cm depth for the two models is shown in Figure 6.10 for all five rain events presented in the previous sections; the head in the preferential flow domain is shown for the dual-permeability model. The 21-day multi-pulse rain event starting on 21 December 2003 is shown starting on 28 December, since the linear-diffusion model cannot simulate such a long period. The pressure heads simulated with the linear-diffusion equation show a relatively slow rise of the pore water pressure in Figures 10 a, d, and e, because the calibrated diffusion coefficients are relatively low. The simulated pore water pressure increase is much faster for the two events with larger calibrated pore diffusion coefficients (Figures 6.10 c-d).

The reliability of the slope stability analysis depends on the accuracy of the simulation of both the arrival time and magnitude of the pressure peak. The pressure response is simulated quite well by both models when the initial groundwater level is high (Figure 6.10b), but performance is mixed when initial groundwater levels are lower (Figures 10a, c, d). For the other events, the linear-diffusion model either underestimates the peaks (Figure 6.10a, and first peak of Figure 6.10c), while the first peak is significantly overestimated in Figure 6.10d. On the other hand, the linear-diffusion model is able to simulate the recession quite well. The dual-permeability model is able to simulate the timing of the peaks quite well for most pulses, but it overestimates the duration of the peak pore water pressure and the simulated recession is faster than observed. The performance for initially low groundwater levels may be improved by using a variable $\alpha_w$, but that is beyond the scope of this paper.

The differences in height and timing of the pressure peaks of the two models are summarized in Table 6.2, which also includes estimates of the observed and simulated depletion factors. Simulation of the peak heights is similar for both models, but the tim-

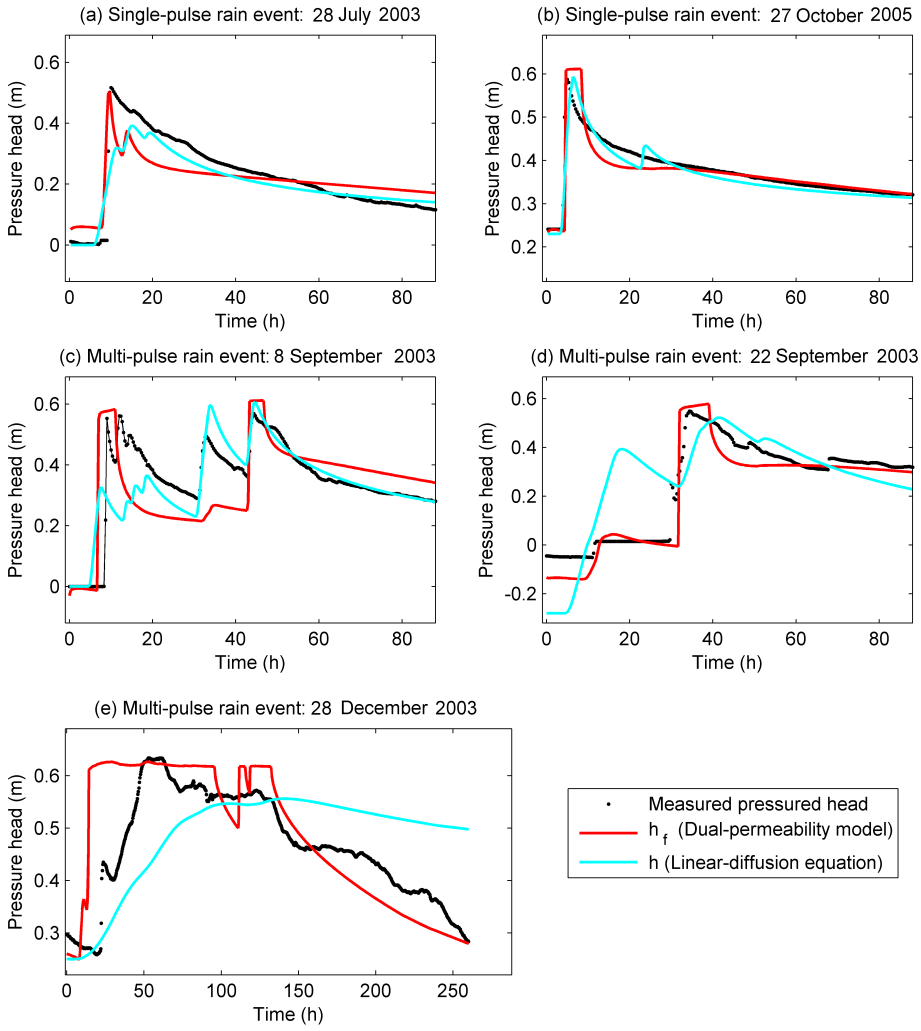


Figure 6.10: Comparison between measured and simulated pressure head at 70 cm depth using the dual-permeability and the linear-diffusion equation for five rainfall events.

ing is significantly better with the dual-permeability model. The depletion factors of the final parts of the recession curves are simulated better by the linear-diffusion model while the dual-permeability model consistently overestimates the depletion factors.

## 6.14. CONCLUSIONS

Berti and Simoni [2010] showed that high pore water pressures in the Rocca Pitigliana

landslide are strongly correlated to landslide movement. Berti and Simoni [2010] simulated the observed pore water pressure response with a 1D linear-diffusion model where the diffusion coefficient was treated as a model parameter (rather than a physical parameter) that needed to be calibrated for each rain event separately. In this paper, a 1D dual-permeability model was developed to simulate the measured pressure response to rainfall. All parameters in the model were taken from Berti and Simoni [2010] and other literature, except for the water exchange coefficient between the matrix domain and the preferential flow domain. Extensive simulations showed that observed pressure response can be simulated quite well by the pressure response in the preferential flow domain for an appropriate value of the water exchange coefficient, while the pressure response in the matrix domain did not match the observed pressure response very well for any values of the water exchange coefficient. Based on the numerical simulations, It is concluded that the pressure response in the preferential flow domain is representative of the observed pressure response and, hence, is expected to be correlated with landslide movement.

The developed dual-permeability model was calibrated on two single-pulse rain events, one on 28 July 2003, and one on 27 October 2005 to obtain a calibrated value of the water exchange coefficient. Performance of the dual-permeability model for these single-pulse rain events was similar to the linear diffusion model (with a different calibrated diffusion coefficient for each event), where the dual-permeability model was better at matching the peaks and the linear-diffusion model was better at simulating the recession.

The calibrated dual-permeability model, with the same parameters, was used to simulate two multi-pulse rain events in late summer, one starting on 8 September, 2003, and the other starting on 22 September 2003. The dual-permeability model was able to simulate the height and timing of the pressure peaks quite well, except for the response to the second pulse on 8 September 2003 (Figure 6.10c). The linear-diffusion model did not do as well for these multi-pulse events, even though a different diffusion coefficient was calibrated for each event.

Finally, the dual-permeability model was applied to simulate the 21-day pressure response to a multi-pulse event in early winter, starting on 21 December 2003. The dual-permeability, again with the parameters calibrated on two single-pulse events, gave an unexpectedly good match: the recession and peaks were simulated quite well although the periods of peak pressure were too long. In contrast, the linear-diffusion model is not able to simulate even a 10-day period of the pressure response to this rain event (Figure 6.10c).

In conclusion, the developed 1D dual-permeability model performed reasonably well to simulate the measured pressure response in the Rocca Pitigliani landslide after it was calibrated on just two single-pulse rain events. The model was able to simulate the pres-

sure response due to rain events consisting of one or more rain pulses in both the summer and the early winter. As such, the 1D dual-permeability model is a promising approach to simulate the pressure response in similar landslides under similar climatological conditions.

# 7

# CONCLUSIONS AND DISCUSSION

## 7.1. CONCLUSIONS

The main objective of this thesis is to investigate the influence of preferential flow on hillslope hydrology and landslide-triggering by a numerical modeling approach. Matrix flow is the relatively slow movement of water through micropores, whereas preferential flow is the rapid water movement through connected macropores and other high-permeability zones, which form only a fraction of the soil pores. Research in the past decades showed that preferential flow is the dominant flow mechanism in soils, whereas the vast majority of numerical models for the simulation of subsurface flow simulate matrix flow only. This results in problems with the quantification of travel times through the subsurface. In a potentially unstable slope, the preferential flow bypasses the soil matrix and results in a fast pressure propagation that affects the timing and magnitude of slope failure. Note that this can be both positive in case of fast drainage of water through preferential flow parallel to the slope, or negative, when the infiltration flux is larger than the drainage flux and the pore-pressure builds up. Hydro-mechanical models need to include preferential flow to quantify and predict the response of slope stability to precipitation.

The necessity of the quantification of the impact of preferential flow on slope stability was discussed in the review of Chapter 2. This review of theories and approaches in hydro-mechanical modeling summarizes the physical processes and mathematical descriptions of soil water transport and slope stability principles, which are strongly intertwined. Different preferential flow models to simulate water flow through matrix and preferential flow paths include the Darcy-Richards equation, the kinematic wave equation, and a simple water storage function. Almost none of these dual-permeability models have been incorporated in soil mechanical models, even through widespread agreement was found that preferential flow takes place in hillslopes and can strongly influence the location, timing, and magnitude of slope failure. The conclusion of this chapter is that an urgent need exists to develop an integrated numerical modeling approach to

study the combined effect of preferential flow on hillslope hydrology and soil stability.

A theoretical analysis of water flow in soils based on the pore bundle model was presented in Chapter 3. The soil is conceptualized as groups of tubes having no interaction between each other, and the celerity is found to equal the maximum water velocity. The celerity equation is derived from the soil hydraulic conductivity function and can be used to derive the breakthrough curve of a conservative tracer through unsaturated soils. Typical soils were analyzed, which showed that preferential flow velocities can be significantly larger than matrix flow velocities, and that the preferential flow dictates the water and tracer transport in the vadose zone. The ratio between the maximum tracer velocity and the average tracer velocity is fairly constant, and its value is related to soil texture. The maximum velocity can be used to predict the first arrival time of a conservative tracer.

In Chapter 4, a synthetic study was described that investigated the effect of preferential flow on the stability of landslides through 2D numerical simulations of rainfall events on a hillslope. Numerical experiments were carried out with both a single-permeability model (no preferential flow) and a dual-permeability model (with 10% preferential flow paths homogeneously distributed through the hillslope). The simulated pressure responses were used in a local factor of safety approach to calculate slope stability and failure area. For low intensity rainfall, the failure area is significantly larger for the single-permeability model; this showed that preferential flow may have a positive effect on slope stability. In this case of low-intensity long-duration rainfall, the preferential flow drains water from the matrix domain and decreases the water pressure. In contrast, during high intensity rainfall, the rainfall intensity is larger than the infiltration capacity of the soil matrix, so that most of the rainfall infiltrates into the preferential flow domain. As a result, the pore water pressure increases very quickly in the preferential flow domain, resulting in a much larger failure area than in the single-permeability model.



In Chapter 6, the Rocca Pitigliana landslide was considered. The Rocca Pitigliana landslide is a well-monitored landslide located roughly 50 km south of Bologna, Italy, and consists mainly of unweathered and weathered clay-shales. This landslide is periodically reactivated with different velocities in response to rain events or snow-melt. Previous studies of the landslide showed that the pressure response in the soil could be modeled using a 1D linear-diffusion approach based on a single-permeability model, where the diffusion coefficient was treated as a model parameter (rather than a physical parameter) that was calibrated for each rain event separately. Field investigations indicated that preferential flow paths (e.g., tension cracks and macropores) are widespread in the Rocca Pitigliana clay landslide cover, so that the fast pressure response is possibly induced by preferential flow, which can not be simulated with the 1D linear-diffusion equation. In this thesis, a 1D dual-permeability model with an infinite-slope stability approach was proposed. In Chapter 5, a new coupled 1D dual-permeability and soil sta-

bility model was developed. The hydrological component of the new model was benchmarked against the HYDRUS-1D software.

The developed 1D dual-permeability model was applied to the Rocca Pitiglana landslide and was calibrated on two single-pulse rain events to obtain a value for the water exchange coefficient between the matrix and preferential flow domains; all other parameters were taken from the literature. The results of this analysis were described in Chapter 6. Performance of the dual-permeability model for these single-pulse rain events was similar to the 1D linear-diffusion model (with a different calibrated diffusion coefficient for each event), where the dual-permeability model was better at matching the peaks and the linear-diffusion model was better at simulating the recession. The calibrated 1D dual-permeability model was used to simulate two multi-pulse rain events in late summer, and was able to simulate the height and timing of the pressure peaks quite well. The 1D linear-diffusion model did not do as well for these multi-pulse events, even though a different diffusion coefficient was calibrated for each event. Finally, the 1D dual-permeability model was applied to simulate a 21-day pressure response to a multi-pulse event in early winter. The dual-permeability, still only calibrated on two single-pulse events in the summer, gave an unexpectedly good match: the recession and peaks were simulated quite well although the periods of peak pressure were too long. In contrast, the 1D linear-diffusion model was not able to simulate even a 10-day period of the 21-day pressure response. In conclusion, the 1D dual-permeability model performed quite well on the Rocca Pitiglana landslide, and is a promising model for other landslides under similar conditions.



## 7.2. DISCUSSION

### 7.2.1. MODELING APPROACH FOR PREFERENTIAL FLOW

The two most common preferential flow modeling approaches are the pore network model and the dual-permeability model. The selection of the modeling approach includes consideration of the computational demands and required parameters. The pore network model requires detailed knowledge of the location, geometry, and hydraulic properties of each individual preferential flow path. A pore network model is well-suited for the simulation of coupled water and solute transport in a network of distinguishable fractures in bedrock or water-sculpted pipes in fine textured soils, but it is not commonly applied in hillslope and catchment hydrological studies. In a natural slope, macropores are abundant, and a detailed investigation and statistical representation of the distribution of macropores at the hillslope scale is cumbersome if not impossible. A dual-permeability model is more appropriate and relatively easy to implement for hillslope hydrology as it considers evenly-distributed preferential flow paths as the second continuum. In this study, the preferential flow domain has no specific direction, and the

pore structure is reflected in the volumetric percentage of macropores and the soil hydraulic functions.

A challenge is how to incorporate the anisotropic soil hydraulic characteristics in a dual-permeability model. Preferential flow paths are not always randomly distributed in the subsurface. For example, drying and swelling cracks in clay soils result in vertical preferential flow paths at the surface. On a hillslope scale, preferential flow paths are often parallel to the slope due to, for example, animal burrows and decayed roots, and the regolith-bedrock interface. Another example is pipe flow, which is defined as a water-sculpted macropore (although it often starts as a regular macropore) where fine-textured soil particles erode due to concentrated throughflow. The measurement of the geometry of preferential flow paths (e.g., density and orientation) is a challenge where geophysical methods such as ground-penetrating radar may aid in the identification of preferential flow paths.

In dual-permeability models, different theories for preferential flow exist, including capillary flow, film flow, and turbulent non-Darcian flow. Correspondingly, the Darcy-Richards equation, Kinematic Wave equation, or non-Darcian flow equation may be selected to simulate preferential flow. When the Kinematic Wave equation is used, it is difficult to simulate the build-up of water pressure in the preferential flow domain, which means it is difficult to be coupled with a soil mechanical model. Furthermore, flow in the preferential flow paths may develop from laminar to turbulent, which means that the relation between specific discharge and pressure gradient becomes non-linear. The non-Darcian flow equation can potentially simulate preferential flow with more comprehensive fluid mechanisms, but it is not widely used. The majority of the current preferential flow models assume that water through a preferential path obeys Darcy's law. The challenge in application of these models lies in the fact that the model performance relies strongly on the parameterization, as discussed in the following.



### 7.2.2. POTENTIAL OF USING A TRACER APPROACH TO PARAMETERIZE DUAL-PERMEABILITY MODELS

The performance of a dual-permeability model in landslide hydrology depends on the parameterization of the hydraulic properties of the matrix and preferential flow domains. The two domains cannot be measured separately in experiments, which makes it difficult to determine representative parameter sets for the two domains. In Chapter 3, the analysis of a bimodal soil hydraulic function shows that different parameter sets may results in similar water retention curves and soil hydraulic functions, but their celerity differs significantly. The celerity can be measured through a tracer experiment (first arrival time), which in turn can be used to estimate a unique parameter set for a dual-permeability model.

Krzeminska et al. [2014] followed a similar idea, but derived volumetric ratios rather than first arrival times. They showed that a tracer experiment in a hillslope can be used to estimate the hydraulic characteristics of the subsurface flow system. Based on tracer and water balance principles, the measured artificial and environmental tracer in groundwater or streamflow can be used to calculate the relative percentages of preferential and matrix flow. Future experimental and numerical modeling studies on rainfall-triggered landslides can use the joint measurements of specific discharge, soil moisture, pressure head, and tracer concentration to infer flow paths and residence times for the parameterization of dual-permeability models to enhance the reliability to simulate hydrological and soil mechanical processes.

### 7.2.3. OTHER PROCESSES THAT AFFECT LANDSLIDE FORECASTING

The performance of hydro-mechanical models for rainfall-induced landslide forecasting depends on the identification of realistic landslide triggering mechanisms and the selection of correct mathematical descriptions reflecting these mechanisms. Landslide-triggering is related to many factors, including hydrological, geomorphological, geotechnical, and ecological processes [Sidle and Bogaard, 2016]. Most of the current studies only focus on one or two of these factors. This thesis mainly focuses on short-term landslide-triggering mechanisms, as the impact of preferential flow on hillslope hydrology and landslide-triggering is usually significant during a rain event. The local factor of safety approach and infinite slope stability approach adopted in this thesis are stress-field based approaches that do not consider plastic deformation of the soil, even through the post failure deformation of the landslide material is an important factor for landslide hazard prediction. It is necessary to couple dual-permeability models with advanced soil mechanical modeling approaches to account for the interaction between preferential flow and slope displacement.

Long-term modeling considers both short-term hydrometeorological triggers and long-term causes of landslide triggering. The prediction of slope stability under long-term processes (multiple years) is still a major challenge. Long-term processes include vegetation dynamics, global changes, and soil weathering processes. The soil hydraulic properties and soil mechanics properties are gradually influenced by a number of processes: chemical weathering and internal erosion in specific flow paths or areas; vegetation dynamics that affect transpiration, interception, and root strength; bioactivity or soil moisture cycling that generate new macropores; and the mechanical feedback of landslide deformation on fissure generation and excess pore-pressure build-up. Current studies commonly focus on one or two of these aspects. The interaction between all these processes and their impact on landslides is not well understood, and requires further research to better forecast the hydrology, slope stability, and movement of landslides.

# REFERENCES


Abramson, L. W.: Slope stability and stabilization methods, John Wiley and Sons Incorporated, 2002.

Aleotti, P. and Chowdhury, R.: Landslide hazard assessment: summary review and new perspectives, Bulletin of Engineering Geology and the Environment, 58, 21–44, doi:10.1007/s100640050066, 1999.

Allaire, S. E., Roulier, S., and Cessna, A. J.: Quantifying preferential flow in soils: A review of different techniques, Journal of Hydrology, 378, 179–204, doi:j.jhydrol.2009.08.013, 2009.

Armstrong, A. C., Matthews, A. M., Portwood, A. M., Leeds-Harrison, P. B., and Jarvis, N. J.: CRACK-NP: A pesticide leaching model for cracking clay soils, Agricultural Water Management, 44, 183–199, doi:S0378-3774(99)00091-8, 2000.

Arnone, E., Noto, L. V., Lepore, C., and Bras, R. L.: Physically-based and distributed approach to analyze rainfall-triggered landslides at watershed scale, Geomorphology, 133, 121–131, doi:j.geomorph.2011.03.019, 2011.

Arora, B., Mohanty, B. P., and McGuire, J. T.: Inverse estimation of parameters for multidomain flow models in soil columns with different macropore densities, Water Resources Research, 47, W04 512, doi:10.1029/2010WR009451, 2011.

Asch, T. V., Buma, J., and Beek, L. V.: A view on some hydrological triggering systems in landslides, Geomorphology, 30, 25 – 32, doi:10.1016/S0169-555X(99)00042-2, 1999.

Baum, R. L., Godt, J. W., and Savage, W. Z.: Estimating the timing and location of shallow rainfall-induced landslides using a model for transient, unsaturated infiltration, Journal of Geophysical Research: Earth Surface, 115, F03 013, doi:10.1029/2009jf001321, 2010.

Bear, J.: Dynamics of fluids in porous media, Dover Publications; Revised edition (September 1, 1988), 1988.

Beckers, J. and Alila, Y.: A model of rapid preferential hillslope runoff contributions to peak flow generation in a temperate rain forest watershed, Water Resources Research, 40, 1–15, doi:10.1029/2003WR002582, 2004.

Berti, M. and Simoni, A.: Field evidence of pore pressure diffusion in clayey soils prone to landsliding, Journal of Geophysical Research: Earth Surface, 115, 1–20, doi:10.1029/2009JF001463, 2010.

Berti, M. and Simoni, A.: Observation and analysis of near-surface pore-pressure measurements in clay-shales slopes, Hydrological Processes, 26, 2187–2205, doi:10.1002/hyp.7981, 2012.

Beven, K.: Kinematic subsurface stormflow, Water Resources Research, 17, 1419–1424, doi:10.1029/WR017i005p01419, 1981.

Beven, K. and Germann, P.: Macropores and water flow in soils, Water Resources Research, 18, 1311–1325, doi:10.1029/WR018i005p01311, 1982.

Beven, K. and Germann, P.: Macropores and water flow in soils revisited, Water Resources Research, 49, 3071–3092, doi:10.1002/wrcr.20156, 2013.

Blume, T. and van Meerveld, H. I.: From hillslope to stream: methods to investigate subsurface connectivity, Wiley Interdisciplinary Reviews: Water, 2, 177–198, doi:10.1002/wat2.1071, 2015.

Bogaard, T.: Analysis of hydrological processes in unstable clayey slopes, Doctoral thesis, Universiteit Utrecht, 2001.

Bogaard, T. A. and Greco, R.: Landslide hydrology: from hydrology to pore pressure, Wiley Interdisciplinary Reviews: Water, 3, 439–459, doi:10.1002/wat2.1126, 2016.

Bogner, C., Trancón y Widemann, B., and Lange, H.: Characterising flow patterns in soils by feature extraction and multiple consensus clustering, Ecological Informatics, 15, 44–52, doi:j.ecoinf.2013.03.001, 2013.

Borga, M., Dalla Fontana, G., and Cazorzi, F.: Analysis of topographic and climatic control on rainfall-triggered shallow landsliding using a quasi-dynamic wetness index, Journal of Hydrology, 268, 56–71, doi:S0022-1694(02)00118-X, 2002a.

Borga, M., Dalla Fontana, G., Gregoretti, C., and Marchi, L.: Assessment of shallow landsliding by using a physically based model of hillslope stability, Hydrological Processes, 16, 2833–2851, doi:10.1002/hyp.1074, 2002b.

Brinkgreve, R., Engin, E., Swolfs, W., Waterman, D., Chesaru, A., Bonnier, P., and Galavi, V.: PLAXIS 2D 2010, Tech. rep., PLAXIS B.V., 2010.

Brooks, R. and Corey, A.: Hydraulic Properties of Porous Media, Colorado State University, 1964.

Brunsden, D.: Some geomorphological considerations for the future development of landslide models, Geomorphology, 30, 13 – 24, doi:10.1016/S0169-555X(99)00041-0, 1999.

Brusseau, M. and Rao, P.: Modeling solute transport in structured soils: a review, Geoderma, 46, 169 – 192, doi:10.1016/0016-7061(90)90014-Z, 1990.

Burdine, N. et al.: Relative permeability calculations from pore size distribution data, Journal of Petroleum Technology, 5, 71–78, doi:10.2118/225-G, 1953.

Campbell, G. S.: A simple method for determining unsaturated conductivity from moisture retention data., Soil science, 117, 311–314, doi:10.1097/00010694-197406000-00001.

Celia, M. A., Reeves, P. C., and Ferrand, L. A.: Recent advances in pore scale models for multiphase flow in porous media, Reviews of Geophysics, 33, 1049–1057, doi:10.1029/95RG00248, 1995.

Chang, X., Hu, C., Zhou, W., Ma, G., and Zhang, C.: A combined continuous-discontinuous approach for failure process of quasi-brittle materials, Science China Technological Sciences, 57, 550–559, doi:10.1007/s11431-014-5482-8, 2014.

Charbeneau, R. J.: Kinematic Models for Soil Moisture and Solute Transport, Water Resources Research, 20, 699–706, doi:10.1029/WR020i006p00699, 1984.

Childs, E. C. and Collis-George, N.: The Permeability of Porous Materials, Proceedings of the Royal Society of London A: Mathematical, Physical and Engineering Sciences, 201, 392–405, doi:10.1098/rspa.1950.0068, 1950.

Christiansen, J. S., Thorsen, M., Clausen, T., Hansen, S., and Christian Refsgaard, J.: Modelling of macropore flow and transport processes at catchment scale, Journal of Hydrology, 299, 136–158, doi:j.jhydrol.2004.04.029, 2004.

Chui, T. and Freyberg, D.: Implementing Hydrologic Boundary Conditions in a Multiphysics Model, Journal of Hydrologic Engineering, 14, 1374–1377, doi:10.1061/(ASCE)HE.1943-5584.0000113, 2009.

Crosta, G. B. and Frattini, P.: Distributed modelling of shallow landslides triggered by intense rainfall, Natural Hazards and Earth System Sciences, 3, 81–93, doi:10.5194/nhess-3-81-2003, 2003.

Crosta, G. B. and Frattini, P.: Rainfall-induced landslides and debris flows, Hydrological Processes, 22, 473–477, doi:10.1002/hyp.6885, 2008.

Dai, F. C., Lee, C. F., and Ngai, Y. Y.: Landslide risk assessment and management: an overview, Engineering Geology, 64, 65–87, doi:S0013-7952(01)00093-X, 2002.

Davies, J. and Beven, K.: Comparison of a Multiple Interacting Pathways model with a classical kinematic wave subsurface flow solution, Hydrological Sciences Journal, 57, 203–216, doi:10.1080/02626667.2011.645476, 2012.

Debieche, T. H., Bogaard, T. A., Marc, V., Emblanch, C., Krzeminska, D. M., and Malet, J. P.: Hydrological and hydrochemical processes observed during a large-scale infiltration experiment at the Super-Sauze mudslide (France), Hydrological Processes, 26, 2157–2170, doi:10.1002/hyp.7843, 2012.

DiCarlo, D. A.: Stability of gravity-driven multiphase flow in porous media: 40 Years of advancements, Water Resources Research, 49, 4531–4544, doi:10.1002/wrcr.20359, 2013.

D'Odorico, P., Fagherazzi, S., and Rigon, R.: Potential for landsliding: Dependence on hyetograph characteristics, Journal of Geophysical Research: Earth Surface, 110, 1007–1021, doi:10.1029/2004JF000127, 2005.

Durner, W.: Hydraulic conductivity estimation for soils with heterogeneous pore structure, Water Resources Research, 30, 211–223, doi:10.1029/93WR02676, 1994.

Dusek, J., Gerke, H. H., and Vogel, T.: Surface Boundary Conditions in Two-Dimensional Dual-Permeability Modeling of Tile Drain Bromide Leaching, Vadose Zone J., 7, 1287–1301, doi:10.2136/vzj2007.0175, 2008.

Flury, M., Flühler, H., Jury, W. A., and Leuenberger, J.: Susceptibility of soils to preferential flow of water: A field study, Water Resources Research, 30, 1945–1954, doi:10.1029/94WR00871, 1994.

Gerke, H. H.: Preferential flow descriptions for structured soils, Journal of Plant Nutrition and Soil Science, 169, 382–400, doi:10.1002/jpln.200521955, 2006.

Gerke, H. H. and Köhne, J. M.: Estimating Hydraulic Properties of Soil Aggregate Skins from Sorptivity and Water Retention, Soil Sci. Soc. Am. J., 66, 26–36, doi:10.2136/sssaj2002.2600, 2002.

Gerke, H. H. and Köhne, J. M.: Dual-permeability modeling of preferential bromide leaching from a tile-drained glacial till agricultural field, Journal of Hydrology, 289, 239 – 257, doi:10.1016/j.jhydrol.2003.11.019, 2004.

Gerke, H. H. and van Genuchten, M.: A dual-porosity model for simulating the preferential movement of water and solutes in structured porous media, Water Resources Research, 29, 305–319, doi:10.1029/92WR02339, 1993a.

Gerke, H. H. and van Genuchten, M.: Evaluation of a first-order water transfer term for variably saturated dual-porosity flow models, Water Resources Research, 29, 1225–1238, doi:10.1029/92wr02467, 1993b.

Germann, P. F. and Beven, K.: Kinematic Wave Approximation to Infiltration Into Soils With Sorbing Macropores, Water Resources Research, 21, 990–996, doi:10.1029/WR021i007p00990, 1985.

Ghestem, M., Sidle, R. C., and Stokes, A.: The influence of plant root systems on subsurface flow: implications for slope stability, BioScience, 61, 869–879, doi:10.1525/bio.2011.61.11.6, 2011.

Godt, J. W., Baum, R. L., Savage, W. Z., Salciarini, D., Schulz, W. H., and Harp, E. L.: Transient deterministic shallow landslide modeling: Requirements for susceptibility and hazard assessments in a GIS framework, Engineering Geology, 102, 214–226, doi:j.enggeo.2008.03.019, 2008.

Greco, R.: Preferential flow in macroporous swelling soil with internal catchment: model development and applications, Journal of Hydrology, 269, 150–168, doi:S0022-1694(02)00215-9, 2002.

Greco, R., Comegna, L., Damiano, E., Guida, A., Olivares, L., and Picarelli, L.: Hydrological modelling of a slope covered with shallow pyroclastic deposits from field monitoring data, hydrology and earth system sciences, 17, 4001–4013, doi:10.5194/hess-17-4001-2013, 2013.

Griffiths, D. and Lane, P.: Slope stability analysis by finite elements, Geotechnique, 49, 387–403, doi:10.1680/geot.1999.49.3.387, 1999.

Griffiths, D. and Lu, N.: Unsaturated slope stability analysis with steady infiltration or evaporation using elasto-plastic finite elements, International Journal for Numerical and Analytical Methods in Geomechanics, 29, 249–267, doi:10.1002/nag.413, 2005.

Griffiths, D., Huang, J., and Fenton, G. A.: Probabilistic infinite slope analysis, Computers and Geotechnics, 38, 577–584, doi:j.compgeo.2011.03.006, 2011.

Guzzetti, F., Carrara, A., Cardinali, M., and Reichenbach, P.: Landslide hazard evaluation: a review of current techniques and their application in a multi-scale study, Central Italy, Geomorphology, 31, 181 – 216, doi:10.1016/S0169-555X(99)00078-1, 1999.

Guzzetti, F., Peruccacci, S., Rossi, M., and Stark, C. P.: The rainfall intensity–duration control of shallow landslides and debris flows: an update, Landslides, 5, 3–17, doi:10.1007/s10346-007-0112-1, 2007.

Gwo, J., Jardine, P., Wilson, G., and Yeh, G.: A multiple-pore-region concept to modeling mass transfer in subsurface media, Journal of Hydrology, 164, 217–237, doi:0022-1694(94)02555-P, 1995.

Hammouri, N., Malkawi, A. H., and Yamin, M. A.: Stability analysis of slopes using the finite element method and limiting equilibrium approach, Bulletin of Engineering Geology and the Environment, 67, 471–478, doi:10.1007/s10064-008-0156-z, 2008.

Hencher, S. R.: Preferential flow paths through soil and rock and their association with landslides, Hydrological Processes, 24, 1610–1630, doi:10.1002/hyp.7721, 2010.

Hendrickx, J. M. and Flury, M.: Uniform and preferential flow mechanisms in the vadose zone, pp. 149–188, National Academy Press, 2001.

Highland, L., Bobrowsky, P. T., et al.: The landslide handbook: a guide to understanding landslides, US Geological Survey Reston, 2008.

Hu, Y., Feng, J., Yang, T., and Wang, C.: A new method to characterize the spatial structure of soil macropore networks in effects of cultivation using computed tomography, Hydrological Processes, 28, 3419–3431, doi:10.1002/hyp.9902, 2014.

Huang, M. and Jia, C.-Q.: Strength reduction FEM in stability analysis of soil slopes subjected to transient unsaturated seepage, Computers and Geotechnics, 36, 93–101, doi:j.compgeo.2008.03.006, 2009.

Šimůnek, J., Jarvis, N. J., van Genuchten, M. T., and Gärdenäs, A.: Review and comparison of models for describing non-equilibrium and preferential flow and transport in the vadose zone, Journal of Hydrology, 272, 14–35, doi:S0022-1694(02)00252-4, 2003.

Šimůnek, J., van Genuchten, M. T., and Šejna, M.: Development and applications of the HYDRUS and STANMOD software packages and related codes, Vadose Zone Journal, 7, 587–600, doi:10.2136/vzj2007.0077, 2008.

Itasca, F.: Fast Lagrangian Analysis of Continua, Version 4.0 User's Guide, Itasca Consulting Group, Inc., Thrasher Square East, 708, 2002.

Iverson, R. M.: Landslide triggering by rain infiltration, Water Resources Research, 36, 1897–1910, doi:10.1029/2000WR900090, 2000.

Jarvis, N. J.: A review of non-equilibrium water flow and solute transport in soil macropores: principles, controlling factors and consequences for water quality, European Journal of Soil Science, 58, 523–546, doi:10.1111/j.1365-2389.2007.00915.x, 2007.

Jarvis, N. J., Jansson, P. E., Dik, P. E., and Messing, I.: Modelling water and solute transport in macroporous soil. I. Model description and sensitivity analysis, Journal of Soil Science, 42, 59–70, doi:10.1111/j.1365-2389.1991.tb00091.x, 1991.

Jing, L.: A review of techniques, advances and outstanding issues in numerical modelling for rock mechanics and rock engineering, International Journal of Rock Mechanics and Mining Sciences, 40, 283–353, doi:S1365-1609(03)00013-3, 2003.

Kampf, S. K. and Burges, S. J.: A framework for classifying and comparing distributed hillslope and catchment hydrologic models, Water Resources Research, 43, 1–25, doi:10.1029/2006WR005370, 2007.

Köhne, J. M. and Mohanty, B. P.: Water flow processes in a soil column with a cylindrical macropore: Experiment and hierarchical modeling, Water Resources Research, 41, W03 010, doi:10.1029/2004wr003303, 2005.

Köhne, J. M., Köhne, S., and Gerke, H. H.: Estimating the hydraulic functions of dual-permeability models from bulk soil data, Water Resources Research, 38, 26–1–26–11, doi:10.1029/2001wr000492, 2002.

Köhne, J. M., Mohanty, B. P., and Šimůnek, J.: Inverse dual-permeability modeling of preferential water flow in a soil column and implications for field-scale solute transport, Vadose Zone Journal, 5, 59–76, doi:10.2136/vzj2005.0008, 2006.

Köhne, J. M., Köhne, S., and Šimůnek, J.: A review of model applications for structured soils: a) Water flow and tracer transport, Journal of Contaminant Hydrology, 104, 4–35, doi:j.jconhyd.2008.10.002, 2009.

Kim, J., Salgado, R., and Yu, H.: Limit Analysis of Soil Slopes Subjected to Pore-Water Pressures, Journal of Geotechnical and Geoenvironmental Engineering, 125, 49–58, doi:doi:10.1061/(ASCE)1090-0241(1999)125:1(49), 1999.

Kirchner, J. W.: A double paradox in catchment hydrology and geochemistry, Hydrological Processes, 17, 871–874, doi:10.1002/hyp.5108, 2003.

Kirchner, J. W.: Catchments as simple dynamical systems: Catchment characterization, rainfall-runoff modeling, and doing hydrology backward, Water Resources Research, 45, WR02 429, doi:doi:10.1029/2008WR006912, 2009.

Kodešová, R., Kozák, J., Šimůnek, J., and Vacek, O.: Single and dual-permeability model of chlorotoluron transport in the soil profile, Plant, Soil and Environment, 51, 310–315, 2005.

Konagai, K. and Johansson, J.: Lagrangian PARTICLEs for Modeling Large Soil Deformations, Proc., Seismic Fault-induced Failures, pp. 99–106, 2001.

Krahn, J.: Stability modeling with SLOPE/W: An engineering methodology, GEO-SLOPE International Ltd, 2004.

Krzeminska, D., Bogaard, T. A., van Asch, T. W. J., and van Beek, L. P. H.: A conceptual model of the hydrological influence of fissures on landslide activity, hydrology and earth system sciences, 16, 1561–1576, doi:10.5194/hess-16-1561-2012, 2012.

Krzeminska, D. M., Bogaard, T. A., Malet, J. P., and van Beek, L. P. H.: A model of hydrological and mechanical feedbacks of preferential fissure flow in a slow-moving landslide, hydrology and earth system sciences, 17, 947–959, doi:10.5194/hess-17-947-2013, 2013.

Krzeminska, D. M., Bogaard, T. A., Debieche, T.-H., Cervi, F., Marc, V., and Malet, J.-P.: Field investigation of preferential fissure flow paths with hydrochemical analysis of small-scale sprinkling experiments, Earth Surface Dynamics, 2, 181–195, doi:10.5194/esurf-2-181-2014, 2014.

Laine-Kaulio, H.: Development and analysis of a dual-permeability model for subsurface stormflow and solute transport in a forested hillslope, Ph.D. thesis, Aalto University, 2011.

Laine-Kaulio, H., Backnäs, S., Karvonen, T., Koivusalo, H., and McDonnell, J. J.: Lateral subsurface stormflow and solute transport in a forested hillslope: A combined measurement and modeling approach, Water Resources Research, pp. 8159–8179, doi:10.1002/2014WR015381, 2014.

Lanni, C., McDonnell, J., Hopp, L., and Rigon, R.: Simulated effect of soil depth and bedrock topography on near-surface hydrologic response and slope stability, Earth Surface Processes and Landforms, 38, 146–159, doi:10.1002/esp.3267, 2013.

Larsbo, M. and Jarvis, N.: MACRO 5.0: a model of water flow and solute transport in macroporous soil: technical description, Tech. Rep. 9157665923, Department of Soil Sciences, Swedish University of Agricultural Sciences, 2003.

Lehmann, P. and Or, D.: Hydromechanical triggering of landslides: From progressive local failures to mass release, Water Resources Research, 48, w03 535–w03 542, doi:10.1029/2011WR010947, 2012.

Leij, F. J.: The UNSODA unsaturated soil hydraulic database: user's manual, Tech. Rep. 95, National Risk Management Research Laboratory, US Environmental Protection Agency, 1996.

Lighthill, M. J. and Whitham, G. B.: On Kinematic Waves. I. Flood Movement in Long Rivers, Proceedings of the Royal Society of London A: Mathematical, Physical and Engineering Sciences, 229, 281–316, doi:10.1098/rspa.1955.0088, 1955.

Lu, N. and Godt, J.: Infinite slope stability under steady unsaturated seepage conditions, Water Resources Research, 44, W11 404, doi:10.1029/2008WR006976, 2008.

Lu, N. and Godt, J. W.: Hillslope hydrology and stability, Cambridge University Press, 2013.

Lu, N., Godt, J. W., and Wu, D. T.: A closed-form equation for effective stress in unsaturated soil, Water Resources Research, 46, W05 515, doi:10.1029/2009wr008646, 2010.

Lu, N., Şener Kaya, B., Wayllace, A., and Godt, J. W.: Analysis of rainfall-induced slope instability using a field of local factor of safety, Water Resources Research, 48, W09 524, doi:10.1029/2012wr011830, 2012.

McDonnell, J.: The influence of macropores on debris flow initiation, Quarterly Journal of Engineering Geology and Hydrogeology, 23, 325–331, 1990.

McDonnell, J. J. and Beven, K.: Debates—The future of hydrological sciences: A (common) path forward? A call to action aimed at understanding velocities, celerities and residence time distributions of the headwater hydrograph, Water Resources Research, 50, 5342–5350, doi:10.1002/2013WR015141, 2014.

McDonnell, J. J., Sivapalan, M., Vaché, K., Dunn, S., Grant, G., Haggerty, R., Hinz, C., Hooper, R., Kirchner, J., Roderick, M. L., Selker, J., and Weiler, M.: Moving beyond heterogeneity and process complexity: A new vision for watershed hydrology, Water Resources Research, 43, 1–6, doi:10.1029/2006WR005467, 2007.

Milledge, D. G., Griffiths, D. V., Lane, S. N., and Warburton, J.: Limits on the validity of infinite length assumptions for modelling shallow landslides, Earth Surface Processes and Landforms, 37, 1158–1166, doi:10.1002/esp.3235, 2012.

Mohammadi, M. H., Neishabouri, M. R., and Rafahi, H.: Predicting the solute breakthrough curve from soil hydraulic properties, Soil science, 174, 165–173, doi:10.1097/SS.0b013e3181998fa7, 2009.

Montgomery, D. R. and Dietrich, W. E.: A physically based model for the topographic control on shallow landsliding, Water Resources Research, 30, 1153–1171, doi:10.1029/93WR02979, 1994.

Montrasio, L. and Valentino, R.: A model for triggering mechanisms of shallow landslides, Natural Hazards and Earth System Science, 8, 1149–1159, doi:10.5194/nhess-8-1149-2008, 2008.

Moonen, P., Carmeliet, J., and Sluys, L.: A continuous–discontinuous approach to simulate fracture processes in quasi-brittle materials, Philosophical Magazine, 88, 3281–3298, doi:10.1080/14786430802566398, 2008.

Mualem, Y.: A new model for Hydrology and Earth System Sciences the hydraulic conductivity of unsaturated porous media, Water Resources Research, 12, 513–522, doi:10.1029/WR012i003p00513, 1976.

Mualem, Y. and Dagan, G.: Hydraulic conductivity of soils: Unified approach to the statistical models, Soil Science Society of America Journal, 42, 392–395, doi:10.2136/sssaj1978.03615995004200030003x, 1978.

Mukhlisin, M., Taha, M., and Kosugi, K.: Numerical analysis of effective soil porosity and soil thickness effects on slope stability at a hillslope of weathered granitic soil formation, Geosciences Journal, 12, 401–410, doi:10.1007/s12303-008-0039-0, 2008.

Mulungu, D. M. M., Ichikawa, Y., and Shiiba, M.: A physically based distributed subsurface-surface flow dynamics model for forested mountainous catchments, Hydrological Processes, 19, 3999–4022, doi:10.1002/hyp.5868, 2005.

Nash, J. and Sutcliffe, J.: River flow forecasting through conceptual models part I — A discussion of principles, Journal of Hydrology, 10, 282 – 290, doi:10.1016/0022-1694(70)90255-6, 1970.

Nemes, A., Schaap, M., Leij, F., and Wösten, J.: Description of the unsaturated soil hydraulic database UNSODA version 2.0, Journal of Hydrology, 251, 151–162, doi:S0022-1694(01)00465-6, 2001.

Ng, C. and Pang, Y.: Influence of Stress State on Soil-Water Characteristics and Slope Stability, Journal of Geotechnical and Geoenvironmental Engineering, 126, 157–166, doi:10.1061/(ASCE)1090-0241(2000)126:2(157), 2000.

Ng, C. W. W. and Shi, Q.: A numerical investigation of the stability of unsaturated soil slopes subjected to transient seepage, Computers and Geotechnics, 22, 1–28, doi:S0266-352X(97)00036-0, 1998.

Nieber, J. L. and Sidle, R. C.: How do disconnected macropores in sloping soils facilitate preferential flow?, Hydrological Processes, 24, 1582–1594, doi:10.1002/hyp.7633, 2010.

Nield, D. A. and Bejan, A.: Convection in porous media, springer, 2006.

Nielsen, D. R., Th. Van Genuchten, M., and Biggar, J. W.: Water flow and solute transport processes in the unsaturated zone, Water Resources Research, 22, 89S–108S, doi:10.1029/WR022i09Sp0089S, 1986.

Nimmo, J. R.: Simple predictions of maximum transport rate in unsaturated soil and rock, Water Resources Research, 43, 1–11, doi:10.1029/2006WR005372, 2007.

Nimmo, J. R.: Preferential flow occurs in unsaturated conditions, Hydrological Processes, 26, 786–789, doi:10.1002/hyp.8380, 2012.

Ogden, F. L., Lai, W., Steinke, R. C., Zhu, J., Talbot, C. A., and Wilson, J. L.: A new general 1-D vadose zone flow solution method, Water Resources Research, 51, 4282–4300, doi:10.1002/2015WR017126, 2015.

Pastor, M., Fernández Merodo, J. A., Herreros, M. I., Mira, P., González, E., Haddad, B., Quecedo, M., Tonni, L., and Drempetic, V.: Mathematical, Constitutive and Numerical Modelling of Catastrophic Landslides and Related Phenomena, Rock Mechanics and Rock Engineering, 41, 85–132, doi:10.1007/s00603-007-0132-0, 2008.

Peters, A., Durner, W., and Wessolek, G.: Consistent parameter constraints for soil hydraulic functions, Advances in Water Resources, 34, 1352–1365, doi:10.1016/j.advwatres.2011.07.006, 2011.

Petley, D.: Global patterns of loss of life from landslides, Geology, 40, 927–930, doi:10.1130/G33217.1, 2012.

Phillips, F. M.: Hydrology: Soil-water bypass, Nature Geoscience, 3, 77–78, doi:10.1038/ngeo762, 2010.

Picarelli, L., Urciuoli, G., Mandolini, A., and Ramondini, M.: Softening and instability of natural slopes in highly fissured plastic clay shales, Natural Hazards and Earth System Sciences, 6, doi:10.5194/nhess-6-529-2006, 2006.

Pierson, T.: Soil pipes and slope stability, Quarterly Journal of Engineering Geology and Hydrogeology, 16, 1–11, doi:10.1144/GSL.QJEG.1983.016.01.01, 1983.

Pirastru, M. and Niedda, M.: Field monitoring and dual permeability modelling of water flow through unsaturated calcareous rocks, Journal of Hydrology, 392, 40–53, doi:j.jhydrol.2010.07.045, 2010.

Qiu, C., Esaki, T., Xie, M., Mitani, Y., and Wang, C.: Spatio-temporal estimation of shallow landslide hazard triggered by rainfall using a three-dimensional model, Environmental Geology, 52, 1569–1579, doi:10.1007/s00254-006-0601-x, 2007.

Rahardjo, H., Satyanaga, A., and Leong, E. C.: Unsaturated soil mechanics for slope stabilization, Southeast Asian Geotechnical Journal, 43, 48–58, 2012.

Rahimi, A., Rahardjo, H., and Leong, E.-C.: Effect of hydraulic properties of soil on rainfall-induced slope failure, Engineering Geology, 114, 135 – 143, doi:10.1016/j.enggeo.2010.04.010, 2010.

Rasmussen, T. C., Baldwin, R. H., Dowd, J. F., and Williams, A. G.: Tracer vs. pressure wave velocities through unsaturated saprolite, Soil Science Society of America Journal, 64, 75–85, doi:10.2136/sssaj2000.64175x, 2000.

Ray, C., Ellsworth, T. R., Valocchi, A. J., and Boast, C. W.: An improved dual porosity model for chemical transport in macroporous soils, Journal of Hydrology, 193, 270–292, doi:S0022-1694(96)03141-1, 1997.

Ray, C., Vogel, T., and Dusek, J.: Modeling depth-variant and domain-specific sorption and biodegradation in dual-permeability media, Journal of Contaminant Hydrology, 70, 63–87, doi:j.jconhyd.2003.08.009, 2004.

Reid, M. E.: A pore-pressure diffusion model for estimating landslide-inducing rainfall, The Journal of Geology, pp. 709–717, 1994.

Romano, N., Nasta, P., Severino, G., and Hopmans, J.: Using bimodal lognormal functions to describe soil hydraulic properties, Soil Science Society of America Journal, 75, 468–480, 2011.

Rosso, R., Rulli, M. C., and Vannucchi, G.: A physically based model for the hydrologic control on shallow landsliding, Water Resources Research, 42, 6410–6426, doi:10.1029/2005WR004369, 2006.

Roulier, S. and Jarvis, N.: Analysis of inverse procedures for estimating parameters controlling macropore flow and solute transport in the dual-permeability model MACRO, Vadose Zone Journal, 2, 349–357, doi:10.2136/vzj2003.3490, 2003.

Savenije, H. H. G. and Veling, E. J. M.: Relation between tidal damping and wave celerity in estuaries, Journal of Geophysical Research: Oceans, 110, 435–466, doi:10.1029/2004JC002278, 2005.

Schaap, M. G. and Van Genuchten, M. T.: A modified Mualem–van Genuchten formulation for improved description of the hydraulic conductivity near saturation, Vadose Zone Journal, 5, 27–34, doi:10.2136/vzj2005.0005, 2006.

Shao, W., Bogaard, T., and Bakker, M.: How to Use {COMSOL} Multiphysics for Coupled Dual-permeability Hydrological and Slope Stability Modeling, Procedia Earth and Planetary Science, 9, 83 – 90, doi:10.1016/j.proeps.2014.06.018, the Third Italian Workshop on Landslides: Hydrological Response of Slopes through Physical Experiments, Field Monitoring and Mathematical Modeling, 2014.

Shao, W., Bogaard, T., Bakker, M., and Greco, R.: Quantification of the influence of preferential flow on slope stability using a numerical modelling approach, Hydrology and Earth System Sciences, 19, 2197–2212, doi:10.5194/hess-19-2197-2015, 2015.

Sharma, R. and Nakagawa, H.: Numerical model and flume experiments of single- and two-layered hillslope flow related to slope failure, Landslides, 7, 425–432, doi:10.1007/s10346-010-0205-0, 2010.

Shuin, Y., Hotta, N., Suzuki, M., and Ogawa, K.-i.: Estimating the effects of heavy rainfall conditions on shallow landslides using a distributed landslide conceptual model, Physics and Chemistry of the Earth, Parts A/B/C, 49, 44–51, doi:j.pce.2011.06.002, 2012.

Sidle, R. C.: Field observations and process understanding in hydrology: essential components in scaling, Hydrological Processes, 20, 1439–1445, doi:10.1002/hyp.6191, 2006.

Sidle, R. C. and Bogaard, T. A.: Dynamic earth system and ecological controls of rainfall-initiated landslides, Earth-Science Reviews, 159, 275 – 291, doi:10.1016/j.earscirev.2016.05.013, 2016.

Sidle, R. C., Noguchi, S., Tsuboyama, Y., and Laursen, K.: A conceptual model of preferential flow systems in forested hillslopes: evidence of self-organization, Hydrological Processes, 15, 1675–1692, doi:10.1002/hyp.233, 2001.

Simoni, S., Zanotti, F., Bertoldi, G., and Rigon, R.: Modelling the probability of occurrence of shallow landslides and channelized debris flows using GEOtop-FS, Hydrological Processes, 22, 532–545, doi:10.1002/hyp.6886, 2008.

Simunek, J., Van Genuchten, M. T., and Sejna, M.: The HYDRUS-1D software package for simulating the movement of water, heat, and multiple solutes in variably saturated media, version 3.0, HYDRUS software series 1, Department of Environmental Sciences, University of California Riverside, Riverside Edition, 2005.

Singh, V. P.: Kinematic wave modeling in water resources, surface-water hydrology, John Wiley & Sons, 1996.

Singh, V. P.: Kinematic wave modeling in water resources, Environmental hydrology, John Wiley & Sons, 1997.

Singh, V. P.: Is hydrology kinematic?, Hydrological Processes, 16, 667–716, doi:10.1002/hyp.306, 2002.

Stead, D., Eberhardt, E., Coggan, J., and Benko, B.: Advanced numerical techniques in rock slope stability analysis—applications and limitations, in: International Conference on Landslides—Causes, Impacts and Countermeasures, pp. 615–624, 2001.

Steenhuis, T., Parlance, J.-Y., and Andreini, M.: A numerical model for preferential solute movement in structured soils, Geoderma, 46, 193 – 208, doi:10.1016/0016-7061(90)90015-2, 1990.

Steenhuis, T. S., Baver, C. E., Hasanpour, B., Stoof, C. R., DiCarlo, D. A., and Selker, J. S.: Pore scale consideration in unstable gravity driven finger flow, Water Resources Research, 49, 7815–7819, doi:10.1002/2013WR013928, 2013.

Stolarski, T., Nakasone, Y., and Yoshimoto, S.: Engineering analysis with ANSYS software, Butterworth-Heinemann, 2011.

Talebi, A., Uijlenhoet, R., and Troch, P. A.: A low-dimensional physically based model of hydrologic control of shallow landsliding on complex hillslopes.

Therrien, R.; McLaren, R. and Sudicky, E.: HydroGeoSphere: A Three-Dimensional Numerical Model Describing Fully-Integrated Subsurface and Surface Flow and Solute Transport, Tech. rep., S.M. Panday, Hydrogeologic Inc./University of Waterloo, 2005.

Tsai, T.-L. and Yang, J.-C.: Modeling of rainfall-triggered shallow landslide, Environmental Geology, 50, 525–534, doi:10.1007/s00254-006-0229-x, 2006.

Tsutsumi, D. and Fujita, M.: Relative importance of slope material properties and timing of rainfall for the occurrence of landslides, International Journal of Erosion Control Engineering, 1, 79–89, 2008.

Uchida, T., Kosugi, K., and Mizuyama, T.: Effects of pipeflow on hydrological process and its relation to landslide: a review of pipeflow studies in forested headwater catchments, Hydrological Processes, 15, 2151–2174, doi:10.1002/hyp.281, 2001.

Uchida, T., Asano, Y., Mizuyama, T., and McDonnell, J. J.: Role of upslope soil pore pressure on lateral subsurface storm flow dynamics, Water Resources Research, 40, W12 401, doi:10.1029/2003WR002139, 2004.

van Dam, J. and Feddes, R.: Numerical simulation of infiltration, evaporation and shallow groundwater levels with the Richards equation, Journal of Hydrology, 233, 72 – 85, doi:10.1016/S0022-1694(00)00227-4, 2000.

van der Spek, J. E., Bogaard, T. A., and Bakker, M.: Characterization of groundwater dynamics in landslides in varved clays, hydrology and earth system sciences, 17, 2171–2183, doi:10.5194/hess-17-2171-2013, 2013.

Van Genuchten, M. T.: A closed-form equation for predicting the hydraulic conductivity of unsaturated soils, Soil science society of America journal, 44, 892–898, doi:10.2136/sssaj1980.03615995004400050002x, 1980.

Van Genuchten, M. T., Leij, F., and Yates, S.: The RETC code for quantifying the hydraulic functions of unsaturated soils, Robert S. Kerr Environmental Research Laboratory, 1991.

van Schaik: The role of macropore flow from plot to catchment scale: a study in a semi-arid area, Doctoral thesis, Universiteit Utrecht, 2010.

Varnes, D. J.: Slope movement types and processes, Transportation Research Board, Washington, DC, United States, 1978.

Vogel, T., Gerke, H., Zhang, R., and Genuchten, M. V.: Modeling flow and transport in a two-dimensional dual-permeability system with spatially variable hydraulic properties, Journal of Hydrology, 238, 78 – 89, doi:10.1016/S0022-1694(00)00327-9, 2000a.

Vogel, T., Van Genuchten, M. T., and Cislerova, M.: Effect of the shape of the soil hydraulic functions near saturation on variably-saturated flow predictions, Advances in water resources, 24, 133–144, doi:10.1016/S0309-1708(00)00037-3, 2000b.

von Ruette, J., Lehmann, P., and Or, D.: Effects of rainfall spatial variability and intermittency on shallow landslide triggering patterns at a catchment scale, Water Resources Research, 50, 7780–7799, doi:10.1002/2013WR015122, 2014.

Vrugt, J. A., Schoups, G., Hopmans, J. W., Young, C., Wallender, W. W., Harter, T., and Bouten, W.: Inverse modeling of large-scale spatially distributed vadose zone properties using global optimization, Water Resources Research, 40, W06 503, doi:10.1029/2003WR002706, 2004.

Wang, Q., Horton, R., and Lee, J.: A Simple Model Relating Soil Water Characteristic Curve and Soil Solute Breakthrough Curve, Soil science, 167, 436–443, doi:10.1097/00010694-200207000-00002, 2002.

Wang, Z., Feyen, J., Nielsen, D. R., and van Genuchten, M. T.: Two-phase flow infiltration equations accounting for air entrapment effects, Water Resources Research, 33, 2759–2767, doi:10.1029/97WR01708, 1997.

Weiler, M.: An infiltration model based on flow variability in macropores: development, sensitivity analysis and applications, Journal of Hydrology, 310, 294–315, doi:j.jhydrol.2005.01.010, 2005.

Westen, C. J., Asch, T. W. J., and Soeters, R.: Landslide hazard and risk zonation—why is it still so difficult?, Bulletin of Engineering Geology and the Environment, 65, 167–184, doi:10.1007/s10064-005-0023-0, 2006.

Wilkinson, P. L., Anderson, M. G., and Lloyd, D. M.: An integrated hydrological model for rain-induced landslide prediction, Earth Surface Processes and Landforms, 27, 1285–1297, doi:10.1002/esp.409, 2002.

Wong, T. S. W.: Influence of upstream inflow on wave celerity and time to equilibrium on an overland plane, Hydrological Sciences Journal, 41, 195–205, doi:10.1080/02626669609491492, 1996.

Wu, Y.-S., Liu, H. H., and Bodvarsson, G. S.: A triple-continuum approach for modeling flow and transport processes in fractured rock, Journal of Contaminant Hydrology, 73, 145–179, doi:j.jconhyd.2004.01.002, 2004.

Zehe, E., Maurer, T., Ihringer, J., and Plate, E.: Modeling water flow and mass transport in a loess catchment, Physics and Chemistry of the Earth, Part B: Hydrology, Oceans and Atmosphere, 26, 487–507, doi:S1464-1909(01)00041-7, 2001.

Zhang, G., Savenije, H., Fenicia, F., and Pfister, L.: Modelling subsurface storm flow with the Representative Elementary Watershed (REW) approach: application to the Alzette River Basin, Hydrology and Earth System Sciences, 10, 937–955, doi:10.5194/hess-10-937-2006, 2006.

Zhou, C., Shao, W., and van Westen, C. J.: Comparing two methods to estimate lateral force acting on stabilizing piles for a landslide in the Three Gorges Reservoir, China, Engineering Geology, 173, 41 – 53, doi:10.1016/j.enggeo.2014.02.004, 2014.

# ACKNOWLEDGEMENT

There are so many people I want to thank who supported me during my Ph.D study.

My biggest thanks goes to my supervisors, promoter Prof. Mark Bakker and co-promoter Dr. Thom Bogaard, for giving me the opportunity to study in the hydrology group of TU Delft. You made enormous efforts in improving the quality of each chapter. Besides, the discussions with Prof. Huub Savenije always gave me additional inspiration and motivation to conduct this research.

Research is a team work that benefits from international cooperation. I am indebted to all co-authors of my publications. Especially, Prof. Roberto Greco and Prof. Matteo Berti gave me valuable suggestions to improve the quality of two research papers that became the main chapters of my thesis. The cooperative work with Cees van Westen, Jakub Langhammer, Chunmei Zhou, and Ye Su gave me the opportunity to gain additional research experience, for which I am very grateful.

I am also grateful to the China Scholarship Council for the financial support. Special thanks goes to Prof. Charles W.W. NG who offered me a chance by providing financial support to visit Hong Kong University of Science and Technology. The 5 months research visit introduced me to experimental studies in geotechnical engineering. Additionally, my final half-year stay in Delft is supported by the funding from the DOMINO project (Dikes and Debris flows monitoring by novel optical fiber sensors). The involvement of this project made me think of using numerical models for engineering designs.

I felt comfortable during my Ph.D study because of the friendly and warm-hearted colleagues: Theo Olsthoorn, Wim Bastiaanssen, Nick van de Giesen, Markus Hrachowitz, Miriam Coenders-Gerrits, Saket Pande, Susan Steele-Dunne, Ronald van Nooyen, Ali Abbasi, Ruud van der Ent, Martijn Westhoff, Remko Nijzink, Elena Cristiano, Bas des Tombe, to name a few. I also want to thank Lydia de Hoog, Luz Ton-Estrada, and Betty Rothfusz for taking care of administrative issue.

The whole period studying overseas left me tons of memories of the beautiful countries and the nice people living in Europe. Also thanks to many of my Chinese friends: Hongkai Gao, Xin Tian, Jianzhi Dong, Lixia Niu, Zheng Duan, Huayang Cai, Lan Wang, Zongji Yang, Congli Dong, Wei Meng, Yingrong Wen, Yang Lv, Yongwei Liu and Zhilin Zhang. Your company in a foreign country made my life more colorful and comfortable.

Finally, thanks go to my parents and grandparents for their unconditional support.

*Wei Shao*
*Delft, September 2016*

# CURRICULUM VITÆ

Wei Shao was born in XinJiang Province in China in June 1986. He received a bachelor's degree in Hydraulic and Hydroelectric Engineering at Tianjin University in 2008, and a master's degree in Hydrology and Water Resources at Hohai University in 2011. In his master thesis, the Lattice Boltzmann method and finite different method were applied to build a one-dimensional dual-permeability model to simulate the process of macropore flow and solute transport in undisturbed soil columns.

In September 2011, with the financial support from Chinese Scholarship Council (CSC), he became a Ph.D student at Delft University of Technology. He join the Hydrology group that is lead by Prof. Huub Savenije, and was supervised by Prof. Mark Bakker and Dr. Thom Bogaard. His research topic was studying the physical principles of subsurface flow and slope instability in mountainous areas, and he developed hydro-mechanical models to simulate the impact of preferential flow on hillslope hydrology and slope stability. Besides, he is also interested in modeling water flow in expansive clays, and water and energy transport in the soil-vegetation-atmosphere continuum.

# List of Publications

## Journal Papers

1. **Shao, W.**, Ni, J.J., Leung, A. K., Su, Y., and Ng, C. W. W.: *Analysis of plant root-induced preferential flow and pore water pressure variation by a dual-permeability model*, Canadian Geotechnical Journal **(under review)**.

2. Ni, J. J., Leung, A. K., Ng, C. W. W., and **Shao, W.**: *A coupled seepage-stability model for considering hydro-mechanical reinforcements by plant roots*, Géotechnique **(under review)**.

3. **Shao, W.**, Su, Y., and Langhammer, J.: *Simulations of coupled non-isothermal soil moisture transport and evaporation fluxes in a forest area*, Journal of Hydrology and Hydromechanics **(under review)**.

4. **Shao, W.**, Bogaard, T. A., Bakker, M., and Berti, M.: *Analysing the influence of preferential flow on pressure propagation and landslide triggering of Rocca Pitigliana landslide*, Journal of Hydrology (2016) **in print**.

5. **Shao, W.**, Bogaard, T. A., Bakker, M., and Greco, R.: *Quantification of the influence of preferential flow on slope stability using a numerical modelling approach*, Hydrology and Earth System Sciences **19**, 2197–2212 (2015).

6. Zhou, C.M., **Shao, W.**, van Westen, C.J.: *Comparing two methods to estimate lateral force acting on stabilizing piles for a landslide in the Three Gorges Reservoir, China*, Engineering Geology **173**, 41–53 (2014).

## Conference Papers

1. **Shao, W.**, Bogaard, T. A., Su, Y., Bakker, M.: *Coupling a 1D dual-permeability model with an infinite slope stability approach to quantify the influence of preferential flow on slope stability*, Procedia Earth and Planetary Science **16**, 128—136 (2016).

2. **Shao, W.**, Bogaard, T. A., Bakker, M., and Greco, R.: *Quantification of the influence of preferential flow on slope stability using a numerical modelling approach*, Procedia Earth and Planetary Science **19**, 2197–2212 (2015).

## Conference Abstracts

1. **Shao, W.**, Bogaard, T. A., Bakker, M., Berti, M. Savenije, H.H.G.: *The influence of preferential flow on pressure propagation and landslide triggering of the Rocca Pitigliana landslide*, Geophysical Research Abstracts **2016**, AGU-H13E-1418 San Francisco 12-16 December 2016.

2. **Shao, W.**, Bogaard, T. A., Bakker, M., Berti, M.: *Analysing the influence of preferential flow on pressure transmission and landslide triggering*, Geophysical Research Abstracts **17**, EGU2015-7571 (2015).

3. **Shao, W.**, Bogaard, T. A., Bakker, M., Su, Y., Savenije, H.: *Can flow velocity distribution at a pore-scale be quantified by a celerity-saturation curve?*, Geophysical Research Abstracts **17**, EGU EGU2015-9611 (2015).

4. Su, Y., **Shao, W.**, Vlcek, L., Langhammer,J.: *Quantifying the feedback of evaporation and transpiration rates to soil moisture dynamics and meteorological condition changes by a numerical model*, Geophysical Research Abstracts **17**, 2015-9456-2 (2015).

5. Cristiano, E., Bogaard, T. A., **Shao, W.**: *The influence of anisotropy on preferential flow in landslides*, Geophysical Research Abstracts **17**, EGU2015-9898 (2015).

6. **Shao, W.**, Bogaard, T. A., Bakker, M.: *Modelling dual-permeability hydrological system and slope stability of the Rocca Pitigliana landslide using COMSOL Multiphysics*, Geophysical Research Abstracts **16**, EGU EGU2014-3723 (2014).

7. **Shao, W.**, Bogaard, T. A., Bakker, M.: *The influence of preferential flow on slope stability*, Geophysical Research Abstracts **15**, EGU EGU2013-2642-1 (2013).